

PHOTOCHEMISTRY OF INORGANIC AND ORGANOMETALLIC  
COMPLEXES IN VARIOUS MEDIA

by

Bentley J. Palmer

THESIS SUBMITTED IN PARTIAL FULFILLMENT OF  
THE REQUIREMENTS FOR THE DEGREE OF  
DOCTOR OF PHILOSOPHY  
in the Department  
of  
Chemistry

Bentley J. Palmer 1992  
SIMON FRASER UNIVERSITY

© All rights reserved. This work may not be  
reproduced in whole or in part, by photocopy  
or other means, without permission of the author.

## APPROVAL

Name: Bentley J. Palmer

Degree: DOCTOR OF PHILOSOPHY

Title of Thesis: PHOTOCHEMISTRY OF INORGANIC AND ORGANO-METALLIC COMPLEXES IN VARIOUS MEDIA

Examining Committee

Chairperson: Dr. F.W.B. Einstein

---

Dr. R.H. Hill, Senior Supervisor

---

Dr. I.D. Gay, Supervisory Committee

---

Dr. D. Sutton, Supervisory Committee

---

Dr. Y.L. Chow, Internal Examiner

---

Dr. J. Takats, External Examiner  
Department of Chemistry  
University of Alberta

Date Approved: 29 July 1992

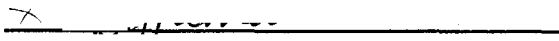
**PARTIAL COPYRIGHT LICENSE**

I hereby grant to Simon Fraser University the right to lend my thesis, project or extended essay (the title of which is shown below) to users of the Simon Fraser University Library, and to make partial or single copies only for such users or in response to a request from the library of any other university, or other educational institution, on its own behalf or for one of its users. I further agree that permission for multiple copying of this work for scholarly purposes may be granted by me or the Dean of Graduate Studies. It is understood that copying or publication of this work for financial gain shall not be allowed without my written permission.

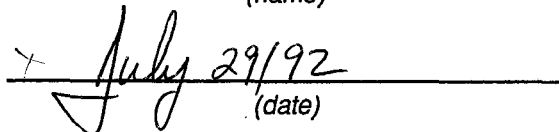
**Title of Thesis/Project/Extended Essay:**

PHOTOCHEMISTRY OF INORGANIC AND ORGANOMETALLIC COMPLEXES IN  
VARIOUS MEDIA

Author:

  
(signature)

BENTLEY J. PALMER  
(name)

  
(date)

## Abstract

This thesis describes the effect of reaction medium upon photochemical and photochemically induced reactions. The media discussed will include glasses and amorphous films. The photochemistry of amorphous inorganic films is a relatively unexplored area of research, which may reveal a different range of reactivity than is possible in other media. The results obtained, as a result of photolysing amorphous films, are compared and contrasted to the wealth of existing knowledge regarding inorganic photochemistry conducted in glass or solution.

The kinetics of the oxidative addition of  $R'_3SiH$  ( $R'_3 = Et_3, Et_2Me, EtMe_2, Et_2H$ ) to photogenerated  $(\eta^5-C_5R_5)Mn(CO)_2$  ( $R_5 = H_5, Me_5, H_4Me$ ) were studied in glasses and the Arrhenius  $E_a$  values varied from 2 kJ/mol ( $R'_3 = EtMe_2$ ) to 35 kJ/mol ( $R'_3 = Et_2Me$ ). The rate constants were amenable to interpretation by a master equation relating energy exchange between reactant molecules and a reaction medium treated as a heat bath. This resulted in a chemically more reasonable range for the  $E_a$  values of 27 kJ/mol to 38 kJ/mol.

The photolysis of *cis*- $(\eta^5-C_5Me_5)Re(CO)_2X_2$  ( $X = Me, Cl, Br, I$ ), in low temperature glasses was found to result in the isomerization to *trans*- $(\eta^5-C_5Me_5)Re(CO)_2X_2$ , through a  $(\eta^5-C_5Me_5)Re(CO)X_2$  intermediate. The intermediate reacted with free CO to yield exclusively *trans*- $(\eta^5-C_5Me_5)Re(CO)_2X_2$ . The photolysis of an amorphous film of

*cis*-( $\eta^5$ -C<sub>5</sub>Me<sub>5</sub>)Re(CO)<sub>2</sub>Br<sub>2</sub>, at 77 K, resulted in the production of two distinct isomers of ( $\eta^5$ -C<sub>5</sub>Me<sub>5</sub>)Re(CO)Br<sub>2</sub>. One of the isomers reacted with free CO to give, exclusively, *cis*-( $\eta^5$ -C<sub>5</sub>Me<sub>5</sub>)Re(CO)<sub>2</sub>Br<sub>2</sub>.

The photolysis of inorganic complexes, in a glass or solution, generally results in the extrusion of a two electron ligand followed by subsequent thermal chemistry. However, in films, the photoextrusion of several ligands from the coordination sphere and the production of metal and metal oxide films is possible.

This has been illustrated by investigating the photochemistry of inorganic complexes of Ti, Mn, Re, Co, and Ni as amorphous films. We have demonstrated the photoextrusion of the following ligands; CO, NH<sub>3</sub>, N<sub>3</sub>, NO, C<sub>5</sub>H<sub>5</sub>, C<sub>5</sub>H<sub>4</sub>Me, PEt<sub>3</sub>, and Br from complexes deposited as films. The mechanisms of these reactions are discussed.

**DEDICATION**

**To those who made it possible...my parents,**

**David L. Palmer**

**and**

**Joyce E. Palmer**

Quotation

"Bimbo limbo is where I've been  
I know you know that it's wearing me thin  
The times are changin' and it's about time  
I'm rearranging all the guilt in my mind..."

-Jimmy Buffett-

(single again, March 29, 1992)

-B.J.P.-

## ACKNOWLEDGEMENTS

My sincere thanks to Dr. Ross H. Hill, for his encouragement, guidance and especially his friendship.

I would also like to thank L. Goetting, and A. Becalska for their valuable friendship and support.

I would like to express my appreciation to Dr. D. Sutton and Dr. A.H. Klahn-Oliva for generously supplying some of the compounds used.

I would also like to express my appreciation to Dr. Brett Heinrich and Mr. K. Myrtle at the Surface Physics Laboratory (Simon Fraser University) for Auger and XPS spectra and to Mr. Vic Bourne, Dept. of Biological Sciences (Simon Fraser University) for the use of the scanning electron microscope.

Finally, I would like to thank Dr. Ross H. Hill and Simon Fraser University for their generous financial support.



## Table of Contents

Title Page .....	i
Approval .....	ii
Abstract .....	iii
Dedication .....	v
Quotation .....	vi
Acknowledgements .....	vii
Table of Contents .....	viii
List of Tables .....	xvi
List of Figures .....	xviii
List of Abbreviations .....	xxiii

### Chapter 1: Introduction

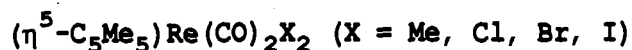
✓ 1.1 Photochemical and thermal reactions of inorganic and organometallic species in various media .....	1
1.2 The use of cryogenics and FTIR spectroscopy to investigate reactions .....	2
✓ 1.3 Surface sensitive analysis techniques .....	5
1.4 Interpretation of Kinetic Data .....	8
1.5 Oxidative Addition Reactions .....	9
✓ 1.6 Photochemistry of Inorganic and Organometallic Complexes .....	11

1.7	Basic Outline of the research plan .....	14
<b>Chapter 2:</b>	<b>Oxidative Addition of Trisubstituted Silanes</b>	
	<b>to Photochemically Generated <math>(\eta^5\text{-C}_5\text{R}_5)\text{Mn}(\text{CO})_2</math></b>	
	<b>Species</b>	
2.1	Introduction .....	16
2.2	Results .....	19
2.2.1	Photogeneration of $(\eta^5\text{-C}_5\text{R}_5)\text{Mn}(\text{CO})_2$ and Oxidative Addition Products .....	19
2.2.2	The Kinetics of the Oxidative Addition of $\text{R}'_3\text{SiH}$ to $(\eta^5\text{-C}_5\text{R}_5)\text{Mn}(\text{CO})_2$ .....	20
2.3	Discussion .....	28
2.3.1	The order of the reaction .....	29
2.3.2	Analysis of the reaction energetics according to Arrhenius law and Eyring theory .....	33
2.3.3	The form of Linert's equation that was used .....	34
2.3.4	Statistical analysis .....	38
2.3.5	Interpretation of the reaction energetics within the framework of Linert's theory .....	40
2.4	Conclusions .....	45
2.5	Experimental Section .....	45
2.5.1	Instruments .....	45
2.5.2	Chemicals .....	46
2.5.3	Kinetic measurements .....	49

2.5.4 N.M.R. Analysis .....	50
-----------------------------	----

**Chapter 3: Mechanistic Study of the Photochemically**

**Induced *cis* - *trans* Isomerization of**



3.1 Introduction .....	51
3.2 Results .....	52
3.2.1 Photochemistry of <i>cis</i> - $(\eta^5\text{-C}_5\text{Me}_5)\text{Re}(\text{CO})_2\text{Me}_2$ in 4-methyl-1-cyclohexene .....	52
3.2.2 Stereochemistry of the product and thermal reactivity of the photogenerated intermediate .....	53
3.3 Discussion .....	62
3.4 Conclusions .....	66
3.5 Experimental Section .....	67
3.5.1 Low-temperature photolysis .....	68

**Chapter 4: Photochemistry of *cis*- $(\eta^5\text{-C}_5\text{Me}_5)\text{Re}(\text{CO})_2\text{Br}_2$  on  
Si(111) Surfaces at Low Temperature.**

4.1 Introduction .....	69
4.2 Results and Discussion .....	69
4.2.1 Calibration of absorbance vs. surface coverage .....	69

4.2.2 Comparison of the IR spectra of <i>cis</i> -( $\eta^5$ -C <sub>5</sub> Me <sub>5</sub> )Re(CO) <sub>2</sub> Br <sub>2</sub> in a low temperature glass and in a film .....	71
4.2.3 Comparison of the IR spectra of <i>trans</i> -( $\eta^5$ -C <sub>5</sub> Me <sub>5</sub> )Re(CO) <sub>2</sub> Br <sub>2</sub> in a low temperature glass and in a film .....	73
4.2.4 Comparison of the photochemistry of ( $\eta^5$ -C <sub>5</sub> Me <sub>5</sub> )Re(CO) <sub>2</sub> Br <sub>2</sub> in a low temperature glass and in a film .....	73
4.3 Conclusions .....	78
4.4 Experimental Section .....	80
4.4.1 Calibration of the absorption of ( $\eta^5$ -C <sub>5</sub> Me <sub>5</sub> )Re(CO) <sub>2</sub> Br <sub>2</sub> on Si(111) .....	81
4.4.2 Photolysis of ( $\eta^5$ -C <sub>5</sub> Me <sub>5</sub> )Re(CO) <sub>2</sub> Br <sub>2</sub> on silicon surfaces .....	81

## Chapter 5: Photochemical Reactions of

**$[(\eta^5\text{-C}_5\text{R}_5)\text{Mn}(\text{CO})_2(\text{NO})]^+$  ( $\text{R}_5 = \text{H}_5, \text{H}_4\text{Me}, \text{Me}_5$ )  
as Films and in Low Temperature Glasses.**

5.1 Introduction .....	82
5.2 Results and Discussion .....	83
5.2.1 Photochemistry of $[(\eta^5\text{-C}_5\text{H}_4\text{Me})\text{Mn}(\text{CO})_2(\text{NO})][\text{PF}_6]$ in a low temperature glass .....	83

5.2.2 Photochemistry of	
$[(\eta^5\text{-C}_5\text{H}_4\text{Me})\text{Mn}(\text{CO})_2(\text{NO})][\text{PF}_6]$ in a film at	
room temperature .....	86
5.2.3 Photochemistry of	
$[(\eta^5\text{-C}_5\text{H}_4\text{Me})\text{Mn}(\text{CO})_2(\text{NO})][\text{PF}_6]$ in a film at	
low temperature .....	92
5.3 Conclusions .....	96
5.4 Experimental Section .....	96
5.4.1 Preparation of $[(\eta^5\text{-C}_5\text{H}_4\text{Me})\text{Mn}(\text{CO})_2(\text{NO})][\text{X}]$	
( $\text{X} = [\text{BF}_4], [\text{ClO}_4]$ ) .....	97
5.4.2 Preparation of	
$[(\eta^5\text{-C}_5\text{H}_4\text{Me})\text{Mn}(\text{CO})_2(^{15}\text{NO})][\text{PF}_6]$ .....	97
5.4.3 Preparation of	
$[(\eta^5\text{-C}_5\text{Me}_5)\text{Mn}(\text{CO})_2(\text{NO})][\text{PF}_6]$ .....	98
5.4.4 Photolysis of the compounds on a silicon	
surface .....	98

**Chapter 6: The Photochemistry of  $\text{trans}-(\text{PEt}_3)_2\text{Ni}(\text{N}_3)_2$ :**

**Photodeposition of Nickel Films.**

6.1 Introduction .....	100
6.2 Results and Discussion .....	101
6.2.1 Spectroscopic data for the complexes .....	101
6.2.2 The photochemistry of $\text{trans}-(\text{PEt}_3)_2\text{Ni}(\text{N}_3)_2$ ..	105
6.3 Conclusions .....	117

6.4	Experimental Section .....	117
6.4.1	Preparation of $\text{trans}-(\text{PEt}_3)_2\text{Ni}(\text{N}_3)_2$ .....	118
6.4.2	Photolysis of complexes in a (1,2-epoxyethyl)-benzene glass .....	119
6.4.3	Calibration of the absorption on a silicon surface .....	119
6.4.4	Spin coating of $\text{trans}-(\text{PEt}_3)_2\text{Ni}(\text{N}_3)_2$ films ..	119
6.4.5	Photolysis of the complexes on a silicon surface .....	120
<b>Chapter 7: The Photochemistry of <math>\text{fac-Co}(\text{NH}_3)_3(\text{NO}_2)_3</math> and <math>\text{mer-Co}(\text{NH}_3)_3(\text{N}_3)_3</math> Films.</b>		
7.1	Introduction .....	121
7.2	Results and Discussion .....	122
7.2.1	Spectroscopic data for the complexes .....	122
7.2.2	Photochemistry of $\text{fac-Co}(\text{NH}_3)_3(\text{NO}_2)_3$ as a film .....	124
7.2.3	Photochemistry of $\text{mer-Co}(\text{NH}_3)_3(\text{N}_3)_3$ as a film .....	129
7.3	Conclusions .....	138
7.4	Experimental Section .....	138
7.4.1	Preparation of $\text{fac-Co}(\text{NH}_3)_3(\text{NO}_2)_3$ .....	139
7.4.2	Preparation of $\text{mer-Co}(\text{NH}_3)_3(\text{N}_3)_3$ .....	140

7.4.3 Deposition of <i>fac</i> -Co(NH <sub>3</sub> ) <sub>3</sub> (NO <sub>2</sub> ) <sub>3</sub> and <i>mer</i> -Co(NH <sub>3</sub> ) <sub>3</sub> (N <sub>3</sub> ) <sub>3</sub> as films .....	140
--	-----

**Chapter 8: The Photochemistry of  $(\eta^5\text{-C}_5\text{H}_5)_2\text{Ti}(\text{N}_3)_2$  on Surfaces and in a Low Temperature Glass: Photodeposition of Titanium Dioxide Films.**

8.1 Introduction .....	142
8.2 Results and Discussion .....	144
8.2.1 Spectroscopic data for the complexes .....	144
8.2.2 Photochemistry of $(\eta^5\text{-C}_5\text{H}_5)_2\text{Ti}(\text{N}_3)_2$ in a low temperature glass .....	150
8.2.3 Photochemistry of $(\eta^5\text{-C}_5\text{H}_5)_2\text{Ti}(\text{N}_3)_2$ as a film .....	151
8.3 Conclusions .....	162
8.4 Experimental Section .....	164
8.4.1 Preparation of ( <sup>15</sup> N)-labelled $(\eta^5\text{-C}_5\text{H}_5)_2\text{Ti}(\text{N}_3)_2$ .....	165
8.4.2 Photolysis of complexes in a (1,2-epoxyethyl)-benzene glass .....	165
8.4.3 Calibration of the absorption on a silicon surface .....	165
8.4.4 The photolysis of complexes on silicon surfaces .....	166

Appendices:

A-2: Appendix for Chapter 2 .....	167
A-6: Appendix for Chapter 6 .....	169
A-8: Appendix for Chapter 8 .....	171
References .....	175



## List of Tables

1-1	Some surface analysis techniques .....	7
2-1	FTIR data for $(\eta^5\text{-C}_5\text{R}_5)\text{Mn}(\text{CO})_2\text{H}(\text{SiR}'_3)$ complexes .....	21
2-2	Rate constants for the reaction of $(\eta^5\text{-C}_5\text{R}_5)\text{Mn}(\text{CO})_2$ with $\text{R}'_3\text{SiH}$ & $\text{R}'_2\text{SiH}_2$ .....	26
2-3	Arrhenius activation parameters for the reaction of $(\eta^5\text{-C}_5\text{R}_5)\text{Mn}(\text{CO})_2$ with $\text{HSiR}'_3$ .....	32
2-4	Linert's activation parameters determined by statistical analysis .....	42
2-5	Percent contraction for solvents at 77 K .....	47
2-6	$^1\text{H}$ NMR of relevant $(\eta^5\text{-C}_5\text{R}_5)\text{Mn}(\text{CO})_2\text{H}(\text{SiR}'_3)$ complexes .....	48
3-1	FTIR and UV-Vis spectral data for $(\eta^5\text{-C}_5\text{Me}_5)\text{Re}(\text{CO})_2\text{X}_2$ ( $\text{X} = \text{Me}, \text{Cl}, \text{Br}, \text{I}$ ) .....	57
4-1	FTIR spectral data for $(\eta^5\text{-C}_5\text{Me}_5)\text{Re}(\text{CO})_2\text{Br}_2$ .....	72
5-1	FTIR spectral data for $[(\eta^5\text{-C}_5\text{R}_5)\text{Mn}(\text{CO})_2(\text{NO})]^+$ ( $\text{R}_5 = \text{H}_5, \text{H}_4\text{Me}, \text{Me}_5$ ) as films and in glass .....	89
6-1	UV/Vis spectral data for nickel complexes .....	102
6-2	FTIR spectral data for nickel complexes on Si(111) .....	106

7-1	UV/Vis spectral data for cobalt complexes .....	123
7-2	FTIR spectral data for cobalt complexes .....	125
8-1	UV/Vis spectral data for titanium complexes .....	145
8-2	FTIR spectral data for titanium complexes .....	147
8-3	Quantities used in the quantum yield calculations for $(\eta^5\text{-C}_5\text{H}_5)_2\text{Ti}(\text{N}_3)_2$ .....	160

## List of Figures

2-1	FTIR spectral changes associated with the photolysis of $(\eta^5\text{-CH}_3\text{C}_5\text{H}_4)\text{Mn}(\text{CO})_3$ in a MCH/Et <sub>2</sub> SiH <sub>2</sub> glass .....	23
2-2	Absorbance difference spectra showing the consumption of $(\eta^5\text{-CH}_3\text{C}_5\text{H}_4)\text{Mn}(\text{CO})_2$ and the formation of $(\eta^5\text{-CH}_3\text{C}_5\text{H}_4)\text{Mn}(\text{CO})_2\text{H}(\text{SiEt}_2\text{H})$ .....	24
2-3	Plot of $\ln[(\eta^5\text{-CH}_3\text{C}_5\text{H}_4)\text{Mn}(\text{CO})_2]_{t=0} / [(\eta^5\text{-CH}_3\text{C}_5\text{H}_4)\text{Mn}(\text{CO})_3]_t$ vs. time .....	25
2-4	Schematic diagram of the energy exchange between reactant molecules and a reactant medium treated as a heat bath .....	36
2-5	Plot of experimental $\ln k$ values vs. $\ln k$ values estimated from Linert's theory .....	41
3-1	<b>(top)</b> The FTIR spectral changes accompanying the UV photolysis of <i>cis</i> - $(\eta^5\text{-C}_5\text{Me}_5)\text{Re}(\text{CO})_2\text{Me}_2$ at 13 K in a 4-methyl-1-cyclohexene glass	

	<b>(bottom)</b> The spectral changes associated with the warming, from 13 K to 100 K, of the glass containing the photoproducted CO and $(\eta^5\text{-C}_5\text{Me}_5)\text{Re}(\text{CO})\text{Me}_2$ .....	55
3-2	<b>(top)</b> The FTIR spectral changes accompanying the UV photolysis of <i>cis</i> - $(\eta^5\text{-C}_5\text{Me}_5)\text{Re}(\text{CO})_2\text{I}_2$ at 13 K in a (1,2-epoxyethyl)benzene glass	
	<b>(bottom)</b> The spectral changes associated with the warming, from 13 K to 100 K, of the glass containing the photoproducted $(\eta^5\text{-C}_5\text{Me}_5)\text{Re}(\text{CO})\text{I}_2$ .....	61
4-1	<b>(a)</b> FTIR spectra of <i>cis</i> - $(\eta^5\text{-C}_5\text{Me}_5)\text{Re}(\text{CO})_2\text{Br}_2$ on a silicon surface	
	<b>(b)</b> Plot of absorbance vs. coverage of <i>cis</i> - $(\eta^5\text{-C}_5\text{Me}_5)\text{Re}(\text{CO})_2\text{Br}_2$ on a silicon surface ...	70
4-2	<b>(a)</b> FTIR spectral changes associated with the photolysis of film of <i>cis</i> - $(\eta^5\text{-C}_5\text{Me}_5)\text{Re}(\text{CO})_2\text{Br}_2$ for 80 seconds	
	<b>(b)</b> Spectral changes associated with warming the sample, shown in figure 4-2 (a), to 150 K and recooling to 77 K .....	74

4-3	<p>(a) FTIR spectral changes associated with the photolysis of a film of <math>cis-(\eta^5-C_5Me_5)Re(CO)_2Br_2</math> for 100 min. and 220 min., using filtered light, and 5 min. using unfiltered light</p> <p>(b) Spectral changes associated with warming the sample, shown in figure 4-3 (a), to 150 K and recooling to 77 K .....</p>	77
4-4	<p>Scheme: Summary of the reactions of <math>cis-(\eta^5-C_5Me_5)Re(CO)_2Br_2</math> in a glass and film ....</p>	79
5-1	<p>(a) FTIR difference spectra for the photolysis of <math>[(\eta^5-C_5H_4Me)Mn(CO)_2(NO)][PF_6]</math> at 77 K in a glass</p> <p>(b) FTIR difference spectra for the photolysis of <math>[(\eta^5-C_5H_4Me)Mn(CO)_2(^{15}NO)][PF_6]</math> at 77 K in a glass</p> <p>(c) FTIR difference spectra for the photolysis of a film of <math>[(\eta^5-C_5H_4Me)Mn(CO)_2(NO)][PF_6]</math> at 298 K .....</p>	84
5-2	<p>Scheme: Summary of the reactions of <math>[(\eta^5-C_5H_4Me)Mn(CO)_2(NO)][PF_6]</math> in a glass and in a film .....</p>	95
6-1	<p>(a) FTIR spectra of <math>trans-(Et_3P)_2Ni(N_3)_2</math> on a silicon surface</p> <p>(b) Plot of absorbance vs. coverage of <math>trans-(Et_3P)_2Ni(N_3)_2</math> on a silicon surface .....</p>	104

6-2	(a) FTIR spectral changes associated with the photolysis of a film of $\text{trans}-(\text{Et}_3\text{P})_2\text{Ni}(\text{N}_3)_2$ on a silicon surface	
	(b) Photolysis of the resultant film (figure 6-2 (a)) for 3 min. ....	108
6-3	Plot of $\ln\{(A(t)-A(f))/(A(0)-A(f))\}$ and $\ln\{A(t)/A(0)\}$ vs. photolysis of $\text{trans}-(\text{Et}_3\text{P})_2\text{Ni}(\text{N}_3)_2$ .....	110
6-4	Scheme: Summary of the photolysis of a $\text{trans}-(\text{Et}_3\text{P})_2\text{Ni}(\text{N}_3)_2$ film .....	115
7-1	FTIR spectra associated with the photolysis of $\text{fac-Co}(\text{NH}_3)_3(\text{NO}_2)_3$ .....	126
7-2	FTIR spectrum of the photoproduced $\text{Co}(\text{NH}_3)_3(\text{NO}_2)(\text{ONO})_2$ intermediate .....	127
7-3	FTIR absorbance difference spectra showing the growth of bands due to $[\text{Co}_2(\text{N}_3)_6]$ .....	131
7-4	Spectra resulting from the addition of starting material absorbances to Figure 7-3 .....	132
7-5	$[\text{Co}_2(\text{N}_3)_6]$ .....	133
7-6	$[\text{Pd}_2(\text{N}_3)_6]^{2-}$ .....	134
7-7	FTIR spectrum of $\{\text{Co}(\text{N}_3)_2\}_n$ .....	136
7-8	Absorbance spectra showing the conversion of $\text{Co}(\text{NH}_3)_3(\text{N}_3)_3$ to $\{\text{Co}(\text{N}_3)_2\}_n$ through the intermediacy of $[\text{Co}_2(\text{N}_3)_6]$ .....	137

8-1	(a) FTIR spectra of $(\eta^5\text{-C}_5\text{H}_5)_2\text{Ti}(\text{N}_3)_2$ on a silicon surface	
	(b) Plot of absorbance vs. coverage of $(\eta^5\text{-C}_5\text{H}_5)_2\text{Ti}(\text{N}_3)_2$ on a silicon surface .....	149
8-2	Room temperature photolysis of $(\eta^5\text{-C}_5\text{H}_5)_2\text{Ti}(\text{N}_3)_2$ on a silicon surface .....	152
8-3	Spectral changes resulting from the prolonged photolysis of a film of $(\eta^5\text{-C}_5\text{H}_5)_2\text{Ti}(\text{N}_3)_2$ <i>in vacuo</i> .....	154
8-4	Scanning electron microscopy image of $\text{TiO}_2$ lines produced by the exhaustive photolysis of a $(\eta^5\text{-C}_5\text{H}_5)_2\text{Ti}(\text{N}_3)_2$ film, through an I.B.M. photomask .....	161
8-5	Scheme: Summary of the reactions of $(\eta^5\text{-C}_5\text{H}_5)_2\text{Ti}(\text{N}_3)_2$ in a glass and a film .....	163

### List of Abbreviations

AES	- Auger emission spectroscopy
Cp	- $\eta^5$ -C <sub>5</sub> H <sub>5</sub>
Cp'	- $\eta^5$ -CH <sub>3</sub> C <sub>5</sub> H <sub>4</sub>
Cp*	- $\eta^5$ -C <sub>5</sub> Me <sub>5</sub>
CT	- charge transfer
CVD	- chemical vapour deposition
DMSO	- dimethyl sulfoxide
ESCA	- electron spectroscopy for chemical analysis
FTIR	- Fourier transform infrared
IR	- infrared
<b>k</b>	- Boltzmann's constant
LF	- ligand field
LMCT	- ligand to metal charge transfer
MCH	- methylcyclohexane
Me	- CH <sub>3</sub>
N <sub>A</sub>	- Avogadro's number
Np	- 1-C <sub>10</sub> H <sub>7</sub> (1-naphthyl)
R	- alkyl group
SEM	- scanning electron microscopy
UV/Vis	- ultraviolet/visible
VLSI	- very large scale integration
XPS	- X-ray photoelectron spectroscopy



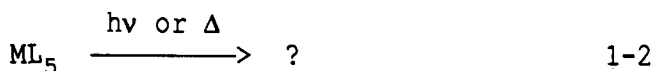
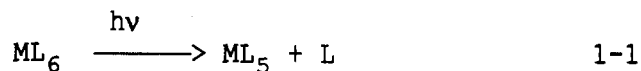
## Chapter 1: Introduction

### 1.1 Photochemical and thermal reactions of inorganic and organometallic species in various media

Discussed in this thesis is the reactivity of inorganic and organometallic species studied in various media; solution, low-temperature glasses, and amorphous films. The photochemistry of inorganic and organometallic compounds has been an active area of research for several years.<sup>1,2</sup> However, the majority of photochemistry has been conducted on molecules that were in solution<sup>3,4</sup> or in low temperature matrices.<sup>5-8</sup> The photoreactivity of inorganic complexes, in each of those media, is well understood.<sup>1,2,9</sup> The study of the photochemistry of inorganic and organometallic solids has progressed at a much slower rate than studies done in other media.<sup>2</sup> The majority of the research conducted on solid-state organometallic complexes has been done by solid-state physicists and material scientists.<sup>10,11</sup> However, the study of the reactions of inorganic and organometallic complexes, as amorphous films, remains a relatively unexplored area. The chemist studying solid-state inorganic and organometallic complexes has a different perspective of the area than solid-state physicists and material scientists.

Commonly, photolysing inorganic and organometallic complexes, in solution, or in low-temperature glasses results in the photo-extrusion

of a ligand (equation 1-1). The photochemically generated species,  $ML_5$ ,



may subsequently undergo another photochemical reaction or a thermal reaction (equation 1-2). However, the range of reactions that are possible depend on the medium in which the reaction is carried out. For example, intermediates that are unobservable in solution studies may be stabilized and characterized when the reaction is carried out in a low-temperature glass<sup>7</sup> or matrix<sup>12</sup>. Discussed in this thesis are the studies done on the photochemical and thermal reactions of inorganic and organometallic complexes in various media. Some of the methods used to characterize reactants, intermediates, and products are uncommon. Therefore, it would be helpful to discuss the various techniques.

## 1.2 The use of cryogenics and FTIR spectroscopy to investigate reactions

The method we used to monitor some of the reactions studied was a variation of the matrix-isolation technique.<sup>13</sup> Matrix isolation is an extremely useful technique for studying unstable intermediates. The theory of matrix-isolation is as follows: If a reactive or unstable species is trapped in a rigid, chemically inert solid at a sufficiently low temperature, then its lifetime may be extended almost indefinitely.

If the solid matrix is rigid enough the trapped, normally unstable, species cannot diffuse. If the possibility of diffusion is removed, a trapped molecule is unable to react with other species in the matrix. Generally, the matrix is supported on a salt window (usually CsI or KBr) which is clamped in a metal holder attached to a refrigeration source. This can be a Dewar containing liquid helium (4 K), liquid H<sub>2</sub> (20 K) or liquid nitrogen (77 K). Some workers favour a closed cycle helium refrigerator, which may operate at any temperature in the range 10 K - 273 K, as the refrigeration source. The majority of the low temperature surface film studies were done with a liquid nitrogen cooled Dewar. The film samples, maintained at approximately 10<sup>-3</sup> torr, were spectroscopically monitored by placing the cell in the sample beam of an FTIR and/or UV/Vis spectrometer.

Ideally, the matrix chosen is transparent in the region used for spectral examination. Traditionally, the matrices most commonly used are methane, nitrogen or argon, which are transparent in the IR, visible and near UV regions.<sup>12</sup>

As mentioned earlier, we used a variation of the standard matrix-isolation technique. Instead of forming the matrix from inert gases, organic solvents which form glasses at low temperature were used. The organometallic complex of interest is dissolved in an organic or organometallic solvent and placed in a CaF<sub>2</sub> faced high conductivity copper cell. The sample is cooled rapidly whereby the solvent forms a glass. Unlike a crystal, glasses possess no long range translational or rotational order.<sup>14</sup> Glasses are not in thermodynamic equilibrium. A glass is formed by rapid cooling, which traps the material in the glassy

state. Thermodynamically, a crystal is of lower energy, but kinetics prevent the system from achieving the global potential minimum. The kinetics at low temperature make the time scale for crystallization essentially infinitely long.<sup>14</sup> Once a glass has been produced, the photochemical reactions of the trapped species may be followed as in the matrix-isolation technique.<sup>15-18</sup> However, the use of glasses has its limitations. In condensed media, IR bands may be broadened causing the loss of some spectral information. Also, there is a considerable body of evidence indicating that glass matrices are not inert.<sup>19</sup> The molecules of the glass matrix may coordinate with a photo-generated unsaturated intermediate. Also, if the glass forms a rigid matrix, recombination of photo-dissociated fragments is efficient and rapid. A rigid matrix gives rise to what is commonly referred to as the "cage effect".<sup>20</sup> The most important problem with monitoring species in a glass is due to the absorbance of the glassy material. However, the primary advantage of a glass is the ability to monitor reactions over a wide temperature range.

Matrix isolation techniques have been used for several years to study main group molecules.<sup>12</sup> Additionally, the study of transition metal carbonyls and related molecules, using matrix isolation techniques, is a rich and active area of research.<sup>21</sup> The combination of FTIR spectroscopy and matrix-isolation techniques has proven to be an extremely useful way to study the kinetics and structural details of highly reactive organometallic fragments.

### 1.3 Surface sensitive analysis techniques

Several studies were done on the photochemistry of inorganic and organometallic compounds deposited as amorphous films on a silicon substrate. In some of the experiments the result of extended photolysis was the photoextrusion of all ligands, as monitored by FTIR spectroscopy. As a result, other surface analysis techniques had to be used to determine the final outcome of the complexes. The techniques used to analyze the films resultant from prolonged photolysis were optical interferometry, Auger emission spectroscopy, X-ray photoelectron spectroscopy and scanning electron microscopy. A summary of the different techniques is given in Table 1-1.

The amorphous inorganic and organometallic films were deposited on the unmasked region of a silicon chip. Removal of the mask resulted in a film-substrate step edge. The film thickness could be measured before or after the film was photolysed. Optical interferometry was used as a means to measure film thicknesses. The technique is based on the same principle as the Michelson interferometer used in Fourier transform infrared spectrometers. In optical interferometry a coherent monochromatic light wave is passed through a beam splitter. One beam strikes the sample and the other is reflected from a mirror. The mirror is then adjusted until interference fringes are observed. At the edge of the film, the light waves travel different distances depending on whether they are reflected from the film or the substrate. The magnitude of the shift of the interference fringes at the film-substrate step edge is then used to determine the film thickness.

X-ray photoelectron spectroscopy (XPS), also known as electron

spectroscopy for chemical analysis (ESCA), is a useful analytical technique for determining elemental composition. In XPS the bombardment of a sample with X-rays results in the ejection of core electrons. The energies of these secondary electrons are then analyzed by means of

$$E_k = hv - E_B \quad 1-3$$

where,  $E_k$  = kinetic energy of the  
           $\beta$ -rays (photoelectrons)

$hv$  = incident photon energy

$E_B$  = electron binding energy

an electrostatic analyser in conjunction with an electron detector. The fundamental equation of XPS spectroscopy is given in equation 1-3. It is the binding energy of the emitted electrons that is reported in an XPS spectrum. The binding energies of electrons are characteristic of the elements (or compounds) they are emitted from. The XPS technique is very useful for distinguishing between the various metals or the oxides or nitrides of those metals.

In Auger emission spectroscopy (AES), a sample is bombarded by a focussed electron beam of 1-10 keV energy which causes the ejection of core electrons from a level  $E_x$  in atoms. The core hole that was generated is then filled by an electron from a level  $E_y$  dropping down into the core hole with the energy difference taken up by a third electron from a level  $E_z$ . The third electron, called an Auger electron, is then ejected from the atom with an energy  $E_a$ , given approximately by

Table 1-1

Some surface analysis techniques

Method	Particle Measured	Process	Information	Monolayer Sensitivity	Effective Probing Depth
Auger Emission Spectroscopy (AES)	Auger electrons	electron in, Auger electron out	-Elements Li-U	$10^{-1}$	20 Å
Scanning Electron Microscopy (SEM)	electrons	electron in, different electron out	-Elements Na-U	none	10000 Å
X-ray Photo-Electron Spectroscopy (XPS or ESCA)	photo-electrons	X-ray in, photo-electron out	-Elements Li-U -Chemical Bonding	$10^{-1}$	30 Å

equation 1-4. The Auger electrons have energies unique to each atom,

$$E_a = E_z + E_y - E_x \quad 1-4$$

therefore, the energies of Auger electrons allow all the elements present (except hydrogen and helium) to be identified. Also, the ratio of the elements may be determined from the yield of Auger electrons. The ratio of the elements is helpful in inferring the stoichiometry of compounds such as metal oxides.

In scanning electron microscopy (SEM) a focussed electron beam, with energies from 1 keV to 20 keV, is directed at a sample. In SEM the focussed electron beam is scanned across a small area of the sample, similar to the process in a television monitor. The scanning electron beam causes the emission of electrons from the sample and the emitted electrons are monitored. The number of emitted electrons is related to the geometry and other properties of the sample. The result is a three-dimensional picture of the surface. The technique is very useful for looking at surface morphology.

#### **1.4 Interpretation of Kinetic Data**

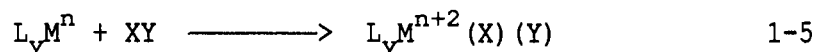
Utilizing low-temperature glasses we were able to measure the kinetics of the oxidative addition of trialkyl silanes to photochemically generated unsaturated organometallic species. Typically, the energetics of such reactions are interpreted using Arrhenius law or Eyring theory. However, the problem with Arrhenius law and Eyring theory is that they may yield little or no chemical insight



as to the factor(s) influencing the rate of reaction. The interpretation of kinetic data using either the Arrhenius law or Eyring theory yields essentially the same energy of activation. The energetics of the oxidative addition of trialkyl silanes to unsaturated organometallic species were interpreted using the Arrhenius law and a theory developed by Linert.<sup>22</sup> Linert's theory allows one to interpret the energetics of an analogous series of reactions based on the energy exchange between reactant molecules and a reaction medium. The application of Linert's theory to our kinetic data yielded a very different, and chemically more reasonable, range of activation energies than an interpretation based on Arrhenius law.

### 1.5 Oxidative Addition Reactions

Oxidative addition reactions<sup>23</sup> are among the most important class of reactions in chemistry. Oxidative addition reactions are the result of the activation of a variety of different bonds that are present in organic and inorganic reagents. Hence, this class of reaction is important for the catalytic application of transition-metal complexes to organic synthesis. Generally, in oxidative addition reactions, the metal undergoes an increase of its formal oxidation state by two units (eq 1-5).



Oxidative addition reactions are thought to proceed by one of three reaction routes. The three different mechanisms observed for oxidative

addition are a concerted addition, a nucleophilic attack, and a free radical mechanism. A concerted addition is the proposed mechanism for the addition of  $H_2$ . A concerted addition invariably occurs in a *cis* manner. Nucleophilic attack is common for the oxidative addition of alkyl halides, although not all alkyl halides are oxidatively added via a nucleophilic attack. The strongest evidence for the oxidative addition of alkyl halides by a nucleophilic attack mechanism comes from the inversion of configuration at the carbon attached to the metal.<sup>24</sup> Alkyl halides which do not oxidatively add to a metal by nucleophilic attack, commonly add by a free radical mechanism.<sup>25,26</sup> The free radical mechanism is characterized by loss of stereochemistry, retardation of the rate by radical inhibitors, and acceleration by oxygen or light.

The reagents, X-Y, which are known to undergo oxidative addition may be divided into three broad classes. The first class is non-polar species such as H-H and also includes low polarity species like  $R_3Si-H$ . The second class is grouped under the heading 'polar electrophilic' and includes such molecules as RX, HX, and  $HgCl_2$ . The third class is multiply bonded molecules such as  $O_2$  or  $MeO_2C\equiv CO_2Me$  which retain one or more X-Y bonds after undergoing oxidative addition. The classifications are important because they give an idea of the type of oxidative addition the reagent will undergo. Non-polar (or low polarity) molecules and multiply bonded molecules tend to undergo a concerted addition to a metal center. In the case of square planar complexes, a concerted addition yields a *cis* stereochemistry. Whereas, alkyl halides tend to undergo oxidative addition, via a nucleophilic attack or free radical mechanism, commonly yielding a *trans*

stereochemistry.

Of interest to us was one of the members of the 'first class' of reagents which was the low polarity species  $R_3Si-H$ . Transition-metal-silyl bonds are most easily formed by the oxidative addition of an Si-H bond.<sup>27</sup> Most importantly, the hydrosilation of olefins,<sup>28</sup> and ketones<sup>29</sup> are all believed to involve the oxidative addition of an Si-H bond. As a result of the importance of the oxidative addition of silicon-hydrogen bonds to transition metal complexes we undertook a kinetic study to try and better understand what governs the rate at which this step proceeds.

Discussed in Chapter 2 are the energetics of the oxidative addition of a silicon-hydrogen bond to an unsaturated organometallic fragment for a series of silanes and organometallic complexes. The variation in the experimentally measured rate constants could not be rationalized within the framework of Eyring theory. A more recently developed theory, which was also applied the kinetic data, appears to explain the variation in the measured rate constants in a chemically more reasonable manner.

## 1.6 Photochemistry of Inorganic and Organometallic Complexes

The use of light is one of the most efficient, and selective, ways in which to induce chemical reactions. The photochemistry of inorganic and organometallic complexes ranges from probing non-dissociative excited-state processes<sup>30</sup> to inducing ligand loss.<sup>31</sup> There are six major types of electronic transitions that result from photolysing transition metal complexes; ligand field (LF), metal to ligand charge-

transfer (MLCT), ligand to metal charge-transfer (LMCT), metal to solvent charge-transfer (MSCT), metal to metal charge-transfer (MMCT), and intraligand (IL). However, only the first three will be discussed since they are the most common and can result in efficient ligand loss.

Ligand field or metal-centered excited states of organometallic complexes are the result of electronic transitions between the metal d orbitals. Since carbon-donor ligands are relatively high on the spectrochemical series,<sup>32</sup> ligand field transitions of organometallic complexes tend to occur in the ultraviolet and visible regions at relatively high energies compared to those observed for the majority of classical coordination compounds.<sup>32, 33</sup> Additionally, metal ligand bonds in organometallic complexes tend to be highly covalent giving rise to metal-centered d-d transitions which have significant ligand character. As a result of the covalency, organometallic complexes tend to have relatively high extinction coefficients that are on the order of  $10^3 - 10^4 \text{ M}^{-1} \text{ cm}^{-1}$  for the LF transitions. However, the d-d transitions of classical coordination compounds generally have extinction coefficients on the order of  $10^1 - 10^2 \text{ M}^{-1} \text{ cm}^{-1}$ .<sup>33</sup> The most important point to note is that excitation into the LF states often results in efficient ligand loss.<sup>34</sup>

Metal to ligand charge-transfer (MLCT) excited states are the result of electronic transitions from a metal based orbital to a ligand based orbital. Formally, MLCT transitions result in the oxidation of the metal and the reduction of the ligand. MLCT transitions are common for organometallic complexes. Depending on the energy difference between the metal based orbitals and the ligand based

orbitals, the MLCT transitions may appear in the near-infrared, visible or ultraviolet regions. Similar to coordination compounds, MLCT transitions for organometallic complexes are usually intense with extinction coefficients in the  $10^4 - 10^5 \text{ M}^{-1} \text{ cm}^{-1}$  range. Also, the energy of a MLCT transition is highly dependent on the solvent used.

The last type of electronic transition to be discussed will be ligand to metal charge-transfer (LMCT) transitions. A LMCT transition is the result of an electronic transition from a mainly ligand based orbital to a mainly metal based orbital. Organometallic complexes exhibit large ligand field splittings since carbon donors are high in the spectrochemical series. Therefore, LMCT transitions tend to be quite high in energy.

Each of the above mentioned electronic transitions can result in ligand loss from inorganic and organometallic complexes in both solution and low temperature matrices. However, would these same electronic transitions give rise to efficient ligand loss for inorganic and organometallic complexes in the solid amorphous phase? If ligand loss occurred, would the unsaturated species be more or less stable in the solid amorphous phase than in solution or in low temperature matrices? If the unsaturated species were relatively long lived, could one affect the sequential photochemical loss of all ligands producing metallic films using a low energy process? These are some of the questions which we wanted to try and answer when we set out to study the photochemistry of amorphous inorganic and organometallic films.

## 1.7 Basic outline of the research plan

The research plan was to study the effects that different phases have on the photochemical and thermal reactions of inorganic and organometallic complexes. Discussed in Chapter 2 is the thermal reactivity of photochemically generated  $(\eta^5\text{-C}_5\text{R}_5)\text{M}(\text{CO})_2$  species. The unsaturated species can be stabilized in a low temperature glass long enough to follow the subsequent thermal reaction with a silane molecule. Hence, the kinetics of these reactions may be obtained. The energetics of these reactions were interpreted within the framework of various theories.

In Chapter 3 a discussion of the mechanism of the photochemical *cis-trans* isomerization of *cis*- $(\eta^5\text{-C}_5\text{Me}_5)\text{Re}(\text{CO})_2\text{X}_2$  ( $\text{X} = \text{Me}, \text{Cl}, \text{Br}, \text{I}$ ) is presented. The study was conducted, utilizing low-temperature glasses, in order to understand the mechanism of the *cis-trans* isomerization. The low-temperature glass stabilized the intermediate in the reaction whereby the mechanism of the reaction could be inferred.

Chapter 4 represents the first of the studies done on organometallic species deposited as amorphous films. The photochemistry of  $(\eta^5\text{-C}_5\text{Me}_5)\text{Re}(\text{CO})_2\text{Br}_2$  deposited as an amorphous film was investigated. The study of  $(\eta^5\text{-C}_5\text{Me}_5)\text{Re}(\text{CO})_2\text{Br}_2$ , as an amorphous film, was an ideal choice since the reactivity of the complex had been studied in solution<sup>35</sup> and in a low-temperature glass.<sup>36</sup> Therefore, the photochemistry of a film of  $(\eta^5\text{-C}_5\text{Me}_5)\text{Re}(\text{CO})_2\text{Br}_2$  could be compared to its photochemistry in solution and a glass.

Chapters 5, 6, and 7 discuss the photochemistry of a variety of inorganic and organometallic complexes deposited as amorphous films.

Where appropriate, complementary studies were done in solution or a low-temperature glass for a basis of comparison.

Discussed in Chapter 8 is the photodecomposition of a titanium complex, deposited as an amorphous film, resulting in the deposition of approximately 2  $\mu\text{m}$  wide  $\text{TiO}_2$  lines. Titanium dioxide is of practical importance in the semiconductor industry for use as a high dielectric constant material.<sup>37</sup> As far as I am aware, the above mentioned deposition of  $\text{TiO}_2$  films is the only single step process using standard photolithography techniques.

## Chapter 2: Oxidative Addition of Trisubstituted Silanes to Photochemically Generated $(\eta^5\text{-C}_5\text{R}_5)\text{Mn}(\text{CO})_2$ species

### 2.1 Introduction

The rate constants for a reaction, or series of reactions, are commonly interpreted using either Arrhenius law or Eyring theory. Using Arrhenius law one may obtain the activation energy ( $E_a$ ) for a reaction. On the other hand, Eyring theory allows one to calculate the enthalpy of activation ( $\Delta H^\ddagger$ ) and the entropy of activation ( $\Delta S^\ddagger$ ).

It has been known for several years that increasing the temperature generally causes a substantial increase in the rate of reactions. It was first discovered empirically by Hood<sup>38</sup> that the rate constant of a reaction varies with the absolute temperature according to equation 2-1, where A and B are constants. Hood's observation was given some

$$\log k = B - (A/T) \quad 2-1$$

theoretical significance by van't Hoff,<sup>39</sup> in 1884, who argued on the basis of the effect of temperature on equilibrium constants. It was these ideas that Arrhenius<sup>40</sup> applied successfully to a large number of reactions and found that the rate constant was related to the temperature by the relationship given in equation 2-2. The Arrhenius

$$k = A \exp(-E_a/RT) \quad 2-2$$

where, A = the frequency factor



law is a completely empirical relationship that has achieved general usage as a result of its applicability to various types of reactions. Using the Arrhenius law, a thorough understanding of the factors determining the rate constant of a reaction requires an understanding of the activation energy and the frequency factor. Although theories have been developed to interpret the Arrhenius parameters, most of these are for gas phase reactions. The interpretation of kinetic data for condensed phase reactions using the Arrhenius law requires the use of several approximations.

The Eyring equation, originally derived from transition state theory, is given in equations 2-3 and 2-4. Eyring theory, like the

$$k = \kappa(kT/h)e^{-\Delta G^\ddagger/RT} \quad 2-3$$

$$k = \kappa(kT/h)e^{(\Delta S^\ddagger/R - \Delta H^\ddagger/RT)} \quad 2-4$$

where,  $k$  = Boltzmann's constant

$h$  = Planck's constant

$\Delta G^\ddagger$  = Gibb's free energy of activation

$\Delta S^\ddagger$  = entropy of activation

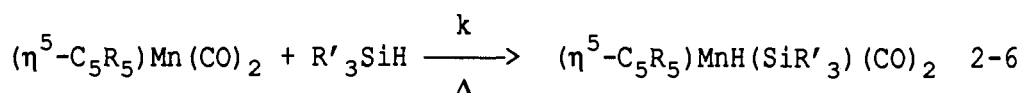
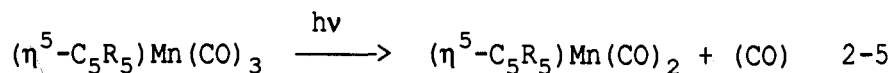
$\Delta H^\ddagger$  = enthalpy of activation

$\kappa$  = transmission coefficient

Arrhenius law, is limited by the information that it provides as to the reasons the rates of analogous reactions may differ. The limitation is, in part, the result of assuming that there is an equilibration of all vibronic states in the reactant system.

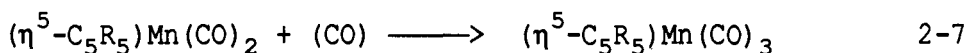
Discussed in this chapter are the results of an experimental study of the oxidative addition of trialkyl silanes to  $d^6$  16e unsaturated species. The organometallic reagents were generated at low temperature

by the irradiation of  $(\eta^5\text{-C}_5\text{R}_5)\text{Mn}(\text{CO})_3$  ( $\text{R}_5 = \text{H}_5, \text{Me}_5, \text{H}_4\text{Me}$ ) species. The photochemical and thermal reactions are summarized in equations 2-5 and 2-6, respectively. It is also possible that the 16e intermediate may react with the photogenerated CO (eq. 2-7). In a low temperature glass



it was possible to cause the photochemical reaction, CO dissociation (eq. 2-5), to occur at a rate substantially faster than the subsequent thermal oxidative addition of the trialkylsilane (eq. 2-6).

Consequently, at low temperatures, reaction 2-5 can be made to occur faster than 2-6 thereby accumulating  $(\eta^5\text{-C}_5\text{R}_5)\text{Mn}(\text{CO})_2$ . Therefore, as long as the back reaction with free CO (eq. 2-7) is too slow to compete for the dicarbonyl, the rate of equation 2-6 is directly measurable.



Oxidative addition by  $d^6$  systems is very important in catalytic<sup>41</sup> and stoichiometric processes including C-H activation by  $(\eta^5\text{-C}_5\text{H}_5)\text{Re}(\text{CO})\text{PMe}_3$ .<sup>42</sup> In solution, the oxidative addition of trisubstituted silane to  $(\eta^5\text{-C}_5\text{H}_5)\text{Mn}(\text{CO})_2$  and  $(\eta^5\text{-C}_5\text{Me}_5)\text{Mn}(\text{CO})_2$  has been shown to result from irradiation of the corresponding tricarbonyl.<sup>43</sup>

The kinetics of the oxidative addition of  $\text{R}'_3\text{SiH}$  ( $\text{R}'_3 = \text{Et}_3, \text{Et}_2\text{Me}, \text{EtMe}_2, \text{Et}_2\text{H}$ ) to photogenerated  $(\eta^5\text{-C}_5\text{R}_5)\text{Mn}(\text{CO})_2$  ( $\text{R}_5 = \text{H}_5, \text{Me}_5, \text{H}_4\text{Me}$ ) have been studied in the temperature range 70 - 130 K. Since

initial results indicated that Arrhenius law and Eyring theory yielded little chemical insight as to the factors that influence reaction rates, the energetics of the reactions were interpreted using an alternate theory. The energetics of the oxidative addition of trialkylsilanes to unsaturated organometallic fragments were interpreted using the Arrhenius law and a theory developed by Linert.<sup>44-50</sup> Linert's theory, which takes into account energy exchange between the solvent and the reactant molecules, allows one to better understand what influences the variation in the rates of similar reactions.

## 2.2 Results

### 2.2.1 Photogeneration of $(\eta^5\text{-C}_5\text{R}_5)\text{Mn}(\text{CO})_2$ and Oxidative Addition Products.

The photolysis of  $(\eta^5\text{-CH}_3\text{C}_5\text{H}_4)\text{Mn}(\text{CO})_3$  in a  $\text{EtMe}_2\text{SiH}$  glass gave rise to bands due to the 16e species,  $(\eta^5\text{-CH}_3\text{C}_5\text{H}_4)\text{Mn}(\text{CO})_2$ , at  $1942\text{ cm}^{-1}$  and  $1870\text{ cm}^{-1}$ , and an unassigned band at  $1845\text{ cm}^{-1}$ . In a dilute trialkylsilane glass (1:1 MCH/ $\text{EtMe}_2\text{SiH}$  mixture by volume at room temperature) photolysis resulted in bands due to  $(\eta^5\text{-CH}_3\text{C}_5\text{H}_4)\text{Mn}(\text{CO})_2$ , at  $1946\text{ cm}^{-1}$  and  $1876\text{ cm}^{-1}$ , and an unassigned band at  $1847\text{ cm}^{-1}$ . The photolysis of  $(\eta^5\text{-C}_5\text{H}_5)\text{Mn}(\text{CO})_3$  in a MCH/ $\text{Et}_2\text{MeSiH}$  glass showed bands due to the 16e species,  $(\eta^5\text{-C}_5\text{H}_5)\text{Mn}(\text{CO})_2$ , at  $1954\text{ cm}^{-1}$  and  $1885\text{ cm}^{-1}$  and two unassigned bands at  $1868\text{ cm}^{-1}$  and  $1834\text{ cm}^{-1}$ . Although the origin of the unexplained bands was unclear, their intensity did not vary on the time scale of the kinetic run. Therefore, it was concluded that equation 2-6 represented the net thermochemistry of all the  $(\eta^5\text{-C}_5\text{R}_5)\text{Mn}(\text{CO})_2$  ( $\text{R}_5 = \text{H}_5, \text{Me}_5, \text{H}_4\text{Me}$ ) species studied.

For each of the systems studied, the photolysis of  $(\eta^5\text{-C}_5\text{R}_5)\text{Mn}(\text{CO})_3$  species in a dilute (50/50 v/v @ room temperature trialkylsilane-methylcyclohexane (MCH) mixture) or neat trialkylsilane ( $\text{R}'_3\text{SiH}$ ) glass led to the loss of IR absorptions due to the starting complexes and the growth of new bands associated with the 16-electron species,  $(\eta^5\text{-C}_5\text{R}_5)\text{Mn}(\text{CO})_2$ , and the oxidative addition product  $(\eta^5\text{-C}_5\text{R}_5)\text{MnH}(\text{SiR}'_3)(\text{CO})_2$ . It was not possible to see free CO ( $\nu = 2132 \text{ cm}^{-1}$ ) in trialkylsilane (or a 1:1 trialkylsilane/MCH mixture) glasses due to the overwhelming Si-H absorption. The stoichiometry of the photochemical loss of CO for the manganese complexes studied has been shown to be one mole of CO produced per mole of  $(\eta^5\text{-C}_5\text{R}_5)\text{Mn}(\text{CO})_3$  consumed.<sup>51</sup> Although the direct monitoring of the increase or decrease in the CO absorption was not possible, it should be noted that photoproducts other than  $(\eta^5\text{-C}_5\text{R}_5)\text{Mn}(\text{CO})_2$  were not detected with the exception of the  $(\eta^5\text{-CH}_3\text{C}_5\text{H}_4)\text{Mn}(\text{CO})_3/\text{EtMe}_2\text{SiH}$  system and the  $(\eta^5\text{-C}_5\text{H}_5)\text{Mn}(\text{CO})_3/\text{Et}_2\text{MeSiH}$  system. Relevant band positions for the compounds studied are summarized in Table 2-1.

### 2.2.2 The Kinetics of the Oxidative Addition of $\text{R}'_3\text{SiH}$ to $(\eta^5\text{-C}_5\text{R}_5)\text{Mn}(\text{CO})_2$ .

A detailed description for studying the kinetics of the oxidative addition reactions is given in the Experimental section. However, the results obtained for a typical kinetic experiment will be discussed here. Before discussing the results of a particular system, it is important to note that in each of the reactions the trialkylsilane was in a large excess and did not change significantly during the course of

**Table 2-1**  
**Spectroscopic Data for Relevant Compounds**

Complex	T, K (± 1 K)	ν(CO) $\text{cm}^{-1}$ neat <sup>a</sup>	T, K (± 1 K)	ν(CO) $\text{cm}^{-1}$ dilute <sup>b</sup>
$(\eta^5\text{-CH}_3\text{C}_5\text{H}_4)\text{Mn}(\text{CO})_3$	298	2023, 1940		
	113	2020, 1935		
$(\eta^5\text{-CH}_3\text{C}_5\text{H}_4)\text{Mn}(\text{CO})_2$	113	1946, 1877		
$(\eta^5\text{-CH}_3\text{C}_5\text{H}_4)\text{MnH}(\text{SiEt}_3)(\text{CO})_2$	113	1971, 1906		
$(\eta^5\text{-CH}_3\text{C}_5\text{H}_4)\text{Mn}(\text{CO})_3$	298	2024, 1941	298	2024, 1941
	113	2020, 1934	114	2021, 1935
$(\eta^5\text{-CH}_3\text{C}_5\text{H}_4)\text{Mn}(\text{CO})_2$	113	1947, 1878	114	1948, 1880
$(\eta^5\text{-CH}_3\text{C}_5\text{H}_4)\text{MnH}(\text{SiEt}_2\text{Me})(\text{CO})_2$	113	1974, 1907	114	1974, 1908
$(\eta^5\text{-CH}_3\text{C}_5\text{H}_4)\text{Mn}(\text{CO})_3$	298	2018, 1933	298	2024, 1941
	90	2016, 1930	110	2018, 1932
$(\eta^5\text{-CH}_3\text{C}_5\text{H}_4)\text{Mn}(\text{CO})_2$	90	1942, 1870	110	1946, 1876
$(\eta^5\text{-CH}_3\text{C}_5\text{H}_4)\text{MnH}(\text{SiEtMe}_2)(\text{CO})_2$	90	1968, 1900 1845 <sup>c</sup>	110	1972, 1905 1847 <sup>c</sup>
$(\eta^5\text{-CH}_3\text{C}_5\text{H}_4)\text{Mn}(\text{CO})_3$	298		298	2024, 1941
	105	2018, 1932	115	2020, 1935
$(\eta^5\text{-CH}_3\text{C}_5\text{H}_4)\text{Mn}(\text{CO})_2$	105	1950, 1879	115	1949, 1880
$(\eta^5\text{-CH}_3\text{C}_5\text{H}_4)\text{MnH}(\text{SiEt}_2\text{H})(\text{CO})_2$	105	1976, 1910	115	1978, 1914
$(\eta^5\text{-C}_5\text{Me}_5)\text{Mn}(\text{CO})_3$	298		298	2010, 1926
	100		108	2006, 1921
$(\eta^5\text{-C}_5\text{Me}_5)\text{Mn}(\text{CO})_2$	100		108	1933, 1864
$(\eta^5\text{-C}_5\text{Me}_5)\text{MnH}(\text{SiEt}_2\text{Me})(\text{CO})_2$	100		108	1954, 1895
$(\eta^5\text{-C}_5\text{Me}_5)\text{Mn}(\text{CO})_3$			298	2009, 1926
			110	2006, 1920
$(\eta^5\text{-C}_5\text{Me}_5)\text{Mn}(\text{CO})_2$			110	1931, 1862
$(\eta^5\text{-C}_5\text{Me}_5)\text{MnH}(\text{SiEtMe}_2)(\text{CO})_2$			110	1954, 1893
$(\eta^5\text{-C}_5\text{H}_5)\text{Mn}(\text{CO})_3$	298		298	2028, 1945
	90		125	2024, 1940
$(\eta^5\text{-C}_5\text{H}_5)\text{Mn}(\text{CO})_2$	90		125	1954, 1885
$(\eta^5\text{-C}_5\text{H}_5)\text{MnH}(\text{SiEt}_2\text{Me})(\text{CO})_2$	90		125	1977, 1910 (1868, 1834) <sup>c</sup>

**a:** Solvent was pure trialkylsilane. **b:** Solvent was a 50/50 mixture (by volume at room temperature) of silane and methylcyclohexane.  
**c:** Additional bands that were observed after photolysis but that did not change on the time scale of the kinetic run.

the reaction.

Initially, a sample containing  $(\eta^5\text{-CH}_3\text{C}_5\text{H}_4)\text{Mn}(\text{CO})_3$  in  $\text{Et}_2\text{SiH}_2/\text{MCH}$  was cooled to 115 K and photolyzed (Figure 2-1). Upon photolysis there was a decrease in absorption bands at  $2020\text{ cm}^{-1}$  and  $1935\text{ cm}^{-1}$  due to  $(\eta^5\text{-CH}_3\text{C}_5\text{H}_4)\text{Mn}(\text{CO})_3$  and the appearance of absorption bands due to  $(\eta^5\text{-CH}_3\text{C}_5\text{H}_4)\text{Mn}(\text{CO})_2$  at  $1949\text{ cm}^{-1}$  and  $1880\text{ cm}^{-1}$  and  $(\eta^5\text{-CH}_3\text{C}_5\text{H}_4)\text{MnH}(\text{SiEt}_2\text{H})(\text{CO})_2$  at  $1978\text{ cm}^{-1}$  and  $1914\text{ cm}^{-1}$ . Subsequently, spectra were obtained as a function of time following the consumption of the  $(\eta^5\text{-CH}_3\text{C}_5\text{H}_4)\text{Mn}(\text{CO})_2$  species and the formation of the oxidative addition product,  $(\eta^5\text{-CH}_3\text{C}_5\text{H}_4)\text{MnH}(\text{SiEt}_2\text{H})(\text{CO})_2$ . Figure 2-2 illustrates a typical result obtained for the reaction of  $(\eta^5\text{-CH}_3\text{C}_5\text{H}_4)\text{Mn}(\text{CO})_2$  with  $\text{Et}_2\text{SiH}_2$  in a  $\text{Et}_2\text{SiH}_2/\text{methylcyclohexane}$  glass. Summarized in Figure 2-2 are the absorbance difference spectra (spectrum after photolysis subtracted from subsequent spectra) showing the consumption of  $(\eta^5\text{-CH}_3\text{C}_5\text{H}_4)\text{Mn}(\text{CO})_2$  (negative peaks) and the formation of  $(\eta^5\text{-CH}_3\text{C}_5\text{H}_4)\text{MnH}(\text{SiEt}_2\text{H})(\text{CO})_2$  (positive peaks). A plot of  $\ln\{[(\eta^5\text{-CH}_3\text{C}_5\text{H}_4)\text{Mn}(\text{CO})_2]_{t=0}/[(\eta^5\text{-CH}_3\text{C}_5\text{H}_4)\text{Mn}(\text{CO})_2]_t\}$  against time (Fig. 2-3) is linear, and the slope yields the rate constant,  $k(3.78 \times 10^{-4}\text{ s}^{-1})$ , according to equation 2-8. For each of the systems studied, the decrease in absorbance due to  $(\eta^5\text{-C}_5\text{R}_5)\text{Mn}(\text{CO})_2$  species (or increase in absorbance due to  $(\eta^5\text{-C}_5\text{R}_5)\text{MnH}(\text{SiR}'_3)(\text{CO})_2$  species) was found to be first order in  $(\eta^5\text{-C}_5\text{R}_5)\text{Mn}(\text{CO})_2$ . In both cases the kinetic results were interpreted in terms of the first-order rate law given in equation 2-8.

$$\frac{-d[(\eta^5\text{-C}_5\text{R}_5)\text{Mn}(\text{CO})_2]}{dt} = k[(\eta^5\text{-C}_5\text{R}_5)\text{Mn}(\text{CO})_2] \quad 2-8$$

$(\eta^5\text{-CH}_3\text{C}_5\text{H}_4)\text{Mn}(\text{CO})_3$ : negative bands at 2020 and 1935  $\text{cm}^{-1}$

$(\eta^5\text{-CH}_3\text{C}_5\text{H}_4)\text{Mn}(\text{CO})_2$ : positive bands at 1949 and 1880  $\text{cm}^{-1}$

$(\eta^5\text{-CH}_3\text{C}_5\text{H}_4)\text{Mn}(\text{H})(\text{SiEt}_2\text{H})(\text{CO})_2$ : positive bands at 1978 and 1914  $\text{cm}^{-1}$

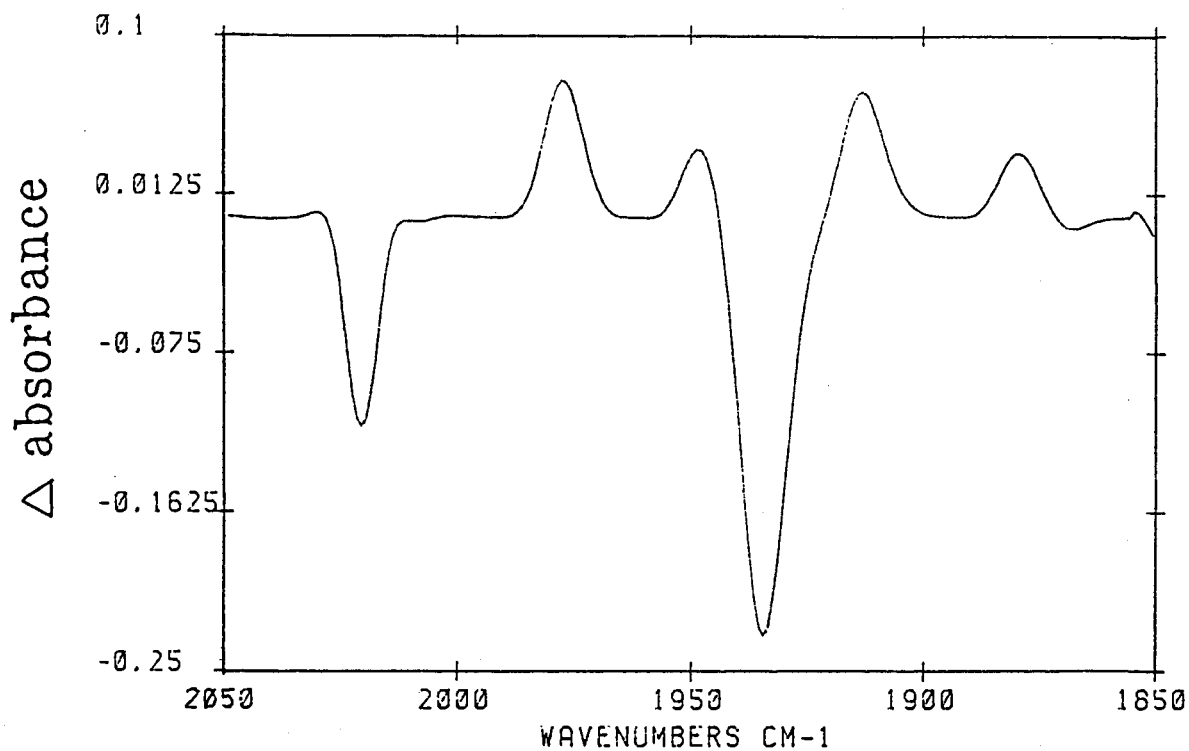


Figure 2-1: FTIR spectral changes associated with the photolysis of  $(\eta^5\text{-CH}_3\text{C}_5\text{H}_4)\text{Mn}(\text{CO})_3$  in a 50/50 (v/v) mixture of  $\text{Et}_2\text{SiH}_2$  and methylcyclohexane. Spectrum prior to photolysis subtracted from spectrum after photolysis.

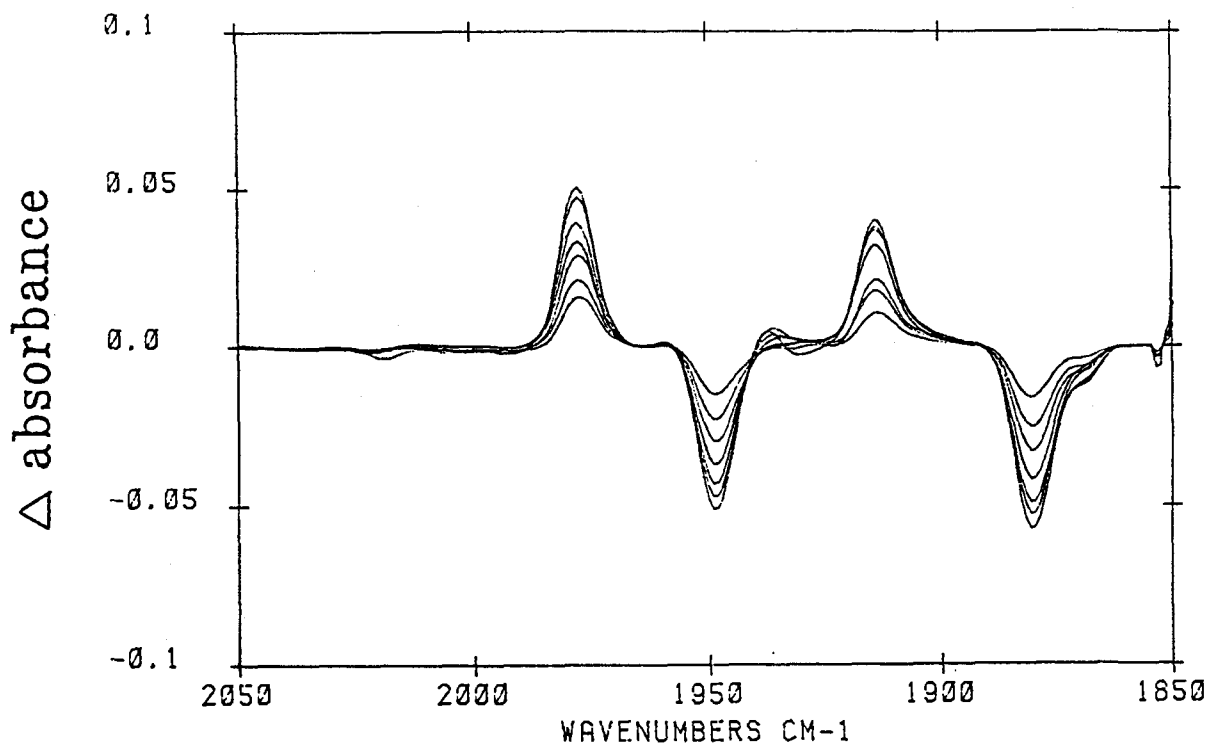


Figure 2-2: Absorbance difference spectra showing the consumption of  $(\eta^5\text{-CH}_3\text{C}_5\text{H}_4)\text{Mn}(\text{CO})_2$  (negative peaks) and the formation of  $(\eta^5\text{-CH}_3\text{C}_5\text{H}_4)\text{MnH}(\text{CO})_2(\text{SiEt}_2\text{H})$  (positive peaks).



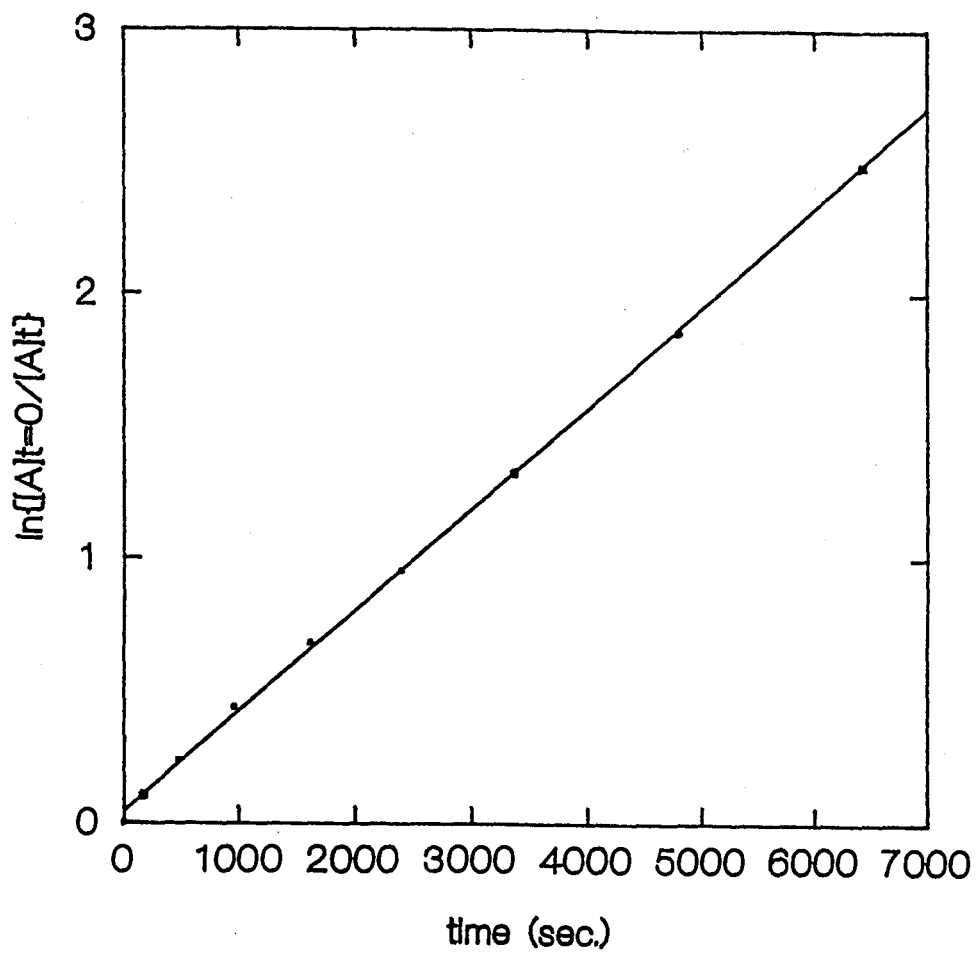


Figure 2-3: A plot of  $\ln\{[(\eta^5\text{-CH}_3\text{C}_5\text{H}_4)\text{Mn}(\text{CO})_2]_{t=0} / [(\eta^5\text{-CH}_3\text{C}_5\text{H}_4)\text{Mn}(\text{CO})_2]_t\}$  vs. time.

Table 2-2

RATE CONSTANTS FOR THE REACTION OF 16e ( $\eta^5\text{-C}_n\text{R}_n$ )Mn(CO)<sub>2</sub> COMPLEXES WITH R'<sub>3</sub>SiH & R'<sub>2</sub>SiH<sub>2</sub>

Complex	R' <sub>3</sub> SiH (M) <sup>a</sup>	T (K) (± 1 K)	k <sub>1</sub> (s <sup>-1</sup> ) (± 10%)
$(\eta^5\text{-CH}_3\text{C}_5\text{H}_4)\text{Mn(CO)}_2$	[Et <sub>2</sub> SiH <sub>2</sub> ] <sup>c</sup>		
	5.1	110	1.55 x 10 <sup>-4</sup>
	5.1	115	3.78 x 10 <sup>-4</sup>
	5.1	120	1.23 x 10 <sup>-3</sup>
	[Et <sub>2</sub> SiH <sub>2</sub> ] <sup>b</sup>		
	15.6	70	1.43 x 10 <sup>-6</sup>
	15.6	80	1.83 x 10 <sup>-6</sup>
	15.6	90	3.20 x 10 <sup>-6</sup>
	15.6	95	3.40 x 10 <sup>-6</sup>
	[Et <sub>2</sub> MeSiH] <sup>c</sup>		
	4.1	105	5.17 x 10 <sup>-6</sup>
	4.1	110	4.76 x 10 <sup>-5</sup>
	4.1	115	2.64 x 10 <sup>-4</sup>
	4.1	120	8.41 x 10 <sup>-4</sup>
	4.1	123	2.11 x 10 <sup>-3</sup>
[Et <sub>2</sub> MeSiH] <sup>b</sup>			
8.5	103	4.10 x 10 <sup>-5</sup>	
8.5	105	8.09 x 10 <sup>-5</sup>	
8.5	108	1.40 x 10 <sup>-4</sup>	
8.5	113	5.12 x 10 <sup>-4</sup>	
8.5	115	1.24 x 10 <sup>-3</sup>	
[EtMe <sub>2</sub> SiH] <sup>c</sup>			
4.8	100	3.88 x 10 <sup>-6</sup>	
4.8	105	2.99 x 10 <sup>-5</sup>	
4.8	110	9.17 x 10 <sup>-5</sup>	
4.8	115	4.72 x 10 <sup>-4</sup>	
4.8	118	8.69 x 10 <sup>-4</sup>	
4.8	120	2.83 x 10 <sup>-3</sup>	
[EtMe <sub>2</sub> SiH] <sup>b</sup>			
13.8	90	5.53 x 10 <sup>-7</sup>	
13.8	112	2.73 x 10 <sup>-4</sup>	
13.8	115	3.16 x 10 <sup>-4</sup>	
13.8	118	1.20 x 10 <sup>-3</sup>	

Table 2-2 (Continued)

Complex	$R_3SiH$ (M) <sup>a</sup>	T (K) (± 1 K)	$k$ (s <sup>-1</sup> ) (± 10%)
	[Et <sub>3</sub> SiH] <sup>b</sup>		
	7.0	103	1.16 x 10 <sup>-5</sup>
	7.0	108	6.43 x 10 <sup>-5</sup>
	7.0	113	2.63 x 10 <sup>-4</sup>
	7.0	115	2.65 x 10 <sup>-4</sup>
	7.0	118	1.13 x 10 <sup>-3</sup>
	7.0	120	1.30 x 10 <sup>-3</sup>
(η <sup>5</sup> -C <sub>5</sub> H <sub>5</sub> )Mn(CO) <sub>2</sub>	[Et <sub>2</sub> MeSiH] <sup>c</sup>		
	4.1	115	2.54 x 10 <sup>-4</sup>
	4.1	120	1.05 x 10 <sup>-3</sup>
	4.1	122	2.08 x 10 <sup>-3</sup>
	4.1	125	3.37 x 10 <sup>-3</sup>
(η <sup>5</sup> -C <sub>5</sub> Me <sub>5</sub> )Mn(CO) <sub>2</sub>	[EtMe <sub>2</sub> SiH] <sup>c</sup>		
	4.8	100	1.85 x 10 <sup>-4</sup>
	4.8	105	3.66 x 10 <sup>-4</sup>
	4.8	110	7.10 x 10 <sup>-4</sup>
	4.8	115	1.22 x 10 <sup>-3</sup>
	[Et <sub>2</sub> MeSiH] <sup>c</sup>		
	4.1	100	8.08 x 10 <sup>-5</sup>
	4.1	104	1.35 x 10 <sup>-4</sup>
	4.1	108	3.28 x 10 <sup>-4</sup>

a. Trialkylsilane concentrations corrected for solvent contraction @ 77 K.

b. Neat trialkylsilane.

c. MCH/silane mixture (50/50 v/v @ room temperature).

The calculated rate constants for reaction of trialkylsilanes with the  $(\eta^5\text{-C}_5\text{R}_5)\text{Mn}(\text{CO})_2$  complexes are summarized in Table 2-2.

### 2.3 Discussion

The photochemical loss of CO from  $(\eta^5\text{-C}_5\text{R}_5)\text{Mn}(\text{CO})_3$  to give coordinatively unsaturated species (eq 2-5) in low temperature trialkylsilane and hydrocarbon/trialkylsilane glasses is consistent with previous work.<sup>51</sup> Unfortunately, the Mn-H stretch could not be observed in the IR. However, the formation of a two band pattern in the IR (at higher frequency, relative to the unsaturated 16e species) concurrent with the disappearance of the two bands due to the intermediate was consistent with the oxidative addition of the trialkylsilane. Concurrent with the appearance of the two carbonyl bands of the product was the observation of a resonance in the  $^1\text{H}$  NMR in the -14.0 - -12.0 ppm region (Table 2-6) consistent with the formation of a metal hydride.

IR absorption spectra of all the  $\text{R}'_3\text{SiH}$  oxidative addition products possess two, approximately equal intensity, CO absorption bands indicative of  $\approx 90^\circ$  OC-Mn-CO angles.<sup>52</sup> Therefore, in agreement with earlier studies, each  $(\eta^5\text{-C}_5\text{R}_5)\text{MnH}(\text{SiR}'_3)(\text{CO})_2$  complex is formulated as the *cis* isomer. This is consistent with the crystallographically determined structure of  $(\eta^5\text{-C}_5\text{H}_4\text{Me})\text{MnH}(\text{SiMePhNp})(\text{CO})_2$  ( $\text{Np} = 1\text{-C}_{10}\text{H}_7$ ) which has a  $91.4^\circ$  OC-Mn-CO angle, and  $(\eta^5\text{-C}_5\text{H}_5)\text{MnH}(\text{SiPh}_3)(\text{CO})_2$  with a  $88.7^\circ$  OC-Mn-CO angle (in the solid state) both prepared by photolysis of the appropriate tricarbonyl in the presence of trialkylsilane.<sup>53</sup> It should be noted that the oxidative addition of an Si-H bond to a transition metal center does not always result in complete Si-H bond

breakage. The incomplete oxidative addition of an Si-H bond may be viewed as a two electron three center (M, Si, H) bond. A two electron three center (Mn, Si, H) interaction has been observed, by neutron diffraction, in the complex  $(\eta^5\text{-C}_5\text{H}_4\text{Me})\text{MnH}(\text{SiFPh}_2)(\text{CO})\text{P}_2$ .<sup>54</sup> Recent X-ray and neutron diffraction results, and studies of  $^{29}\text{Si}$  NMR to obtain the coupling constants  $J(\text{SiMH})$ , show that the extent to which the oxidative addition is complete is greater when there are electron-releasing ligands on M and/or highly electron withdrawing substituents (R') on Si.<sup>53</sup> Based on the NMR data, of the systems reported here, the oxidative addition of the Si-H bond to the metal center should be considered more or less complete.

### 2.3.1 The order of the reaction

The trialkylsilane concentration, for experiments conducted in a neat trialkylsilane glass, was not incorporated into the rate equation. The rate of a bimolecular reaction can be thought of as being dependent on two main factors; 1) the frequency of collision between reacting molecules, and 2) the collision energy (and geometry of the two species) being appropriate to surmount the activation barrier. Generally, for the case of gas phase reactions, the incorporation of reactant concentration is crucial. In gas phase reactions (assuming relatively low concentrations and pressure) there are a limited number of reactants and a great deal of empty space. Therefore, including the concentration of the reactive species is important in determining the rate of the reaction. Analogously, in solution, concentrations are important as a result of diffusional processes. However, in a neat trialkylsilane

glass, it is clear that each  $(\eta^5\text{-C}_5\text{R}_5)\text{Mn}(\text{CO})_2$  species is entirely surrounded by trialkylsilane molecules. Therefore, the probability of each  $(\eta^5\text{-C}_5\text{R}_5)\text{Mn}(\text{CO})_2$  molecule being surrounded by a sphere of trialkylsilane molecules is unity. Hence, each collision that a  $(\eta^5\text{-C}_5\text{R}_5)\text{Mn}(\text{CO})_2$  molecule undergoes is with a trialkylsilane molecule. For this reason, the trialkylsilane concentration in a neat trialkylsilane glass may be neglected.

For kinetic experiments done in a 50/50 mixture of trialkylsilane/methylcyclohexane one can not simply neglect the trialkylsilane concentration. The probability of a  $(\eta^5\text{-C}_5\text{R}_5)\text{Mn}(\text{CO})_2$  species colliding with a trialkylsilane molecule, in a solvent mixture, can not be assumed to be unity. In a neat trialkylsilane glass there is no doubt that the probability of the unsaturated species colliding with a trialkylsilane molecule is one. However, in a glass containing a mixture of two solvents the reduced probability of a  $(\eta^5\text{-C}_5\text{R}_5)\text{Mn}(\text{CO})_2$  species colliding with a trialkylsilane molecule must be taken into consideration. In a neat trialkylsilane glass the number of collisions between a  $(\eta^5\text{-C}_5\text{R}_5)\text{Mn}(\text{CO})_2$  molecule and a trialkylsilane molecule may be expressed by the general relationship given in equation 2-10. In equation 2-10,  $f(c)$  is the frequency of collision and  $P(\text{HSiR}'_3)$  is the probability of colliding with a trialkylsilane molecule.

$$\text{number of collisions} \propto f(c) \times P(\text{HSiR}'_3) \quad 2-10$$

The rate of the reaction may then be expressed by equation 2-11. However, a very different situation arises in a dilute trialkylsilane

glass. In a 50/50 silane/MCH mixture it may be possible that during the

$$k = f(c) \times P(\text{HSiR}'_3) e^{-E_a/RT} \quad 2-11$$

process of forming a glass, MCH preferentially forms a coordination sphere around the  $(\eta^5\text{-C}_5\text{R}_5)\text{Mn}(\text{CO})_3$  molecules. However, this possibility does seem remote. The other extreme, which seems just as unlikely, is that in a 50/50 mixture the trialkylsilane preferentially forms a sphere around the tricarbonyl complex. The only workable assumption, and the one that was made, was that the  $(\eta^5\text{-C}_5\text{R}_5)\text{Mn}(\text{CO})_3$  molecules have a statistical ratio of trialkylsilane and MCH surrounding them. The relationship given in equation 2-10 would still apply but clearly the probability of colliding with a trialkylsilane molecule changes. The probability of  $(\eta^5\text{-C}_5\text{R}_5)\text{Mn}(\text{CO})_2$  colliding with a trialkylsilane molecule would now be dependent on the concentration of trialkylsilane molecules surrounding the fragment (eq. 2-12). Therefore, the rate of reaction in a dilute glass may be expressed by combining equation 2-11 and 2-12 to yield equation 2-13. Subsequently, the rate constants obtained in a

$$P(\text{HSiR}'_3)_{\text{dilute}} \propto \frac{[\text{HSiR}'_3]_{\text{dilute}}}{[\text{HSiR}'_3]_{\text{dilute}} + [\text{MCH}]_{\text{dilute}}} \quad 2-12$$

$$k = f(c) \times \frac{[\text{HSiR}'_3]_{\text{dilute}}}{[\text{HSiR}'_3]_{\text{dilute}} + [\text{MCH}]_{\text{dilute}}} e^{-E_a/RT} \quad 2-13$$

Table 2-3

Arrhenius Activation Parameters for the Reaction of 16e ( $\eta^5\text{-C}_5\text{R}_5$ )M(CO)<sub>2</sub> with R'<sub>3</sub>SiH

COMPLEX	SOLVENT	SILANE	E <sub>a</sub> (kJ/mol)	A (s <sup>-1</sup> )
( $\eta^4\text{-C}_4\text{H}_4$ )Fe(CO) <sub>3</sub>	neat	Et <sub>3</sub> SiH <sup>a</sup>	38 ± 3	(1.86 ± 0.186) × 10 <sup>13</sup>
( $\eta^5\text{-C}_5\text{Me}_5$ )Mn(CO) <sub>3</sub>	neat	Et <sub>3</sub> SiH <sup>a</sup>	36 ± 2	(2.08 ± 0.116) × 10 <sup>16</sup>
( $\eta^5\text{-C}_5\text{H}_5$ )Mn(CO) <sub>3</sub>	neat	Et <sub>3</sub> SiH <sup>a</sup>	35 ± 2	(4.96 ± 0.176) × 10 <sup>13</sup>
( $\eta^5\text{-C}_5\text{Cl}_5$ )Mn(CO) <sub>3</sub>	neat	Et <sub>3</sub> SiH <sup>b</sup>	41 ± 4	(1.36 ± 0.169) × 10 <sup>7</sup>
( $\eta^5\text{-CH}_3\text{C}_5\text{H}_4$ )Mn(CO) <sub>3</sub>	neat	Et <sub>3</sub> SiH	29 ± 2	(4.14 ± 3.85) × 10 <sup>9</sup>
( $\eta^5\text{-CH}_3\text{C}_5\text{H}_4$ )Mn(CO) <sub>3</sub>	neat	EtMe <sub>2</sub> SiH	23 ± 2	(1.89 ± 0.183) × 10 <sup>7</sup>
	dil.	EtMe <sub>2</sub> SiH	31 ± 3	(5.36 ± 0.397) × 10 <sup>10</sup>
( $\eta^5\text{-C}_5\text{Me}_5$ )Mn(CO) <sub>3</sub>	dil.	EtMe <sub>2</sub> SiH	12 ± 1	(3.94 ± 0.121) × 10 <sup>1</sup>
( $\eta^5\text{-CH}_3\text{C}_5\text{H}_4$ )Mn(CO) <sub>3</sub>	neat	Et <sub>2</sub> SiH <sub>2</sub>	2 ± 1	(4.65 ± 4.30) × 10 <sup>-5</sup>
	dil.	Et <sub>2</sub> SiH <sub>2</sub>	23 ± 3	(8.36 ± 0.132) × 10 <sup>6</sup>
( $\eta^5\text{-C}_5\text{H}_5$ )Mn(CO) <sub>3</sub>	dil.	Et <sub>2</sub> MeSiH	32 ± 3	(6.94 ± 0.612) × 10 <sup>10</sup>
( $\eta^5\text{-CH}_3\text{C}_5\text{H}_4$ )Mn(CO) <sub>3</sub>	neat	Et <sub>2</sub> MeSiH	26 ± 2	(1.05 ± 0.110) × 10 <sup>9</sup>
	dil.	Et <sub>2</sub> MeSiH	35 ± 2	(1.83 ± 0.115) × 10 <sup>12</sup>
( $\eta^5\text{-C}_5\text{Me}_5$ )Mn(CO) <sub>3</sub>	dil.	Et <sub>2</sub> MeSiH	16 ± 3	(1.14 ± 0.397) × 10 <sup>4</sup>

a : from reference 51 a) & 51 b).

b : from reference 51 c) after correcting for solvent contraction.

dil. : diluted sample, 50/50 mixture (by volume) with methylcyclohexane.

neat : pure trialkylsilane.



trialkylsilane/MCH mixture were multiplied by the concentration ratio  $\{[\text{HSiR}'_3]_{\text{dilute}}/([\text{HSiR}'_3]_{\text{dilute}} + [\text{MCH}]_{\text{dilute}})\}$  to correct for dilution. The concentration ratios given in equations 2-12 and 2-13 represent the concentrations of the contracted media. The rate constants (quoted in Table 2-2) obtained in neat trialkylsilane omit the trialkylsilane concentration and those obtained in dilute trialkylsilane have been corrected as summarized above.

### 2.3.2 Analysis of the reaction energetics according to Arrhenius law and Eyring theory

For each  $(\eta^5\text{-C}_5\text{R}_5)\text{Mn}(\text{CO})_3/\text{R}'_3\text{SiH}$  system summarized in Table 2-2, the activation energy was determined using Arrhenius law. The Arrhenius activation energies summarized in Table 2-3, for the systems that we studied, varied from 2 kJ/mol to 38 kJ/mol. Such a variation in the activation energies of these systems did not seem chemically reasonable. The effect of solvent on the energetics of these reactions also appeared unreasonable. For example, the activation energy for reaction of  $(\eta^5\text{-CH}_3\text{C}_5\text{H}_4)\text{Mn}(\text{CO})_2$  with  $\text{Et}_2\text{SiH}_2$  increased from 2 kJ/mol to 23 kJ/mol upon changing the media from neat trialkylsilane to a trialkylsilane/MCH mixture. It seemed intuitive that the unsaturated organometallic fragments would oxidatively add an Si-H bond with approximately the same energy. Since the wide variation in  $E_a$  values did not seem reasonable to us we chose to look at alternative theories to interpret the kinetic data. A preliminary analysis of the kinetic data using Eyring theory gave essentially the same energies of activation as the Arrhenius equation did. Additionally, interpretation of the kinetic data using

Eyring theory showed a very good linear relationship between the enthalpy of activation and the entropy of activation. Such a correlation is indicative of an isokinetic relationship (IKR), but an IKR does not explain what governs the reaction rates. As a result of our kinetic data being consistent with an isokinetic relationship we were led to a theory developed by Linert. Linert's theory was derived in an attempt to put the isokinetic relationship on firmer theoretical ground. However, our interest in Linert's theory was not to obtain an isokinetic temperature but to try to understand what caused the variation in the observed reaction rates.

### **2.3.3 The form of Linert's equation that was used**

It would be useful to know, specifically, what the dominant effect is on reaction rates for a given series of analogous reactions. In a series of papers, Linert has developed a 'master equation' in an effort to interpret reaction rates.<sup>22,44-50</sup> Linert has shown that the variation in reaction rates for an analogous set of reactions may be interpreted in terms of the ability of the reactant molecules' to couple with the reaction medium, treated as a heat bath, and thereby exchange energy. The energy exchange between reactant molecules and a reactant medium treated as a heat bath is shown schematically in Figure 2-4. Schematically, the heat-bath system represents the vibronic transitions of the solvent molecules in the glassy state. The reactant system represents the vibrational transitions of the reactant molecule. It is the reactant systems ability to couple and exchange energy with specific heat-bath transitions which gives rise to the non-Boltzmann distributed

population of the vibrational levels in the reactant system. We were interested in determining whether the kinetic data we obtained were interpretable in terms of energy exchange between the reactant molecules and the heat bath. Using Linert's theory we set out to determine what parameter governed the kinetics of the reactions. The equation which Linert developed is given in equation 2-14. Linert's equation is based on the assumption that during a reaction a non-equilibrium steady state distribution of reactant species is present. This nature of the steady state distribution is controlled by energy transfer from the heat bath to the reactant system. While Linert's assumption is approximate, it does remove Eyring's assumption of an equilibrium distribution. The terms  $A_0$ ,  $s_N h \omega$ , and  $\nu$  represent constants involving the collision number, the energy barrier height, and the vibrational heat bath frequency, respectively. The actual form of the equation used will be

$$k = A_0 s_N (h \omega x_{\text{bath}})^2 \exp[s_N (\omega/\nu - h \omega x_{\text{bath}})] \quad 2-14$$

where;

$A_0$  = constant

$s_N$  = is the number of reactant levels with energy lower than the reaction barrier

$h$  = Planck's constant

$\omega$  = is the vibrational frequency of the reaction site of the reactant

$x_{\text{bath}}$  = defined as  $1/kT$

$\nu$  = the active frequency of the heat-bath system in resonance with the reactant vibrations

discussed here. However, the derivation of the equation we used is summarized in the appendix. In order to interpret the kinetic results

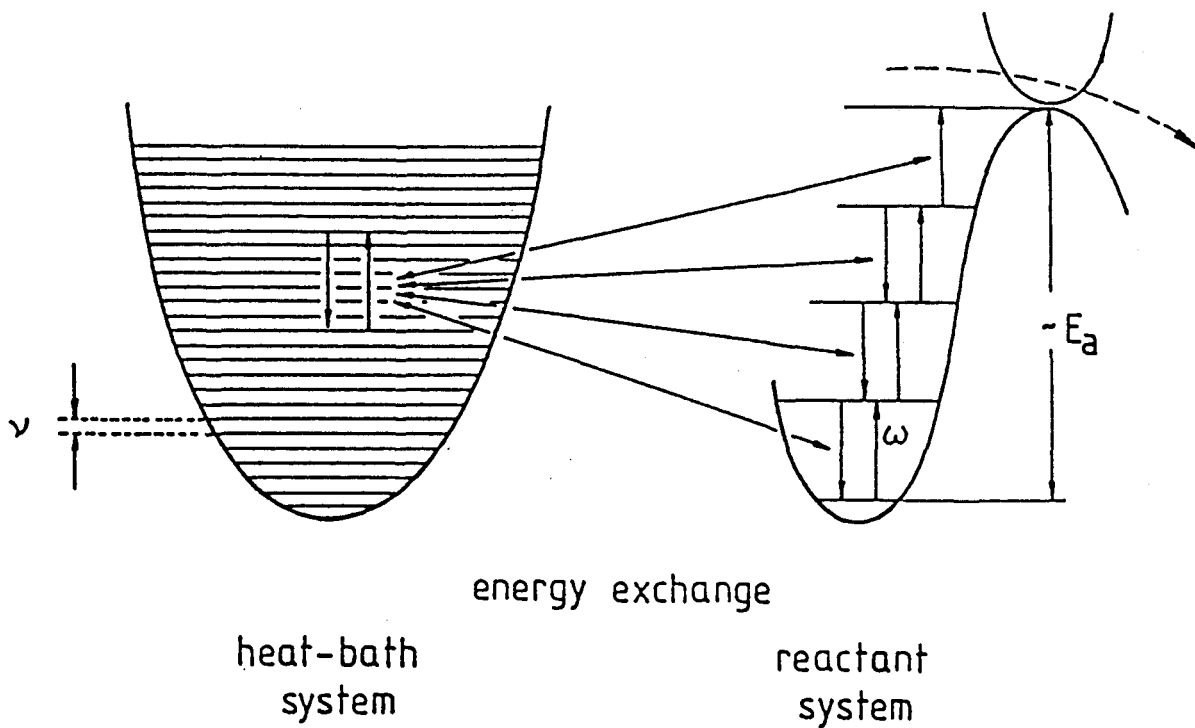


Figure 2-4

Schematic diagram of the energy exchange between reactant molecules and a reactant medium treated as a heat bath.

that are fit to an equation one must identify the parameters that are varying within the reaction series. Linert's equation gives two parameters characterizing the reactants; 1) the number of energy levels of the reactant system with an energy less than the activation energy ( $s_N$ ), and 2) the vibrational frequency of the reaction site of the reactant ( $\omega$ ). However, it was not clear which parameter ( $s_N$  or  $\omega$ ) would influence the rates of reaction to a greater extent. Therefore,  $\omega$  was held constant for all the data, while  $s_N$  was assumed to have a unique value for each set of metal complex, trialkylsilane, and solvent yielding equation 2-15. Equation 2-16 was arrived at by assuming  $\omega$  changes for each set of metal complex, trialkylsilane and solvent while  $s_N$  was a constant for all the data. The vibrational heat bath frequency,  $\nu$ , was treated as a constant in equations 2-15 and 2-16 because the vibronic modes of the trialkylsilanes are similar. As mentioned earlier, the details of the derivation of equations 2-15 and 2-16 are given in the appendix. Each of these equations allow for the determination of a single parameter,  $E_a$ , which corresponds to the energy of the reaction barrier. Both  $A$  and  $\nu$  are constants independent of complex, trialkylsilane and solvent.

$$\ln k = \ln(A \times E_a / (RT)^2) + E_a/\nu - E_a/RT \quad 2-15$$

where;

$$A = A_0 h \omega N_A$$

$$E_a = s_N h \omega N_A$$

$$\nu = h \nu N_A$$

$$\ln k = \ln(A \times (E_a/RT)^2) + E_a/v - E_a/RT \quad 2-16$$

where;      $A = A_0/s_N$   
                $E_a = s_N h \omega N_A$   
                $v = h \nu N_A$

Statistical analysis (discussed in section 2.3.4) showed that equations 2-15 and 2-16 fit the experimental data equally well. It should be noted that the kinetic data for all of the systems, summarized in Table 2-4, were fit to equations 2-15 and 2-16. This is in contrast to Arrhenius law or Eyring theory where  $E_a$  values are determined independently.  $E_a$  values calculated from Linert's theory are summarized in Table 2-4.

#### 2.3.4 Statistical analysis

The kinetic data were analyzed using a statistical package called SYSTAT.<sup>56</sup> A program within the SYSTAT package called NONLIN was used to fit the data. NONLIN is a non-linear least squares fit of an equation with two or more variables. NONLIN estimates parameters for a variety of nonlinear models. A 'model' is a statement of the equation being fit, where a variable is set equal to a function. The statistical analysis was conducted on two models; equation 2-15 and equation 2-16. The experimental data ( $k$ 's and  $T$ 's) were fit to equations 2-15 and 2-16 by minimizing the sum of least squares. There are two minimization algorithms available for NONLIN to use: Quasi-Newton<sup>57</sup> and Simplex<sup>58,59</sup>. The quasi-Newton method uses numeric estimates of the first and second derivatives of the error function to search for a minimum, whereas the

Simplex algorithm is a direct search procedure. Simplex calculates the error, for a set of parameters, and checks if the error is reduced for a different set of parameters. Simplex is usually slower than the quasi-Newton method because it cannot use information from the second derivative of the error function to choose a step size. Both methods, and various starting values, were used in the statistical analysis to avoid converging at a false minimum. A tolerance criterion, within the program, was used to determine convergence. A tolerance value of 0.0001 was used for all calculations. A tolerance value of 0.0001 represents one ten-thousandths of the absolute magnitude of each parameter. With this value, iterations would normally end when the displayed values of the parameter estimates were less than or equal to the tolerance value.

Linert's equation (Eq. 2-14) was obtained under the condition of large barriers for a non-equilibrium distribution of reactant molecules among discrete energy levels, coupled to the surrounding heat bath. Therefore, Linert's equation only applies to systems whose energy of activation is much larger than ' $kT$ '. The  $(\eta^5\text{-CH}_3\text{C}_5\text{H}_4)\text{Mn}(\text{CO})_3/\text{Et}_2\text{SiH}_2$  system was not included in the final statistical analysis since its  $E_a$  value (2 kJ/mol), determined by a preliminary fit to Arrhenius law, was not significantly larger than ' $kT$ ' (1.1 kJ/mol). Four analogous systems have been reported in the literature;  $(\eta^4\text{-C}_4\text{H}_4)\text{Fe}(\text{CO})_3/\text{Et}_3\text{SiH}^{51a)}$ ,  $(\eta^5\text{-C}_5\text{Me}_5)\text{Mn}(\text{CO})_3/\text{Et}_3\text{SiH}^{51a)}$ ,  $(\eta^5\text{-C}_5\text{H}_5)\text{Mn}(\text{CO})_3/\text{Et}_3\text{SiH}^{51a)}$ , and  $(\eta^5\text{-C}_5\text{Cl}_5)\text{Mn}(\text{CO})_3/\text{Et}_3\text{SiH}^{51c)}$ . It should be noted that the  $(\eta^5\text{-C}_5\text{Cl}_5)\text{Mn}(\text{CO})_3/\text{Et}_3\text{SiH}$  system was not included in the final statistical analysis with the other systems. Initially, the system was included but its inclusion resulted in an unrealistically high value of

the active heat-bath frequency ( $\nu \approx 38000 \text{ cm}^{-1}$ ). However, when the data for the  $(\eta^5\text{-C}_5\text{Cl}_5)\text{Mn}(\text{CO})_3/\text{Et}_3\text{SiH}$  system was dropped from the statistical analysis a far more reasonable heat-bath frequency was found. Fitting the kinetic data to equations 2-15 and 2-16 gave a heat-bath frequency of  $174 \text{ cm}^{-1}$  and  $507 \text{ cm}^{-1}$ , respectively.

It is important to point out that fitting equations 2-15 and 2-16 to just the kinetic data for the  $(\eta^5\text{-C}_5\text{Cl}_5)\text{Mn}(\text{CO})_3/\text{Et}_3\text{SiH}$  system revealed a heat-bath frequency which was in accord with the analysis of the other kinetic data mentioned above. For example, fitting eq. 2-15 to the data for the  $(\eta^5\text{-C}_5\text{Cl}_5)\text{Mn}(\text{CO})_3/\text{Et}_3\text{SiH}$  system gave a  $\nu$  value of  $292 \text{ cm}^{-1}$  and a fit to eq. 2-16 gave a  $\nu$  value of  $374 \text{ cm}^{-1}$ .

Calculated parameters, from a statistical fit of the data to equations 2-15 and 2-16 are summarized in Table 2-4. A plot of experimental  $\ln k$  values versus estimated  $\ln k$  values (from Linert's theory) is given in Figure 2-5. Figure 2-5 is the result of fitting the kinetic data to eq. 2-16, however, the correlation coefficient for a fit to both equations is essentially the same. The correlation coefficients when the experimental data were fit to equations 2-15 and 2-16 were 0.994 and 0.995 respectively. The results for the fit to equations 2-15 and 2-16 are discussed below.

### **2.3.5 Interpretation of the reaction energetics within the framework of Linert's theory**

It is quite likely that the unsaturated complex is coordinated, by a solvent molecule, to some extent. In neat trialkylsilane, the solvent (trialkylsilane) may coordinate through a C-H bond. However, in dilute



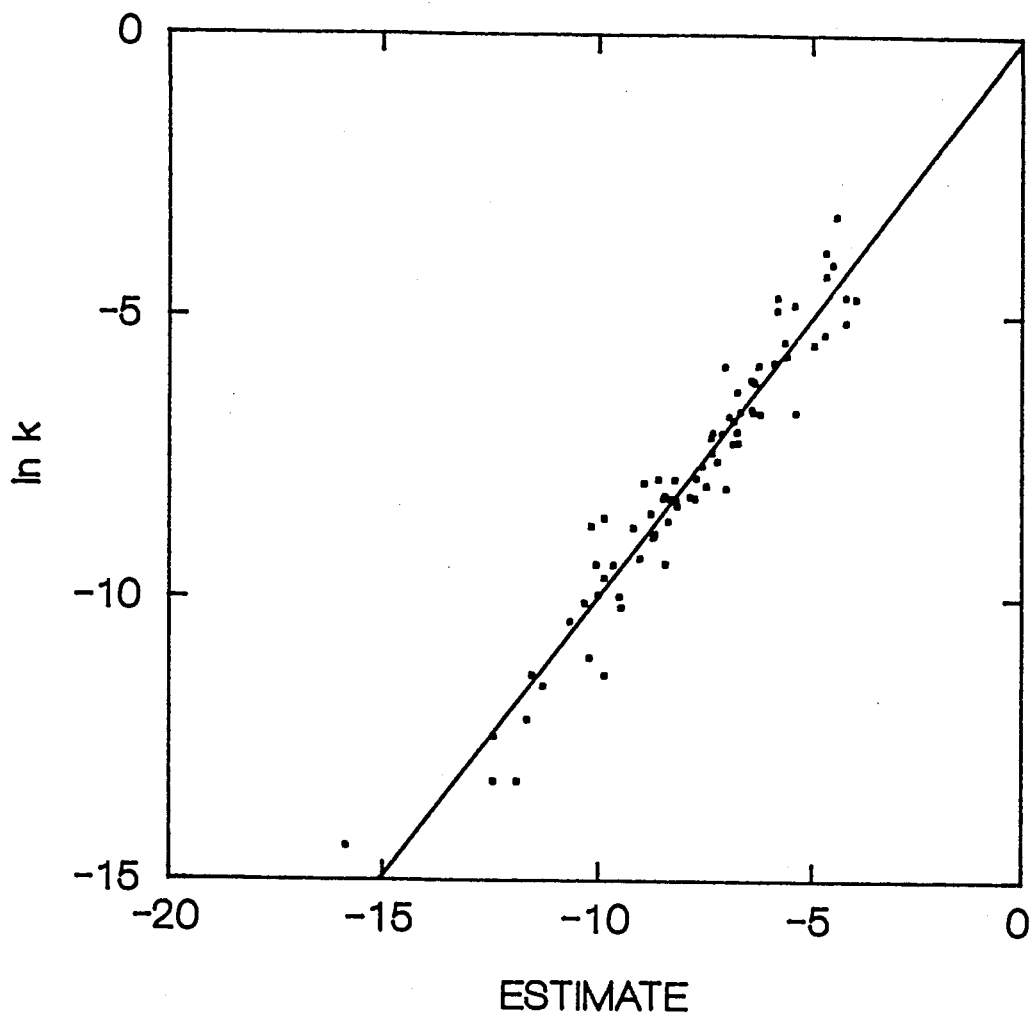


Figure 2-5

A plot of experimental  $\ln k$  values versus estimated  $\ln k$  values (from Linert's theory) for the kinetic data fit to equation 2-16. The coefficient of correlation is 0.995.

Table 2-4

Linert's Activation Parameters determined by statistical analysis

METAL	SOLVENT	SILANE	$E_a^a$ (kJ/mol) ( $\pm 3$ )	$E_a^b$ (kJ/mol) ( $\pm 3$ )
$(\eta^4-C_4H_4)Fe(CO)_3$	neat	$Et_3SiH$	36 <sup>c</sup>	38
$(\eta^5-C_5Me_5)Mn(CO)_3$	neat	$Et_3SiH$	28 <sup>c</sup>	27
$(\eta^5-C_5H_5)Mn(CO)_3$	neat	$Et_3SiH$	32 <sup>c</sup>	31
$(\eta^5-CH_3C_5H_4)Mn(CO)_3$	neat	$Et_3SiH$	34	35
$(\eta^5-CH_3C_5H_4)Mn(CO)_3$	neat	$EtMe_2SiH$	33	33
	dil.	$EtMe_2SiH$	34	34
$(\eta^5-C_5Me_5)Mn(CO)_3$	dil.	$EtMe_2SiH$	31	30
$(\eta^5-CH_3C_5H_4)Mn(CO)_3$	dil.	$Et_2SiH_2$	34 <sup>d</sup>	35
$(\eta^5-C_5H_5)Mn(CO)_3$	dil.	$Et_2MeSiH$	35	36
$(\eta^5-CH_3C_5H_4)Mn(CO)_3$	neat	$Et_2MeSiH$	33	33
	dil.	$Et_2MeSiH$	35	36
$(\eta^5-C_5Me_5)Mn(CO)_3$	dil.	$Et_2MeSiH$	31	31
Calculated value of A ( $\times 10^6$ ) ( $s^{-1}$ )			4.00	3.90
Calculated value of $\nu$ (J/mol)			6067	2080
Calculated value of $\nu$ determined from $\nu$ ( $cm^{-1}$ )			507	174
Coefficient of Correlation ( $R^2$ )			0.995	0.994
Corrected Coefficient of Correlation <sup>e</sup> ( $R^2$ )			0.936	0.926

a: values calculated from Eq. 2-16 using the Quasi-Newton algorithm.

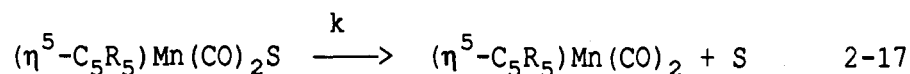
b: values calculated from Eq. 2-15 using the Simplex algorithm.

c: values from reference 51 a)

d: The  $E_a$  value determined for  $(\eta^5-CH_3C_5H_4)Mn(CO)_3$  in neat  $Et_2SiH_2$  was approximately the same magnitude as ' $kT$ ' and therefore could not be included in the statistical analysis (see refs. 44-50).

e: Coefficient of Correlation corrected for the number of parameters used.

trialkylsilane the coordinating species could be MCH or the trialkylsilane. Therefore, it is possible that the measured rate constant actually represents the rate of dissociation of the coordinating solvent, S (eq. 2-17). After solvent dissociation, the oxidative addition of the trialkylsilane would occur very fast.



This hypothesis is consistent with the statistical analysis. The computed  $E_a$  values changed very little (Table 2-4). The calculated  $E_a$  values fell in the range  $32 \pm 5$  kJ/mol. This is not surprising since the various unsaturated fragments should coordinate a solvent molecule with approximately the same energy. The unsaturated fragments should also have approximately the same barrier for oxidative addition. If solvent dissociation is the rate-limiting step, it is not surprising that the  $(\eta^5\text{-C}_5\text{Cl}_5)\text{Mn}(\text{CO})_3/\text{Et}_3\text{SiH}$  system could not be included in the full statistical analysis. The  $(\eta^5\text{-C}_5\text{Cl}_5)\text{Mn}(\text{CO})_2$  fragments ability to coordinate a solvent molecule should be much greater as a result of the electron withdrawing nature of the  $(\eta^5\text{-C}_5\text{Cl}_5)$  ligand. The  $(\eta^5\text{-C}_5\text{Cl}_5)$  ligand should also affect the oxidative addition step. The calculated  $E_a$  value of 45 kJ/mol for the  $(\eta^5\text{-C}_5\text{Cl}_5)\text{Mn}(\text{CO})_3/\text{Et}_3\text{SiH}$  system is consistent with the  $(\eta^5\text{-C}_5\text{Cl}_5)\text{Mn}(\text{CO})_2$  fragments enhanced ability to coordinate a solvent molecule strongly.

As mentioned earlier equations 2-15 and 2-16 were found to fit the experimental data equally well. In equation 2-15,  $s_N$  was a variable and  $\omega$  was treated as a constant, whereas, in equation 2-16  $s_N$  was a

constant and  $\omega$  was a variable. In a condensed phase such as a glass, or matrix, the number of reactant levels ( $s_N$ ) and the vibrational frequencies of the reaction site ( $\omega$ ) of the reactant should be extremely large. It is likely that  $s_N$  and  $\omega$  would approach a continuum for media in the glassy state. Therefore, it seemed reasonable that we were unable to determine which parameter ( $s_N$  or  $\omega$ ) dominated the energy exchange between the heat-bath and the reactant system. However, it was clear that the ability of the reactants to couple and exchange energy with the heat-bath system gave rise to the variation in the experimentally determined rates of reaction. It is also interesting to note that the calculated heat-bath frequencies,  $\nu$ , of 507 and 174  $\text{cm}^{-1}$  are in the range expected for low energy librational modes of the condensed media.

The variation in the experimentally determined rates of reaction most likely reflect a combination of different modes of solvent coordination and cage effects. Conversely, in a gas phase reaction, it is not obvious why there should be a measurable difference in the energy barrier for the oxidative addition of analogous  $\text{R}'_3\text{SiH}$  species to  $(\eta^5\text{-C}_5\text{R}_5)\text{Mn}(\text{CO})_2$  ( $\text{R}_5 = \text{H}_5, \text{Me}_5, \text{H}_4\text{Me}$ ) fragments.

In summary, fitting the experimental data to Linert's theory showed that the reactant systems ability to couple and exchange energy with the heat-bath system dominated the observed variation in the experimentally determined  $E_a$ 's. Chemically, a very small difference in  $E_a$  values for the oxidative addition of trialkylsilanes to  $(\eta^5\text{-C}_5\text{R}_5)\text{Mn}(\text{CO})_2$  fragments makes sense.

## 2.4 Conclusions

In this study the energetics of a series of analogous reactions has been interpreted using Linert's theory. Using this theory we were able to explain the wide variation in the observed reaction rates in a way that, chemically, made more sense than the energies of activation determined using the Arrhenius law. The large variation in reaction rates was consistent with the differing degree with which the reactant molecules were able to couple and exchange energy with the heat-bath. Whereas, using the Arrhenius law, the variation in reaction rates was reflected in a wide range of activation energies. However, such a wide range of activation energies does not seem reasonable for these systems.

## 2.5 Experimental Section

### 2.5.1 Instruments

Infrared spectral data were recorded by using a Bruker IFS 85 Fourier transform infrared spectrometer operating at  $1\text{ cm}^{-1}$  resolution.  $^1\text{H}$  NMR spectra were run on room temperature solutions using a Bruker SY100 NMR spectrometer. Chemical shifts are referenced to TMS. Irradiations were carried out by using the  $\text{H}_2\text{O}$ -filtered output (10 cm path length/pyrex optics) from an Osram 100-W high-pressure Hg lamp.

Low temperature spectra were possible by means of a CTI - Cryogenics Model 22 cryocooler and a 350R compressor system equipped with a Lake Shore Cryotronics DRC 80C temperature controller. The temperature of the cell was monitored with a Lake Shore Cryotronics silicon diode sensor (DT500 DRC). The IR cell was constructed of high conductivity copper and contained  $\text{CaF}_2$  windows. The sample path length

was 0.127mm.

The trialkylsilane concentrations were corrected for temperature contraction. As a result of the experiments being conducted in the temperature range 70 K - 130 K, the volume of solvent was reduced considerably. In an effort to correct for the volume change, the percent contraction was measured at 77 K. Both the neat trialkylsilane and the trialkylsilane/MCH mixtures were measured for contraction. Neat trialkylsilane was placed in an NMR tube and the height of the meniscus was measured. The NMR tube was then placed in a liquid nitrogen bath and allowed to equilibrate. Once the sample had equilibrated, at 77 K, the height of the meniscus was measured again and the percent contraction calculated. The percent contraction of the trialkylsilane/MCH equal volume mixtures were measured in the same manner. Even though this method is not the most accurate method of measuring the solvent contraction, it is better than neglecting the volume contraction entirely. The estimated error in the percent contraction is 10%. The percent contraction for each solvent is summarized in Table 2-5.

### 2.5.2 Chemicals

The trialkylsilanes used,  $\text{Et}_3\text{SiH}$ ,  $\text{Et}_2\text{MeSiH}$ ,  $\text{EtMe}_2\text{SiH}$  and  $\text{Et}_2\text{SiH}_2$  were obtained from Petrarch Systems Inc. and used without further purification. The  $(\eta^5\text{-CH}_3\text{C}_5\text{H}_4)\text{Mn}(\text{CO})_3$  was obtained from Alfa Products and used without further purification. The  $(\eta^5\text{-C}_5\text{H}_5)\text{Mn}(\text{CO})_3$  and  $(\eta^5\text{-C}_5\text{Me}_5)\text{Mn}(\text{CO})_3$  were purchased from Strem Chemicals and were recrystallized prior to their use.

Table 2-5

Percent contraction of solvents at 77 K

<u>Solvent</u>	<u>% contraction<sup>a</sup></u>
Et <sub>3</sub> SiH	10
EtMe <sub>2</sub> SiH	45
Et <sub>2</sub> SiH <sub>2</sub>	50
Et <sub>2</sub> MeSiH	20
Et <sub>3</sub> SiH/MCH	14
EtMe <sub>2</sub> SiH/MCH	20
Et <sub>2</sub> SiH <sub>2</sub> /MCH	24
Et <sub>2</sub> MeSiH/MCH	18

a) error in percent contraction is estimated to be 10%.

Table 2-6

<sup>1</sup>H NMR OF RELEVANT COMPOUNDS

COMPOUND	δ (Mn-H <sup>a</sup> )
(η <sup>5</sup> -CH <sub>3</sub> C <sub>5</sub> H <sub>4</sub> )MnH(SiEt <sub>3</sub> )(CO) <sub>2</sub>	-13.50
(η <sup>5</sup> -CH <sub>3</sub> C <sub>5</sub> H <sub>4</sub> )MnH(SiMeEt <sub>2</sub> )(CO) <sub>2</sub>	-13.27
(η <sup>5</sup> -CH <sub>3</sub> C <sub>5</sub> H <sub>4</sub> )MnH(SiMe <sub>2</sub> Et)(CO) <sub>2</sub>	-13.09
(η <sup>5</sup> -CH <sub>3</sub> C <sub>5</sub> H <sub>4</sub> )MnH(SiEt <sub>2</sub> H)(CO) <sub>2</sub>	-12.63
(η <sup>5</sup> -C <sub>5</sub> H <sub>5</sub> )MnH(SiMeEt <sub>2</sub> )(CO) <sub>2</sub>	-13.50
(η <sup>5</sup> -C <sub>5</sub> Me <sub>5</sub> )MnH(SiMeEt <sub>2</sub> )(CO) <sub>2</sub>	-13.33
(η <sup>5</sup> -C <sub>5</sub> Me <sub>5</sub> )MnH(SiMe <sub>2</sub> Et)(CO) <sub>2</sub>	-13.01

a) Chemical shifts quoted, in ppm, relative to TMS.



### 2.5.3 Kinetic Measurements

All the kinetic measurements were conducted in a similar manner and a typical one will be described in detail. A 50/50 Et<sub>2</sub>SiH<sub>2</sub>-methylcyclohexane solution containing ( $\eta^5$ -CH<sub>3</sub>C<sub>5</sub>H<sub>4</sub>)Mn(CO)<sub>3</sub> was purged with N<sub>2</sub>, and placed in a copper cell. The sample was then loaded into the cold head of the cryocooler, cooled to the appropriate temperature, and allowed to equilibrate. The solutions of ( $\eta^5$ -C<sub>5</sub>R<sub>5</sub>)Mn(CO)<sub>3</sub> (where R<sub>5</sub>=H<sub>5</sub>, MeH<sub>4</sub>, Me<sub>5</sub>) were prepared so that the most intense absorption due to the CO ligands was between 0.2 and 1.0 ( $\approx 1 \times 10^{-4}$  M). Subsequently, the sample was removed from the IR bench and photolyzed, using the pyrex/water filtered output (bandpass  $\lambda > 313$  nm) of a high pressure Hg lamp, so that approximately 15% - 20% of the ( $\eta^5$ -CH<sub>3</sub>C<sub>5</sub>H<sub>4</sub>)Mn(CO)<sub>3</sub> had been consumed and ( $\eta^5$ -CH<sub>3</sub>C<sub>5</sub>H<sub>4</sub>)Mn(CO)<sub>2</sub> was detected by FTIR. After photolysis the IR spectrum typically showed a mixture of ( $\eta^5$ -CH<sub>3</sub>C<sub>5</sub>H<sub>4</sub>)Mn(CO)<sub>3</sub>, ( $\eta^5$ -CH<sub>3</sub>C<sub>5</sub>H<sub>4</sub>), and ( $\eta^5$ -CH<sub>3</sub>C<sub>5</sub>H<sub>4</sub>)MnH(SiR'<sub>3</sub>)(CO)<sub>2</sub>. It should be pointed out that the relative amounts of these species depended on temperature, photolysis time, and reactants. Generally, photolysis was conducted in 10 second intervals until the absorbance due to the intermediate was 0.1. After generating the 16e intermediate, FTIR spectra were then obtained as a function of time, in the dark, to monitor the disappearance of the ( $\eta^5$ -CH<sub>3</sub>C<sub>5</sub>H<sub>4</sub>)Mn(CO)<sub>2</sub> and the formation of the oxidative addition product, ( $\eta^5$ -CH<sub>3</sub>C<sub>5</sub>H<sub>4</sub>)MnH(SiEt<sub>2</sub>H)(CO)<sub>2</sub>. Care was taken to ensure that the IR beam of the spectrometer did not accelerate the "dark" reactions between the 16e species and the trialkylsilane. For some of the experiments, the sample was left in the IR beam continuously. Duplicate experiments were conducted where the

sample was placed in the IR beam only when spectra were collected. No beam-induced chemistry on the time scale of data acquisition was observed.

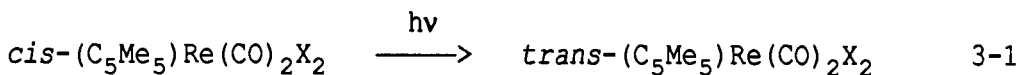
#### 2.5.4 N.M.R. Analysis

A NMR characterization of the starting materials and their photo-generated oxidative addition products was conducted using a Bruker SY100 spectrometer. The typical procedure was as follows: To a 5mm NMR tube containing approximately 0.5 mL of  $C_6D_6$  was added 0.025 mL of  $Et_2SiH_2$  and 0.003 mL of  $(\eta^5-CH_3C_5H_4)Mn(CO)_3$ . The NMR spectrum of the light yellow solution was obtained. The sample was then photolyzed for 1 min using the water filtered (10 cm path length, pyrex optics) output of a 100 W high pressure Hg lamp. Another NMR spectrum was obtained and the sample was then photolyzed for an additional 5 minutes whereupon a final NMR spectrum was obtained. Relevant chemical shifts are quoted in Table 2-6.

Chapter 3: Mechanistic study of the photochemically induced *cis-trans* isomerization of  $(\eta^5\text{-C}_5\text{Me}_5)\text{Re}(\text{CO})_2\text{X}_2$  (X = Me, Cl, Br, I).

3.1 Introduction

Preliminary work, conducted in our group, indicated that the room temperature photolysis of *cis*- $(\eta^5\text{-C}_5\text{Me}_5)\text{Re}(\text{CO})_2\text{Me}_2$  led to the production of *trans*- $(\eta^5\text{-C}_5\text{Me}_5)\text{Re}(\text{CO})_2\text{Me}_2$  and  $(\eta^5\text{-C}_5\text{Me}_5)\text{Re}(\text{CO})_3$ . At lower temperatures, the *cis-trans* isomerization was the only detectable reaction. This result prompted the study of the *cis-trans* isomerization, in more detail, for the following reason: In an earlier study<sup>35</sup> the compounds  $(\eta^5\text{-C}_5\text{Me}_5)\text{Re}(\text{CO})_2\text{X}_2$  (X = Cl, Br, I) were made and shown to undergo photochemical *cis-trans* isomerization as summarized in



equation 3-1. Also of interest was the fact that when *cis*- $(\eta^5\text{-C}_5\text{Me}_5)\text{Re}(\text{CO})_2\text{I}_2$  was photolyzed in a chlorinated solvent, the major product was *trans*- $(\eta^5\text{-C}_5\text{Me}_5)\text{Re}(\text{CO})_2\text{Cl}_2$ . This result indicated that the mechanism of isomerization involved photochemistry resulting in halogen loss. There is some literature precedent indicating that halogen loss may be responsible for the reactivity of transition-metal halides.<sup>2</sup> For example, the *trans*  $\rightarrow$  *cis* isomerization of  $\text{Pt}(\text{PEt}_3)_2\text{PhCl}$  has been reported to occur via photochemical chlorine radical loss.<sup>60</sup> Although halogen loss seemed reasonable for the rhenium dihalides, such a mechanism did not seem likely for the dimethyl complex where analogous chemistry would result in methyl radicals.

Reductive elimination has been inferred in the photoreactions of

several molecules containing *cis* one-electron ligands, such as  $(\eta^5\text{-C}_5\text{Me}_5)\text{IrPMe}_3\text{H}_2$ ,<sup>61</sup>  $(\eta^5\text{-C}_5\text{Me}_5)\text{IrPMe}_3\text{H(R)}$ ,<sup>61</sup>  $(\eta^5\text{-C}_4\text{H}_4)\text{Fe(CO)}_2\text{H(SiEt}_3)$ ,<sup>7</sup> and  $(\eta^5\text{-C}_5\text{H}_5)\text{Mn(CO)}_2\text{H(SiEt}_3)$ .<sup>62</sup> Interestingly, the last two compounds undergo reductive elimination of the *cis* groups as opposed to CO loss. There is also some evidence, in the literature, for the photochemical reductive elimination of methyl groups.<sup>63</sup> Other possible reactions of metal alkyl groups include radical cleavage<sup>64</sup> and alkyl group transfer to a ring carbon as shown in the photoreaction of  $(\eta^5\text{-C}_5\text{Me}_5)\text{Fe(CO)}_2\text{R}$  (R = Me, benzyl).<sup>8</sup> Notably, in the case of  $(\eta^5\text{-C}_5\text{Me}_5)\text{Fe(CO)}_2\text{R}$ , the photodissociation of the alkyl group occurred in competition with CO loss.

The studies on *cis*- $(\eta^5\text{-C}_5\text{Me}_5)\text{Re(CO)}_2\text{X}_2$  were conducted to determine the primary photoprocess responsible for the isomerization and to examine the origin of its uni-directional nature. We studied the dimethyl complex as well as the series of dihalides to determine if a common mechanism could account for the isomerization in these complexes or if they react via different pathways.

## 3.2 Results

### 3.2.1 Photochemistry of *cis*- $(\eta^5\text{-C}_5\text{Me}_5)\text{Re(CO)}_2\text{Me}_2$ in 4-methyl-1-cyclohexene

Photolysis of 4-methyl-1-cyclohexene solutions of *cis*- $(\eta^5\text{-C}_5\text{Me}_5)\text{Re(CO)}_2\text{Me}_2$  at room temperature led to the loss of FTIR absorptions due to the starting complex, at  $2011\text{ cm}^{-1}$  and  $1919\text{ cm}^{-1}$ , and the production of  $(\eta^5\text{-C}_5\text{Me}_5)\text{Re(CO)}_3$ . *Trans*- $(\eta^5\text{-C}_5\text{Me}_5)\text{Re(CO)}_2\text{Me}_2$  was

also formed giving rise to bands at  $1994\text{ cm}^{-1}$  and  $1919\text{ cm}^{-1}$ . Upon prolonged photolysis, bands due to a new dicarbonyl complex appear at  $1948\text{ cm}^{-1}$  and  $1876\text{ cm}^{-1}$ . The new dicarbonyl species was complexed to the olefin solvent and was formulated as  $(\eta^5\text{-C}_5\text{Me}_5)\text{Re}(\text{CO})_2(\eta^2\text{-4-methyl-1-cyclohexene})$  by comparison to an authentic sample.<sup>65</sup> This product, which only appeared after  $(\eta^5\text{-C}_5\text{Me}_5)\text{Re}(\text{CO})_3$  was produced, was probably a result of photolysis of the tricarbonyl. To confirm this interpretation, a 4-methyl-1-cyclohexene solution containing  $(\eta^5\text{-C}_5\text{Me}_5)\text{Re}(\text{CO})_3$  was photolyzed. The only observed photoreaction was the conversion of  $(\eta^5\text{-C}_5\text{Me}_5)\text{Re}(\text{CO})_3$  to  $(\eta^5\text{-C}_5\text{Me}_5)\text{Re}(\text{CO})_2(\eta^2\text{-4-methyl-1-cyclohexene})$ .

At 100 K, in a 4-methyl-1-cyclohexene glass, the photoreaction of  $\text{cis}-(\eta^5\text{-C}_5\text{Me}_5)\text{Re}(\text{CO})_2\text{Me}_2$  proceeded without the production of the tricarbonyl. The *cis*  $\rightarrow$  *trans* isomerization was the only process observed by FTIR spectroscopy.

### 3.2.2 Stereochemistry of the product and thermal reactivity of the photogenerated intermediate.

The photoproduct,  $\text{trans}-(\eta^5\text{-C}_5\text{Me}_5)\text{Re}(\text{CO})_2\text{Me}_2$ , was assigned a *trans* stereochemistry based on the relative intensity of the symmetric and antisymmetric IR bands of the carbonyl ligands. The ratio  $I_{\text{asym}}/I_{\text{sym}}$  is given by  $\tan^2\theta$ , where  $\theta$  is one half of the C-Re-C angle.<sup>66</sup> For the *trans* isomer, the higher energy symmetric band was less intense and the C-Re-C angle,  $2\theta$ , was calculated to be  $113^\circ$ . The angle calculated for the *cis* isomer was  $86^\circ$ . In the case of  $\text{trans}-(\eta^5\text{-C}_5\text{Me}_5)\text{Re}(\text{CO})_2\text{Br}_2$ , where an analogous calculation was done, the predicted angle was

115°. X-ray crystal analysis yielded a value of 104°. <sup>54</sup>

There was no intermediate observed, by FTIR spectroscopy, following the photolysis of *cis*-( $\eta^5$ -C<sub>5</sub>Me<sub>5</sub>)Re(CO)<sub>2</sub>Me<sub>2</sub> at 100 K. However, the intermediate was observed following photolysis at lower temperatures. The photolysis of *cis*-( $\eta^5$ -C<sub>5</sub>Me<sub>5</sub>)Re(CO)<sub>2</sub>Me<sub>2</sub>, at 13 K led to the changes shown in Figure 3-1. The loss of FTIR absorptions due to the starting complex at 1978 cm<sup>-1</sup> and 1894 cm<sup>-1</sup> occurred upon photolysis. The appearance of two new absorptions at 2128 cm<sup>-1</sup> and 1861 cm<sup>-1</sup> was observed and found to coincide with the loss of intensity due to *cis*-( $\eta^5$ -C<sub>5</sub>Me<sub>5</sub>)Re(CO)<sub>2</sub>Me<sub>2</sub>. The band at 2128 cm<sup>-1</sup> was due to the formation of free CO in the matrix.<sup>7</sup> The other absorption, at 1861 cm<sup>-1</sup>, was assigned to the CO loss product ( $\eta^5$ -C<sub>5</sub>Me<sub>5</sub>)Re(CO)Me<sub>2</sub>. The assignment of the 1861 cm<sup>-1</sup> band as being due to ( $\eta^5$ -C<sub>5</sub>Me<sub>5</sub>)Re(CO)Me<sub>2</sub> was consistent with a single absorption, as expected for a monocarbonyl. The assignment is also consistent with the subsequent chemistry of the photoproducted intermediate.

When the glass, containing ( $\eta^5$ -C<sub>5</sub>Me<sub>5</sub>)Re(CO)Me<sub>2</sub> and CO, was warmed to 100 K the absorptions due to the unsaturated complex and free CO disappeared. New absorptions appeared at 1988 cm<sup>-1</sup> and 1910 cm<sup>-1</sup> as shown in Figure 3-1. These bands were assigned as due to *trans*-( $\eta^5$ -C<sub>5</sub>Me<sub>5</sub>)Re(CO)<sub>2</sub>Me<sub>2</sub> by comparison with the FTIR spectrum of an authentic sample. At low temperature the formation of ( $\eta^5$ -C<sub>5</sub>Me<sub>5</sub>)Re(CO)Me<sub>2</sub> appeared to be quantitative since all the free CO was consumed, upon warming, and no tricarbonyl was observed by FTIR spectroscopy. The thermal reaction to produce

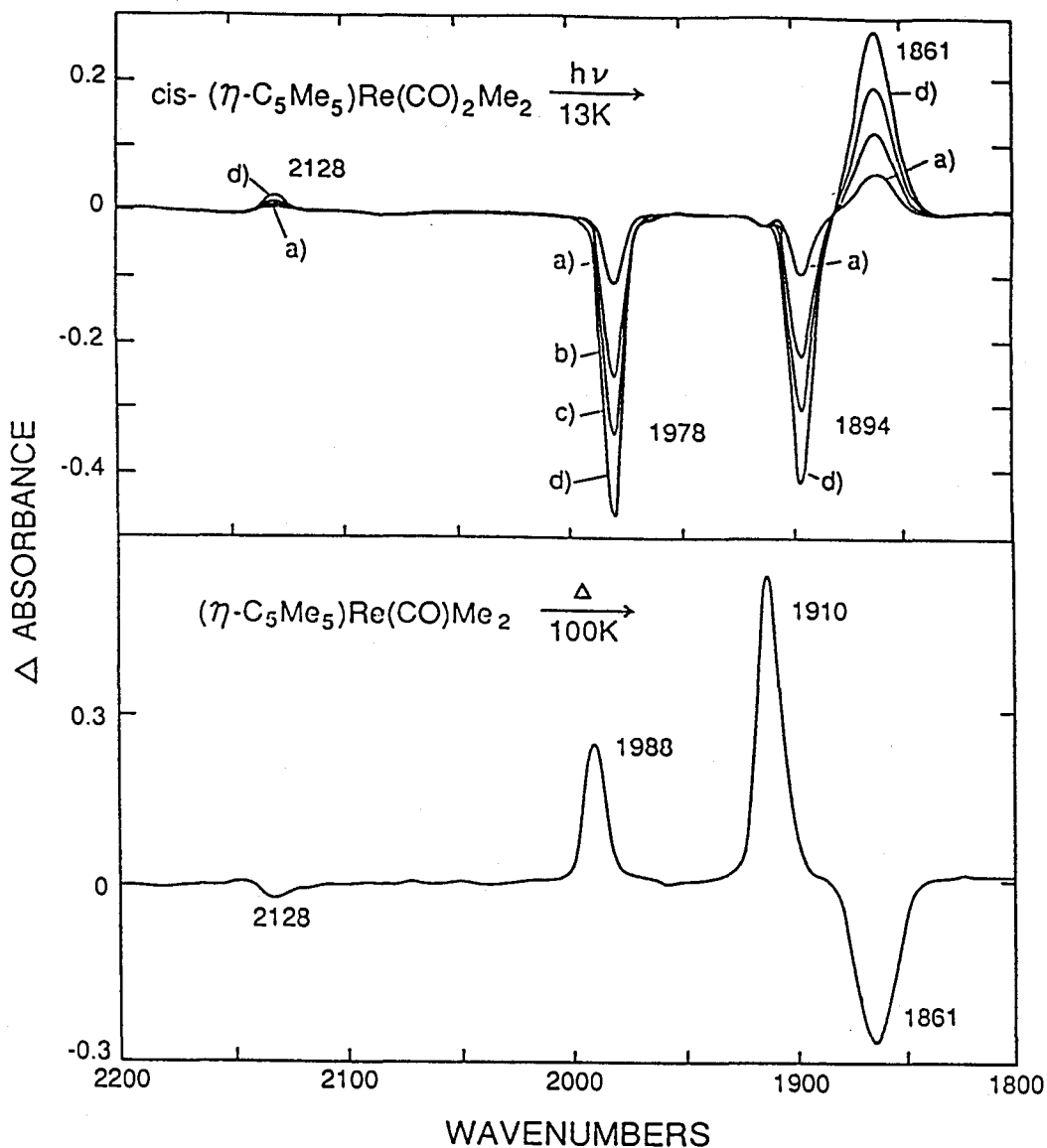


Figure 3-1

(Top). The FTIR spectral changes accompanying the UV photolysis of  $\text{cis-}(\eta^5\text{-C}_5\text{Me}_5)\text{Re(CO)}_2\text{Me}_2$  at 13 K in a 4-methyl-1-cyclohexene glass. The negative peaks at 1978  $\text{cm}^{-1}$  and 1894  $\text{cm}^{-1}$  indicate the loss of  $\text{cis-}(\eta^5\text{-C}_5\text{Me}_5)\text{Re(CO)}_2\text{Me}_2$ . The positive peak at 2128  $\text{cm}^{-1}$  is due to the formation of free CO trapped in the matrix. The positive band at 1861  $\text{cm}^{-1}$  is due to the photogenerated intermediate  $(\eta^5\text{-C}_5\text{Me}_5)\text{Re(CO)Me}_2$ . Photolysis times were (a) 5 s, (b) 10 s, (c) 25 s, (d) 85 s. (Bottom). FTIR spectral change associated with the warming, from 13 K to 100 K, of the glass containing photoproducted  $(\eta^5\text{-C}_5\text{Me}_5)\text{Re(CO)Me}_2$ . The positive bands, at 1988  $\text{cm}^{-1}$  and 1910  $\text{cm}^{-1}$ , represent the formation of  $\text{trans-}(\eta^5\text{-C}_5\text{Me}_5)\text{Re(CO)}_2\text{Me}_2$ .

*trans*-( $\eta^5$ -C<sub>5</sub>Me<sub>5</sub>)Re(CO)<sub>2</sub>Me<sub>2</sub> confirmed the assignment of the intermediate as a simple CO loss product. If, as a result of photolysis, the methyl groups as well as CO were lost the product of the intermediate reacting with free CO would not have been the *trans* isomer. The photochemically generated intermediate must have retained the other portions of its coordination sphere and was therefore ( $\eta^5$ -C<sub>5</sub>Me<sub>5</sub>)Re(CO)Me<sub>2</sub>.

The photolysis of *cis*-( $\eta^5$ -C<sub>5</sub>Me<sub>5</sub>)Re(CO)<sub>2</sub>Me<sub>2</sub>, in a methylcyclohexane glass, gave essentially the same results as in a 4-methyl-1-cyclohexene glass. The FTIR absorptions are given in Table 3-1. However, due to the low solubility and poor optical characteristics of *cis*-( $\eta^5$ -C<sub>5</sub>Me<sub>5</sub>)Re(CO)<sub>2</sub>Me<sub>2</sub> in methylcyclohexane it was difficult to confirm, based on FTIR data, that no *cis*-( $\eta^5$ -C<sub>5</sub>Me<sub>5</sub>)Re(CO)<sub>2</sub>Me<sub>2</sub> was formed upon warming. Also it could not be confirmed, with any degree of accuracy, that all the free CO was consumed during the back reaction at 100 K. However, since all the ( $\eta^5$ -C<sub>5</sub>Me<sub>5</sub>)Re(CO)Me<sub>2</sub> was consumed and no tricarbonyl was formed the efficient recoordination of CO was indicated.

Unfortunately, *cis*-( $\eta^5$ -C<sub>5</sub>Me<sub>5</sub>)Re(CO)<sub>2</sub>X<sub>2</sub> (X = Cl, Br, I) were only slightly soluble in methylcyclohexane or 4-methyl-1-cyclohexene. The most soluble of the three halogen compounds was *cis*-( $\eta^5$ -C<sub>5</sub>Me<sub>5</sub>)Re(CO)<sub>2</sub>I<sub>2</sub>, however, when a 4-methyl-1-cyclohexene solution containing the iodine complex was cooled, the FTIR spectra showed that the compound had precipitated before reaching temperatures low enough to stabilize an intermediate. Therefore, the study of the halogen complexes in those solvents was not practical. Consequently, (1,2-epoxyethyl)-benzene was chosen as an alternate solvent for the halogen compounds. All of the halogen complexes were soluble in (1,2-epoxyethyl)-benzene. (1,2-



Table 3-1

## FTIR and UV-Vis spectral data for relevant complexes

complex	$\nu(\text{CO}),^{\text{a}} \text{cm}^{-1}$ (rel intensity)
<i>cis</i> -( $\eta^5\text{-C}_5\text{Me}_5$ )Re(CO) <sub>2</sub> Me <sub>2</sub>	1978 (1.1), 1894 (1.0) <sup>b</sup>
( $\eta^5\text{-C}_5\text{Me}_5$ )Re(CO)Me <sub>2</sub>	1861 <sup>b</sup>
<i>trans</i> -( $\eta^5\text{-C}_5\text{Me}_5$ )Re(CO) <sub>2</sub> Me <sub>2</sub>	1988 (1.0), 1910 (2.2) <sup>b</sup>
<i>cis</i> -( $\eta^5\text{-C}_5\text{Me}_5$ )Re(CO) <sub>2</sub> Me <sub>2</sub>	1968 (1.2), 1879 (1.0)
( $\eta^5\text{-C}_5\text{Me}_5$ )Re(CO)Me <sub>2</sub>	1840
<i>trans</i> -( $\eta^5\text{-C}_5\text{Me}_5$ )Re(CO) <sub>2</sub> Me <sub>2</sub>	1976 (1.0), 1892 (2.3)
<i>cis</i> -( $\eta^5\text{-C}_5\text{Me}_5$ )Re(CO) <sub>2</sub> Me <sub>2</sub>	1982 (1.2), 1900 (1.0) <sup>c</sup>
( $\eta^5\text{-C}_5\text{Me}_5$ )Re(CO)Me <sub>2</sub>	1864 <sup>c</sup>
<i>trans</i> -( $\eta^5\text{-C}_5\text{Me}_5$ )Re(CO) <sub>2</sub> Me <sub>2</sub>	1992 (1.0), 1918 (2.2) <sup>c</sup>
<i>cis</i> -( $\eta^5\text{-C}_5\text{Me}_5$ )Re(CO) <sub>2</sub> Cl <sub>2</sub>	2032 (1.3), 1953 (1.0)
( $\eta^5\text{-C}_5\text{Me}_5$ )Re(CO)Cl <sub>2</sub>	1912
<i>trans</i> -( $\eta^5\text{-C}_5\text{Me}_5$ )Re(CO) <sub>2</sub> Cl <sub>2</sub>	2048 (1.0), 1966 (2.2)
<i>cis</i> -( $\eta^5\text{-C}_5\text{Me}_5$ )Re(CO) <sub>2</sub> Br <sub>2</sub>	2028 (1.5), 1953 (1.0)
( $\eta^5\text{-C}_5\text{Me}_5$ )Re(CO)Br <sub>2</sub>	1910
<i>trans</i> -( $\eta^5\text{-C}_5\text{Me}_5$ )Re(CO) <sub>2</sub> Br <sub>2</sub>	2039 (1.0), 1966 (2.2)
<i>cis</i> -( $\eta^5\text{-C}_5\text{Me}_5$ )Re(CO) <sub>2</sub> I <sub>2</sub>	2017 (1.6), 1947 (1.0)
<i>cis</i> -( $\eta^5\text{-C}_5\text{Me}_5$ )Re(CO)I <sub>2</sub>	1905
<i>trans</i> -( $\eta^5\text{-C}_5\text{Me}_5$ )Re(CO) <sub>2</sub> I <sub>2</sub>	2020 (1.0), 1951 (2.7)

Table 3-1 (Continued)

complex	UV-Vis <sup>d</sup> ( $\epsilon$ , M <sup>-1</sup> cm <sup>-1</sup> )
<i>cis</i> -( $\eta^5$ -C <sub>5</sub> Me <sub>5</sub> )Re(CO) <sub>2</sub> Me <sub>2</sub>	340 (500) <sup>e</sup>
<i>trans</i> -( $\eta^5$ -C <sub>5</sub> Me <sub>5</sub> )Re(CO) <sub>2</sub> Me <sub>2</sub>	320 (400 sh)
<i>cis</i> -( $\eta^5$ -C <sub>5</sub> Me <sub>5</sub> )Re(CO) <sub>2</sub> Cl <sub>2</sub>	344 (380), 403 (360), 470 (170 sh)
<i>trans</i> -( $\eta^5$ -C <sub>5</sub> Me <sub>5</sub> )Re(CO) <sub>2</sub> Cl <sub>2</sub>	386 (390), 460 (130 sh)
<i>cis</i> -( $\eta^5$ -C <sub>5</sub> Me <sub>5</sub> )Re(CO) <sub>2</sub> Br <sub>2</sub>	340sh (1200), 426 (710)
<i>trans</i> -( $\eta^5$ -C <sub>5</sub> Me <sub>5</sub> )Re(CO) <sub>2</sub> Br <sub>2</sub>	401 (770)
<i>cis</i> -( $\eta^5$ -C <sub>5</sub> Me <sub>5</sub> )Re(CO) <sub>2</sub> I <sub>2</sub>	368 (1040), 486 (550)
<i>trans</i> -( $\eta^5$ -C <sub>5</sub> Me <sub>5</sub> )Re(CO) <sub>2</sub> I <sub>2</sub>	365 (1290), 484 (360)

**a** All data of glasses recorded at 13 K. The solvent was (1,2-epoxyethyl)-benzene unless otherwise noted.

**b** Solvent was 4-methyl-1-cyclohexene.

**c** Solvent was methylcyclohexane.

**d** Data was all from room-temperature benzene solutions unless otherwise stated. In addition to the bands listed all the complexes exhibited higher energy charge-transfer bands at  $\approx$  280 nm.

**e** Toluene solution.

epoxyethyl)-benzene formed a glass which was optically transparent at temperatures as low as 12 K, and appears to be inert toward several unsaturated organometallic complexes.<sup>67</sup> In order to more directly compare the reactivity of the dimethyl and dihalogen complexes, a more thorough study of the photochemistry of  $(\eta^5\text{-C}_5\text{Me}_5)\text{Re}(\text{CO})_2\text{Me}_2$  in (1,2-epoxyethyl)-benzene was conducted.

A (1,2-epoxyethyl)-benzene solution of *cis*- $(\eta^5\text{-C}_5\text{Me}_5)\text{Re}(\text{CO})_2\text{Me}_2$  was prepared and cooled to 13 K, forming a glass. Photolysis, at 13 K, led to the formation of the monocarbonyl,  $(\eta^5\text{-C}_5\text{Me}_5)\text{Re}(\text{CO})\text{Me}_2$ , and free CO. The pertinent FTIR absorptions are listed in Table 3-1. Upon warming to 100 K the photogenerated intermediate reacted with the free CO producing *trans*- $(\eta^5\text{-C}_5\text{Me}_5)\text{Re}(\text{CO})_2\text{Me}_2$ . All of the free CO, produced during photolysis at 13 K, was consumed in the thermal reaction upon warming to 100 K, as was observed in a 4-methyl-1-cyclohexene glass. The sample was also photolyzed with the light of wavelength 320-400 nm. In the 320-400 nm region only d-d absorptions occur (see Table 3-1). Although the required photolysis times using 320-400 nm light were longer than those required with unfiltered light, no difference in the photochemistry was observable.

*Trans*- $(\eta^5\text{-C}_5\text{Me}_5)\text{Re}(\text{CO})_2\text{Me}_2$  was photolyzed in an analogous manner to the *cis* isomer. Once again CO was lost to produce an unsaturated species. The unsaturated intermediate was the same as that produced by the *cis* isomer based on its identical IR absorption and reactivity upon warming. Only *trans*- $(\eta^5\text{-C}_5\text{Me}_5)\text{Re}(\text{CO})_2\text{Me}_2$  was formed in the thermal reaction with CO. When the unfiltered output of the lamp was used, CO loss from the *trans* isomer was not observable on the same time scale as

CO loss from the *cis* isomer. However, when the wavelength range 320-400 nm was used, the efficiency of the reaction was comparable to CO loss from the *cis* isomer.

The d-d transitions at room temperature showed a maximum at 340 nm for the *cis* dimethyl complex. At approximately 290 nm the absorption edge of the charge-transfer bands obscured any higher energy d-d transitions. In the case of the *trans* dimethyl complex the d-d absorption appeared as a shoulder on the more intense charge-transfer transitions. The qualitative ordering of wavelength dependence was expected to be followed at low temperature in (1,2-epoxyethyl)-benzene. Utilizing the 320-400 nm wavelength region, the sample was irradiated in a region where both isomers displayed d-d absorbances. Under these conditions, both the *cis* and *trans* isomers displayed approximately the same photosensitivity. However, if the unfiltered light was used, the *trans* isomer was less sensitive than the *cis* isomer since the d-d absorption band of the *trans* isomer overlaps to a much greater extent with its higher energy charge-transfer absorptions.

The above series of experiments were repeated for the halogen complexes *cis*- and *trans*- $(\eta^5\text{-C}_5\text{Me}_5)\text{Re}(\text{CO})_2\text{X}_2$  (X = Cl, Br, I). The results were qualitatively the same. FTIR absorption bands for the halogen complexes are summarized in Table 3-1, and Figure 3-2 shows the spectral changes associated with photolysis and subsequent warming of the *cis* diiodide complex.

Irradiation, at 13 K, resulted in the loss of CO and the formation of  $(\eta^5\text{-C}_5\text{Me}_5)\text{Re}(\text{CO})\text{X}_2$  (X = Cl, Br, I). When the glass was warmed to 100 K, the bands due to the unsaturated species and free CO disappeared and

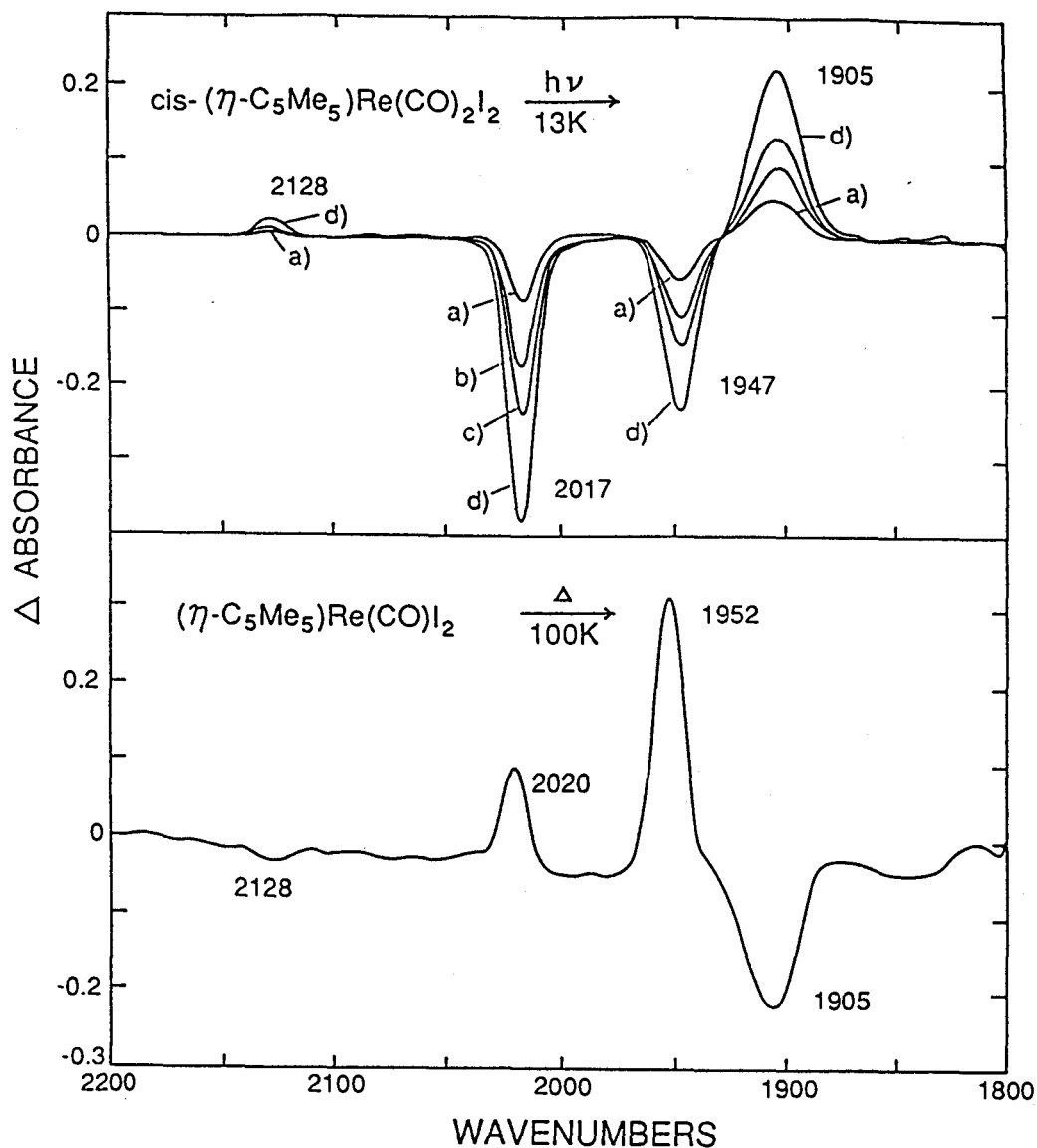


Figure 3-2

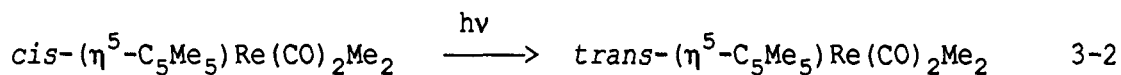
(Top). The FTIR spectral changes accompanying the UV photolysis of  $\text{cis-}(\eta^5\text{-C}_5\text{Me}_5)\text{Re(CO)}_2\text{I}_2$  at 13 K in a (1,2-epoxyethyl)benzene glass. The negative bands at 2017  $\text{cm}^{-1}$  and 1947  $\text{cm}^{-1}$  are a result of the loss of  $\text{cis-}(\eta^5\text{-C}_5\text{Me}_5)\text{Re(CO)}_2\text{I}_2$ . The positive band at 2128  $\text{cm}^{-1}$  is due to free CO in the matrix. The positive band at 1905  $\text{cm}^{-1}$  was due to the formation of the photogenerated intermediate  $(\eta^5\text{-C}_5\text{Me}_5)\text{Re(CO)I}_2$ . The photolysis times were (a) 5 s, (b) 15 s, (c) 25 s, (d) 145 s.

(Bottom) FTIR spectral change associated with the warming, from 13 K to 100 K, of the glass containing photoproducted  $(\eta^5\text{-C}_5\text{Me}_5)\text{Re(CO)I}_2$ . The positive bands at 2020  $\text{cm}^{-1}$  and 1952  $\text{cm}^{-1}$  are due to the formation of  $\text{trans-}(\eta^5\text{-C}_5\text{Me}_5)\text{Re(CO)}_2\text{I}_2$ .

new bands due to  $trans-(\eta^5-C_5Me_5)Re(CO)_2X_2$  ( $X = Cl, Br, I$ ) appeared. Analogous to the dimethyl complex, when narrow wavelengths were used (in particular  $\lambda = 320-400$  nm, pass  $\lambda > 380$  nm and pass  $\lambda > 310$  nm) to selectively irradiate the d-d transitions the course of the reaction was not affected. The dihalogen complexes, both *cis* and *trans* isomers, exhibited resolved d-d absorptions at lower energy than their respective charge-transfer bands.

### 3.3 Discussion

Previous studies on the photochemistry of  $cis-(\eta^5-C_5Me_5)Re(CO)_2X_2$  ( $X = Cl, Br, I$ ) showed that they underwent *cis*  $\rightarrow$  *trans* isomerization.<sup>35</sup> This study demonstrated that the related complex,  $cis-(\eta^5-C_5Me_5)Re(CO)_2Me_2$ , also underwent the unidirectional *cis*  $\rightarrow$  *trans* isomerization as shown in equation 3-2. In a low temperature glass

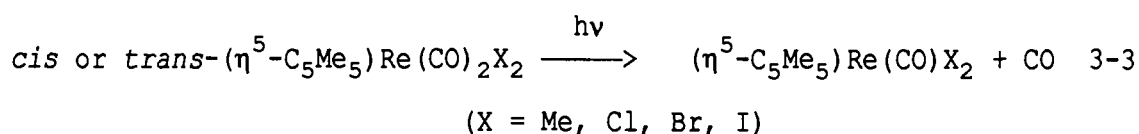


the reaction was found to be nearly quantitative. The reaction was also found to be unidirectional, at or below a temperature of 100 K, where photolysis of  $trans-(\eta^5-C_5Me_5)Re(CO)_2Me_2$  did not produce the *cis* isomer.

As mentioned above, the reaction was nearly quantitative at low temperature but at ambient temperature the production of  $(\eta^5-C_5Me_5)Re(CO)_3$  and its photoproducts were also observed. It is possible that the tricarbonyl complex was formed by the reaction of the photogenerated unsaturated species with the starting complex which led ultimately to  $(\eta^5-C_5Me_5)Re(CO)_3$ .

The primary photoprocess for the complexes *cis* and *trans*-

$(\eta^5\text{-C}_5\text{Me}_5)\text{Re}(\text{CO})_2\text{X}_2$  (X = Me, Cl, Br, I) was CO loss to generate the unsaturated complexes  $(\eta^5\text{-C}_5\text{Me}_5)\text{Re}(\text{CO})\text{X}_2$  (X = Me, Cl, Br, I) as shown in equation 3-3. In each instance the observed photoreaction was independent of irradiation wavelength. There was no observed difference in reactivity if only the ligand field (LF) transitions were irradiated as opposed to irradiating both the ligand field and charge-transfer (CT) states.



The unsaturated intermediates did not appear to be coordinated by the matrix molecules. The degree of solvent coordination was assessed by monitoring the change in absorption energies upon varying the solvent. For example, the carbonyl absorption frequency of  $(\eta^5\text{-C}_5\text{Me}_5)\text{Re}(\text{CO})\text{Me}_2$  shifted from  $1861\text{ cm}^{-1}$  to  $1840\text{ cm}^{-1}$  upon changing the solvent from 4-methyl-1-cyclohexene to (1,2-epoxyethyl)-benzene. The carbonyl absorption of  $(\eta^5\text{-C}_5\text{Me}_5)\text{Re}(\text{CO})\text{Me}_2$ , in the non-coordinating solvent methylcyclohexane, was  $1864\text{ cm}^{-1}$ . The similarity between the carbonyl absorption in methylcyclohexane and 4-methyl-1-cyclohexene indicated that the olefin did not coordinate strongly to the unsaturated intermediate. There was a substantial shift observed,  $24\text{ cm}^{-1}$  for the CO stretch of  $(\eta^5\text{-C}_5\text{Me}_5)\text{Re}(\text{CO})\text{Me}_2$ , upon switching from methylcyclohexane to (1,2-epoxyethyl)-benzene. However, the CO absorption bands of *cis*- $(\eta^5\text{-C}_5\text{Me}_5)\text{Re}(\text{CO})_2\text{Me}_2$  were  $1982\text{ cm}^{-1}$  and  $1900\text{ cm}^{-1}$  in methylcyclohexane and  $1968\text{ cm}^{-1}$  and  $1879\text{ cm}^{-1}$  in (1,2-epoxyethyl)-benzene, which was a shift of  $14\text{ cm}^{-1}$  for the symmetric and  $21\text{ cm}^{-1}$  for the antisymmetric

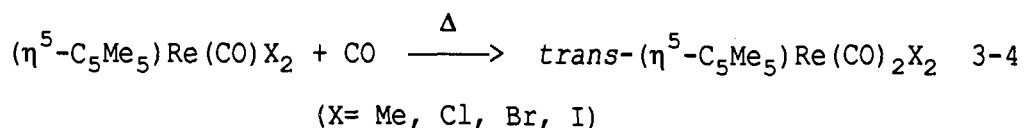
vibrations. Comparatively, the absorption frequency shift of the CO loss product was only slightly larger than the shift observed for the coordinatively saturated starting complex. Therefore, for all three solvents used in this study, it was concluded that any interaction between the unsaturated complex and solvent was very weak.

The dihalide complexes,  $cis-(\eta^5-C_5Me_5)Re(CO)_2X_2$  ( $X = Cl, Br, I$ ), were sparingly soluble in hydrocarbon solvents. The characterization of the CO loss product of the dihalides was unachievable in both methylcyclohexane and 4-methyl-1-cyclohexene. Consequently, an analysis of the CO stretching frequencies of the dihalides in methylcyclohexane or 4-methyl-1-cyclohexene was not feasible. However, it was possible to compare the differences in frequency between the saturated complexes and their CO loss product in (1,2-epoxyethyl)-benzene. The CO stretching frequencies of the CO loss products of the dihalides,  $(\eta^5-C_5Me_5)Re(CO)X_2$  ( $X = Cl, Br, I$ ) were approximately  $80\text{ cm}^{-1}$  lower in energy than the average band positions of the starting complexes. The frequency differences of the CO stretches, between the saturated and unsaturated dihalide complexes were similar to the frequency difference of  $83\text{ cm}^{-1}$  between the average band position of  $cis-(\eta^5-C_5Me_5)Re(CO)_2Me_2$  and the absorption band of  $(\eta^5-C_5Me_5)Re(CO)Me_2$ . As a result of the similarity in frequency shifts it was concluded that the CO loss products of the dihalide complexes are best considered as effectively unsaturated species.

When a glass containing  $(\eta^5-C_5Me_5)Re(CO)X_2$  ( $X = Me, Cl, Br, I$ ) and free CO was warmed, reaction occurred to produce the *trans* isomer as shown in equation 3-4. In each instance only the *trans* isomer, and none



of the *cis* isomer, was formed in the thermal back-reaction.



In each case all the photoproduct carbon monoxide, formed at 13 K, was consumed in reaction 3-4. No detectable amounts of other products were observed by FTIR spectroscopy. Therefore the reactions must have been essentially quantitative. The fact that CO recoordination occurred upon warming the sample to 100 K is probably not reflective of the energetics of CO reacting with the unsaturated fragment. All of the unsaturated complexes,  $(\eta^5\text{-C}_5\text{Me}_5)\text{Re}(\text{CO})\text{X}_2$  (X= Me, Cl, Br, I), reacted with free CO by the time the glass was warmed to 100 K, indicative of the rate of CO diffusion through the glass. The spectra of  $(\eta^5\text{-C}_5\text{Me}_5)\text{Re}(\text{CO})\text{Me}_2$  in 4-methyl-1-cyclohexene showed that some recombination with free CO was observable at temperatures as low as 20 K, although the bulk of the recombination occurred between 60 K and a 100 K. The limited thermal back reaction at 20 K was probably a result of only the unsaturated molecules which had free CO occupying the same solvation sphere reacting. At 20 K the rate of reaction would be affected by both the rate of rotational motion in the glass and the energetics of the recoordination. At low temperatures, near 20 K, CO cannot diffuse and therefore molecules which did not have CO in the same solvation shell would not react. However, at 100 K the glass was far less rigid which would allow the CO to diffuse more readily and react with  $(\eta^5\text{-C}_5\text{Me}_5)\text{Re}(\text{CO})\text{X}_2$ . The fact that some back-reaction was observed at 20 K did support the premise that the CO loss product,

$(\eta^5\text{-C}_5\text{Me}_5)\text{Re}(\text{CO})\text{Me}_2$ , was indeed a coordinatively unsaturated molecule.

The photochemistry of each of the *trans* isomers was the same as their respective *cis* isomers; CO loss to generate unsaturated species. The unsaturated species reacted with free CO, upon warming, to regenerate the *trans* isomer and therefore no net photochemistry was observed. The *trans* isomers were found to be less photosensitive. The reduced photosensitivity of the *trans* isomers, relative to the *cis* isomers, was partially due to the higher energy of the d-d absorption bands. In the case of the dimethyl complex the d-d transition was, for the most part, concealed by the charge-transfer band. The overall *cis-trans* isomerization for all the complexes studied proceeded by the same process. Initially, CO loss occurred to produce the unsaturated intermediate followed by the thermal reaction of the intermediate, with free CO, to produce only the *trans* product. When photolyzed the *trans* isomer led to the same intermediate as produced by the *cis* isomer and therefore did not undergo *trans*  $\rightarrow$  *cis* isomerization. The observation, mentioned previously, that when *cis*- $(\eta^5\text{-C}_5\text{Me}_5)\text{Re}(\text{CO})_2\text{I}_2$  was photolyzed in a chlorinated solvent it produced *trans*- $(\eta^5\text{-C}_5\text{Me}_5)\text{Re}(\text{CO})_2\text{Cl}_2$  cannot be a result of the simple isomerization. The product, *trans*- $(\eta^5\text{-C}_5\text{Me}_5)\text{Re}(\text{CO})_2\text{Cl}_2$ , must have been produced by either a concurrent exchange process or the subsequent reactivity of the *trans* isomer at room temperature.

### 3.4 Conclusions

In this study it was demonstrated that the photolysis of *cis*- $(\eta^5\text{-C}_5\text{Me}_5)\text{Re}(\text{CO})_2\text{Me}_2$  at 13 K in methylcyclohexane,

methylcyclohexene, or (1,2-epoxyethyl)-benzene resulted in the loss of a carbonyl ligand and the formation of  $(\eta^5\text{-C}_5\text{Me}_5)\text{Re}(\text{CO})\text{Me}_2$ . It was also shown that the unsaturated complex underwent reaction with the photoproduct CO, upon warming to 100 K, to yield exclusively *trans*- $(\eta^5\text{-C}_5\text{Me}_5)\text{Re}(\text{CO})_2\text{Me}_2$ . Photolysis of the *trans* isomer leads to the same unsaturated intermediate as the *cis* isomer. Additionally, the mechanism of the *cis*  $\rightarrow$  *trans* isomerization for the analogous dihalides, *cis*- $(\eta^5\text{-C}_5\text{Me}_5)\text{Re}(\text{CO})_2\text{X}_2$  (X = Cl, Br, I), in (1,2-epoxyethyl)-benzene was found to occur by the same mechanism as the dimethyl complex.

### 3.5 Experimental Section

The complexes *cis*- $(\eta^5\text{-C}_5\text{Me}_5)\text{Re}(\text{CO})_2\text{Me}_2$  and  $(\eta^5\text{-C}_5\text{Me}_5)\text{Re}(\text{CO})_2\text{X}_2$  (X = Cl, Br, I) were obtained from the laboratories of D. Sutton and A.H. Klahn-Oliva. However, the complexes may be prepared by published procedures.<sup>35, 68, 69</sup> FTIR spectra were obtained using a Bruker IFS 85 spectrophotometer operating at  $1\text{ cm}^{-1}$  resolution. The samples were cooled in  $\text{CaF}_2$  faced IR cells using a CTI-cyrogenics Model 22 cryocooler and a 350R compressor system equipped with a Lake Shore Cryotronics DRC 80C temperature controller. The temperature was monitored by a Lake Shore Cryotronics silicon diode sensor (DT500 DRC). The solvents, methylcyclohexane, 4-methyl-1-cyclohexene and (1,2-epoxyethyl)-benzene, were purchased from Aldrich and used without further purification.

The photolysis source was a 100-W high pressure Hg lamp. For all of the experiments, the light was passed through a 10 cm path length water filter equipped with quartz optics. To isolate specific wavelengths, specific filters were used; Corning 7-51 (pass  $\lambda = 320\text{-}$

400nm), 3-75 (pass  $\lambda > 380\text{nm}$ ) and 0-54 (pass  $\lambda > 310\text{nm}$ ).

**3.5.1 Low-temperature photolysis.** All of the experiments were conducted in a similar manner, therefore, a typical one will be described. A solution of *cis*-( $\eta^5\text{-C}_5\text{Me}_5$ )Re(CO)<sub>2</sub>Me<sub>2</sub> was prepared such that the optical density of the most intense absorption, due to the CO ligands, was between 0.3 and 1. The solution was loaded into a CaF<sub>2</sub>-faced FTIR cell and cooled with the cryocooler to a temperature of 13 K and allowed to equilibrate. FTIR spectra were then obtained in the region from 2200 cm<sup>-1</sup> to 1700 cm<sup>-1</sup>. The sample was then removed from the optical bench and irradiated with the water-filtered output of a 100-W high-pressure Hg lamp for 5 seconds. Subsequently, the sample was reinserted into the optical bench and the FTIR spectrum obtained. This process was repeated until no appreciable change in the FTIR spectra was observed upon subsequent irradiation. The sample was then allowed to warm and FTIR spectra were collected at 10 K intervals up to 100 K. The sample was stabilized at 100 K and FTIR spectra were obtained until no further change occurred (see Figure 3-1). Consequently, the sample temperature was raised to 298 K and its FTIR spectrum obtained. The sample, which now contained predominantly *trans*-( $\eta^5\text{-C}_5\text{Me}_5$ )Re(CO)<sub>2</sub>Me<sub>2</sub>, was again cooled to 13 K and its FTIR spectrum obtained.

Analogous experiments were conducted in the other solvents and with the dihalides in (1,2-epoxyethyl)-benzene. In (1,2-epoxyethyl)-benzene the experiments were done by using different optical filters to assess the effect of wavelength on the reaction.

## Chapter 4: Photochemistry of $(\eta^5\text{-C}_5\text{Me}_5)\text{Re}(\text{CO})_2\text{Br}_2$ on Si(111) surfaces at low temperature.

### 4.1 Introduction

Very little is known about the photochemistry of inorganic compounds in the solid state. Therefore, we were interested in learning how chemical reactivity may differ in the solid state as opposed to in a solution or a glass.

The compound, *cis*- $(\eta^5\text{-C}_5\text{Me}_5)\text{Re}(\text{CO})_2\text{Br}_2$ , was chosen to be studied as an amorphous film since its chemistry in solution<sup>35</sup> and glasses<sup>36</sup> had been extensively studied. Hence, the photochemical studies of a film of *cis*- $(\eta^5\text{-C}_5\text{Me}_5)\text{Re}(\text{CO})_2\text{Br}_2$  could be compared with the studies done in different media.

In this chapter the photochemical reactions of a film of  $(\eta^5\text{-C}_5\text{Me}_5)\text{Re}(\text{CO})_2\text{Br}_2$  deposited on a silicon surface are discussed. Silicon was chosen as the substrate since it was inexpensive and transmitted infrared wavelengths. The results are compared to those obtained from the photolysis of *cis*- $(\eta^5\text{-C}_5\text{Me}_5)\text{Re}(\text{CO})_2\text{Br}_2$  in a glass.

### 4.2 Results and Discussion

#### 4.2.1 Calibration of absorbance vs. surface coverage

The absorbance of *cis*- $(\eta^5\text{-C}_5\text{Me}_5)\text{Re}(\text{CO})_2\text{Br}_2$  as a function of the amount of film deposited on a silicon surface was determined in order to provide a means to approximate the coverages used in subsequent experiments. A stock solution with a known concentration of *cis*- $(\eta^5\text{-C}_5\text{Me}_5)\text{Re}(\text{CO})_2\text{Br}_2$ , in dichloromethane, was prepared and a drop of

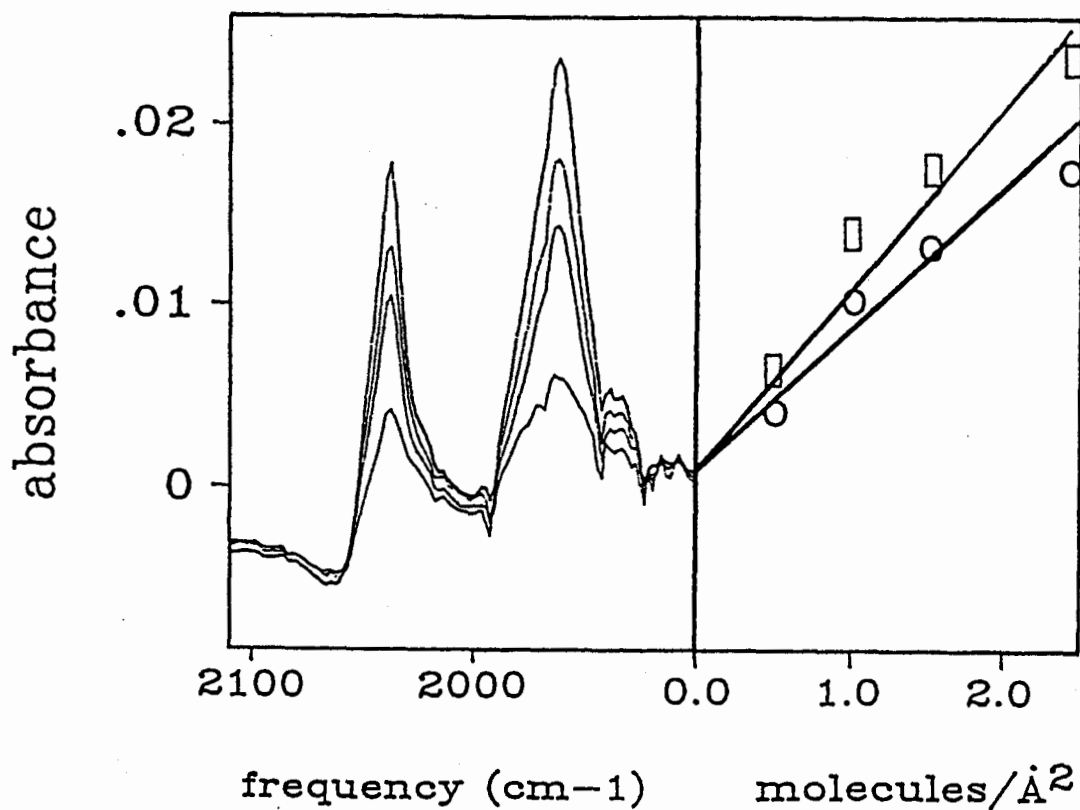


**Figure 4-1** (a) FTIR spectra for 0.5, 1.1, 1.6, and 2.2 molecules of  $\text{cis}-(\eta^5\text{-C}_5\text{Me}_5)\text{Re}(\text{CO})_2\text{Br}_2$  per  $\text{\AA}^2$  on a silicon (111) surface. (b) Plot of the absorbance of the symmetric ( $\square$ ) and antisymmetric ( $\circ$ ) CO stretches of  $\text{cis}-(\eta^5\text{-C}_5\text{Me}_5)\text{Re}(\text{CO})_2\text{Br}_2$  vs. coverage (data from Fig. 4-1(a)).

the solution was deposited on a silicon wafer. The solvent was allowed to evaporate leaving a film of *cis*-( $\eta^5$ -C<sub>5</sub>Me<sub>5</sub>)Re(CO)<sub>2</sub>Br<sub>2</sub>. FTIR spectra of the films were obtained over an absorbance range of 0 - 0.02 (for the carbonyl stretches) and the results are summarized in Figure 4-1. A more detailed description of the absorbance vs. coverage plot is given in the Experimental Section. As a result of knowing the concentration of *cis*-( $\eta^5$ -C<sub>5</sub>Me<sub>5</sub>)Re(CO)<sub>2</sub>Br<sub>2</sub> deposited as a film, and assuming that the average footprint of a molecule of *cis*-( $\eta^5$ -C<sub>5</sub>Me<sub>5</sub>)Re(CO)<sub>2</sub>Br<sub>2</sub> was 100 Å<sup>2</sup>, an absorbance of 0.02 corresponded to more than 300 monolayers. The absorbance measurements described here are not sufficiently sensitive to detect the interfacial layers (i.e., 2 in 300 monolayers). Consistent with this, the observed photochemistry was occurring in the film and did not appear to be influenced by the silicon surface environment. Although the substrate did not appear to effect the observed chemistry, very thin films (less than 50 monolayers) were not used in order to maintain good signal to noise characteristics.

#### 4.2.2 Comparison of the IR spectra of *cis*-( $\eta^5$ -C<sub>5</sub>Me<sub>5</sub>)Re(CO)<sub>2</sub>Br<sub>2</sub> in a low temperature glass and in a film.

The FTIR spectrum of *cis*-( $\eta^5$ -C<sub>5</sub>Me<sub>5</sub>)Re(CO)<sub>2</sub>Br<sub>2</sub> on the silicon surface consisted of two absorptions in the metal carbonyl region. The bands at 2017 cm<sup>-1</sup> and 1938 cm<sup>-1</sup> were assigned as due to the symmetric and antisymmetric carbonyl stretches, respectively. Both the positions and relative intensities of the two CO stretching absorptions were consistent with the results from a low temperature glass where the

Table 4-1

FTIR spectral data for relevant complexes

Complex	Medium <sup>a</sup>	$\nu(\text{CO}) \text{ cm}^{-1}$ (relative intensity)
<i>cis</i> -( $\eta^5\text{-C}_5\text{Me}_5$ )Re(CO) <sub>2</sub> Br <sub>2</sub>	Si(111)	2017(1.6), 1938(1.0)
	Glass	2028(1.5), 1935(1.0)
<i>trans</i> -( $\eta^5\text{-C}_5\text{Me}_5$ )Re(CO) <sub>2</sub> Br <sub>2</sub>	Si(111)	2040(1.0), 1967(1.2)
	Glass	2039(1.0), 1963(2.5)
Isomer 1 ( $\eta^5\text{-C}_5\text{Me}_5$ )Re(CO)Br <sub>2</sub>	Si(111)	1900
Isomer 2	Si(111)	1909
	Glass	1910

<sup>a</sup>Data in a (1,2-epoxyethyl)-benzene glass were obtained at 13 K, data obtained on a Si(111) surface were at 77 K.



symmetric and antisymmetric carbonyl absorptions appeared at  $2028\text{ cm}^{-1}$  and  $1935\text{ cm}^{-1}$ , respectively (see Table 4-1).

#### 4.2.3 Comparison of the IR spectra of *trans*-( $\eta^5\text{-C}_5\text{Me}_5$ )Re(CO)<sub>2</sub>Br<sub>2</sub> in a low temperature glass and in a film.

The carbonyl stretches of *trans*-( $\eta^5\text{-C}_5\text{Me}_5$ )Re(CO)<sub>2</sub>Br<sub>2</sub> were found to occur at approximately the same frequency in a glass and a film. The symmetric and antisymmetric carbonyl stretches of the *trans* isomer, in a film, were at  $2040\text{ cm}^{-1}$  and  $1967\text{ cm}^{-1}$ , respectively. In a glass the carbonyl stretches of the *trans* isomer appeared at  $2039\text{ cm}^{-1}$  and  $1963\text{ cm}^{-1}$ . However, the relative intensities differed considerably in the different media. The relative intensity of the antisymmetric stretch was reduced in a film. The relative intensities of the *trans* isomer in a film were used to calculate the C-Re-C angle,<sup>66</sup> and found to be  $95^\circ$ . The angle calculated for the same isomer in a glass was  $115^\circ$ . The angle observed in the crystal structure<sup>35</sup> was  $104^\circ$ . The reason for the change in the C-Re-C angle, of the *trans* isomer, upon switching from a glass to a film may have been due to an orientation effect of the surface or the increased molecule-molecule interaction that is possible in a film.

#### 4.2.4 Comparison of the photochemistry of ( $\eta^5\text{-C}_5\text{Me}_5$ )Re(CO)<sub>2</sub>Br<sub>2</sub> in a low temperature glass and in a film.

Irradiation of an amorphous film of *cis*-( $\eta^5\text{-C}_5\text{Me}_5$ )Re(CO)<sub>2</sub>Br<sub>2</sub>, at 77 K, into the lowest energy d-d absorption (bandpass > 420 nm) led to the difference spectrum shown in Figure 4-2(a). The loss of the starting material's absorptions at  $2017\text{ cm}^{-1}$  and  $1938\text{ cm}^{-1}$  and the

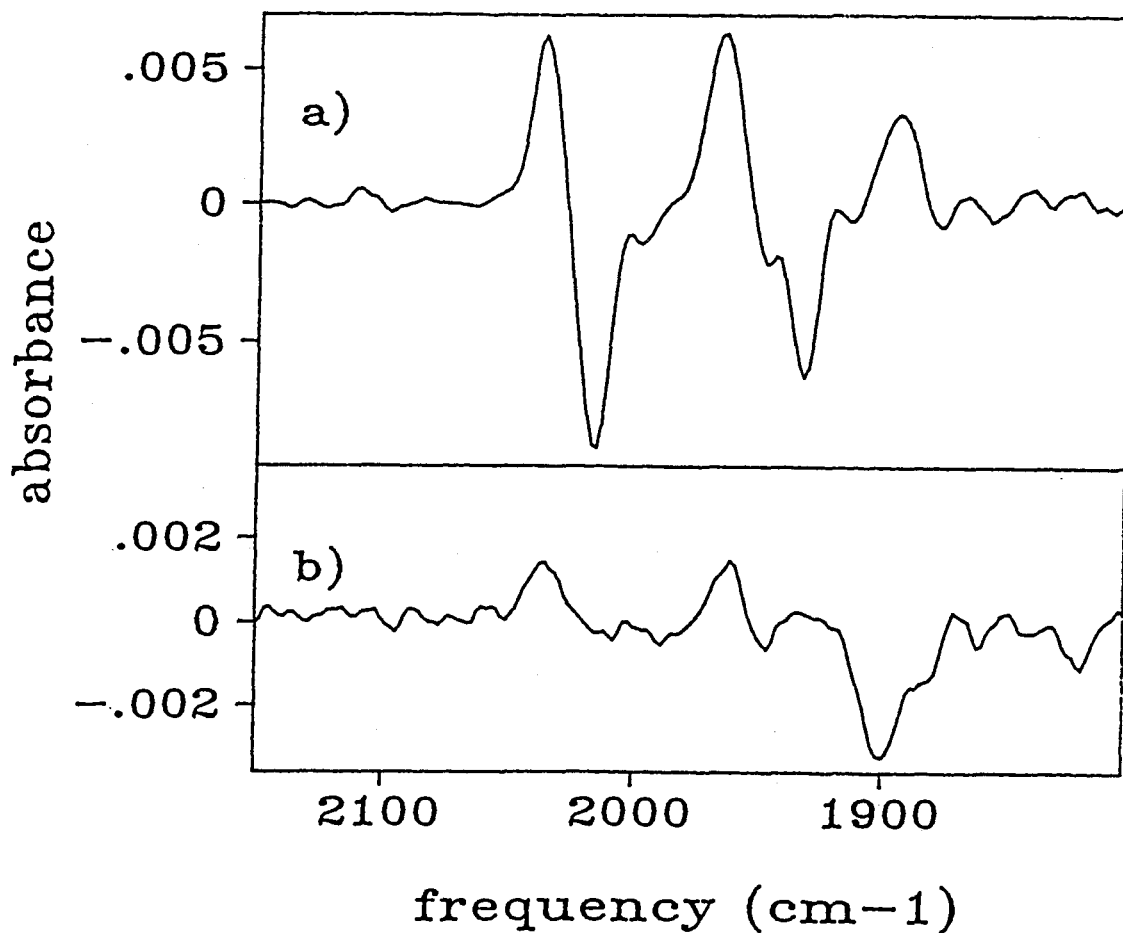


Figure 4-2. FTIR spectral change associated with (a) the photolysis of a film of  $cis-(\eta^5-C_5Me_5)Re(CO)_2Br_2$  on Si(111) for 80 s followed by (b) the spectral change associated with warming the sample to 150 K and re-cooling to 77 K.

appearance of three new absorption bands at  $2042\text{ cm}^{-1}$ ,  $1970\text{ cm}^{-1}$  and  $1900\text{ cm}^{-1}$  was observed. The two higher energy bands were assigned to *trans*- $(\eta^5\text{-C}_5\text{Me}_5)\text{Re}(\text{CO})_2\text{Br}_2$ . An authentic sample of *trans*- $(\eta^5\text{-C}_5\text{Me}_5)\text{Re}(\text{CO})_2\text{Br}_2$  was deposited on a silicon surface and cooled to 77 K where its spectrum was obtained. The CO stretching frequencies of the authentic sample were found to occur at  $2040\text{ cm}^{-1}$  and  $1967\text{ cm}^{-1}$ . The band positions of the authentic *trans*- $(\eta^5\text{-C}_5\text{Me}_5)\text{Re}(\text{CO})_2\text{Br}_2$  isomer and the photogenerated *trans*- $(\eta^5\text{-C}_5\text{Me}_5)\text{Re}(\text{CO})_2\text{Br}_2$  isomer agree within the  $4\text{ cm}^{-1}$  resolution at which the spectra were obtained, confirming the assignment of the photoproduct.

The lower energy band at  $1900\text{ cm}^{-1}$ , produced by the photolysis of *cis*- $(\eta^5\text{-C}_5\text{Me}_5)\text{Re}(\text{CO})_2\text{Br}_2$ , was assigned to the unsaturated complex  $(\eta^5\text{-C}_5\text{Me}_5)\text{Re}(\text{CO})\text{Br}_2$ . At lower conversions, the production of free CO was not observed due to its low extinction coefficient in the film. When the sample was warmed to 150 K, reaction occurred consuming  $(\eta^5\text{-C}_5\text{Me}_5)\text{Re}(\text{CO})\text{Br}_2$ , and free CO, to produce *trans*- $(\eta^5\text{-C}_5\text{Me}_5)\text{Re}(\text{CO})_2\text{Br}_2$  (see Figure 4-2(b)). The overall reaction pathway is summarized in Figure 4-4, pathways (i) and (ii). The photoreaction is completely analogous to the results found in a (1,2-epoxyethyl)-benzene glass.<sup>36</sup> A similar result was found if the sample was irradiated with light of wavelengths longer than 300 nm.

The unsaturated species,  $(\eta^5\text{-C}_5\text{Me}_5)\text{Re}(\text{CO})\text{Br}_2$ , was also photosensitive. The spectral changes are shown in Figure 4-3(a). Initially, photolysis resulted in the formation of both *trans*- $(\eta^5\text{-C}_5\text{Me}_5)\text{Re}(\text{CO})_2\text{Br}_2$  at  $2040\text{ cm}^{-1}$  and  $1967\text{ cm}^{-1}$  and the unsaturated species at  $1900\text{ cm}^{-1}$ . Continued photolysis resulted in the appearance

of an absorption band at  $1909\text{ cm}^{-1}$  which was assigned to a second isomer of  $(\eta^5\text{-C}_5\text{Me}_5)\text{Re}(\text{CO})\text{Br}_2$ . At higher conversions, free CO could be seen at  $2132\text{ cm}^{-1}$ . The photochemical steps and proposed geometries for each unsaturated isomer are outlined in Figure 4-4. When the sample was warmed, the second isomer reacted with free CO to produce only *cis*- $(\eta^5\text{-C}_5\text{Me}_5)\text{Re}(\text{CO})_2\text{Br}_2$  as illustrated by the spectral change in Figure 4-3(b). The result of warming was insensitive to the irradiation wavelength used at low temperature.

As shown earlier, from results obtained in a (1,2-epoxyethyl)-benzene glass, only one isomer of  $(\eta^5\text{-C}_5\text{Me}_5)\text{Re}(\text{CO})\text{Br}_2$  was formed in the glass. This isomer underwent a reaction with free CO resulting in the formation of *trans*- $(\eta^5\text{-C}_5\text{Me}_5)\text{Re}(\text{CO})_2\text{Br}_2$ . However, photolysis of isomer 1 on a silicon surface led to the photoproduction of a second isomer of  $(\eta^5\text{-C}_5\text{Me}_5)\text{Re}(\text{CO})\text{Br}_2$ . The two unsaturated isomers were found to react thermally with free CO to produce the two isomers of  $(\eta^5\text{-C}_5\text{Me}_5)\text{Re}(\text{CO})_2\text{Br}_2$ . The structure of each of the unsaturated isomers was probably a result of the molecule retaining a four legged piano stool geometry. Although the assignment of the structure of the two CO loss isomers was not conclusive, it does seem plausible that the geometry of the basal ligands would be retained throughout the thermal reaction. The reaction of isomer 1, with free CO, resulted in a *trans* product. Consequently, isomer 1 was assigned as having CO *trans* to the vacant coordination site. Since the thermal reaction of isomer 2, with free CO, resulted in the *cis* product, isomer 2 was assigned as having CO *cis* to the vacant site.

Previous work showed that the photolysis of the isoelectronic

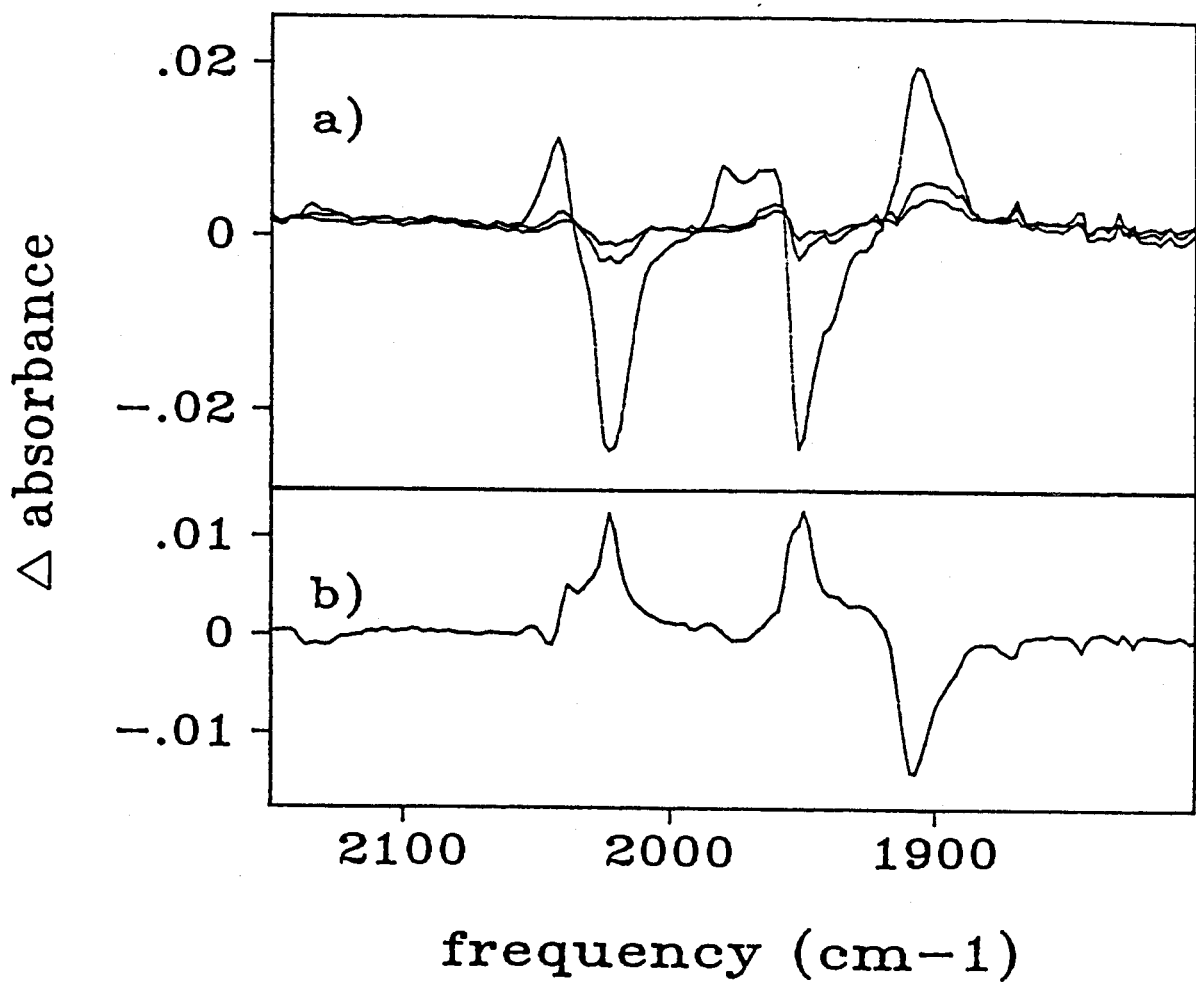


**Figure 4-3.** FTIR spectral changes associated with (a) the photolysis of a film of  $\text{cis}-(\eta^5\text{-C}_5\text{Me}_5)\text{Re}(\text{CO})_2\text{Br}_2$  on Si(111) for 100 min and 220 min using filtered light (band pass  $> 420$  nm) and 5 min using unfiltered light followed by (b) the spectral change associated with warming the sample to 150 K and re-cooling to 77 K.

molecules,  $(\eta^5\text{-C}_5\text{H}_5)\text{Mo}(\text{CO})_2\text{PR}_3\text{X}$  ( $\text{R} = \text{Ph}, \text{Bu}; \text{X} = \text{Cl}, \text{Br}, \text{I}$ ) in glasses, produced two isomeric unsaturated species following CO loss.<sup>70</sup> In each case the reaction of  $(\eta^5\text{-C}_5\text{H}_5)\text{Mo}(\text{CO})\text{PR}_3\text{X}$  with free CO resulted in the specific generation of an isomer of  $(\eta^5\text{-C}_5\text{H}_5)\text{Mo}(\text{CO})_2\text{PR}_3\text{X}$ . Also, the photolysis of *cis* and *trans*- $(\eta^5\text{-C}_5\text{H}_5)\text{V}(\text{CO})_2\text{L}_2$  ( $\text{L} = \text{P}(\text{OMe})_3, \text{P}(\text{OEt})_3$ ) in a glass produced distinct unsaturated species depending on the stereochemistry of the starting compound. The back reaction, with free CO, resulted in the formation of the starting material in its original configuration.<sup>71</sup> In contrast, it was found that the photolysis of *cis* or *trans*- $(\eta^5\text{-C}_5\text{H}_5)\text{W}(\text{CO})_2\text{IL}$  ( $\text{L} = \text{P}(\text{OMe})_3, \text{PPh}_3, \text{P}(\text{n-Bu})_3$ ) in a glass showed temperature dependent intermediates. At 12 K the results were analogous to the vanadium compounds mentioned above. However, at 77 K, the production of a mixture of *cis* and *trans* complexes was observed upon reaction with uncoordinated CO.<sup>71</sup>

Photolysis of a film of *trans*- $(\eta^5\text{-C}_5\text{Me}_5)\text{Re}(\text{CO})_2\text{Br}_2$  resulted in no observable change in the FTIR spectrum regardless of the photolysis wavelength used. Contrasted with this, was the result obtained by the photolysis of *trans*- $(\eta^5\text{-C}_5\text{Me}_5)\text{Re}(\text{CO})_2\text{Br}_2$  in a low temperature glass where CO loss was observed.

#### 4.3 Conclusions

Previously, it was shown that  $(\eta^5\text{-C}_5\text{Me}_5)\text{Re}(\text{CO})_2\text{Br}_2$ , in low temperature glasses, underwent efficient CO loss to generate  $(\eta^5\text{-C}_5\text{Me}_5)\text{Re}(\text{CO})\text{Br}_2$ .<sup>36</sup> The  $(\eta^5\text{-C}_5\text{Me}_5)\text{Re}(\text{CO})\text{Br}_2$  intermediate was produced by the photolysis, at 13 K, of either *cis* or *trans*- $(\eta^5\text{-C}_5\text{Me}_5)\text{Re}(\text{CO})_2\text{Br}_2$ . Upon warming the glass containing  $(\eta^5\text{-C}_5\text{Me}_5)\text{Re}(\text{CO})\text{Br}_2$ , only the *trans* isomer was formed

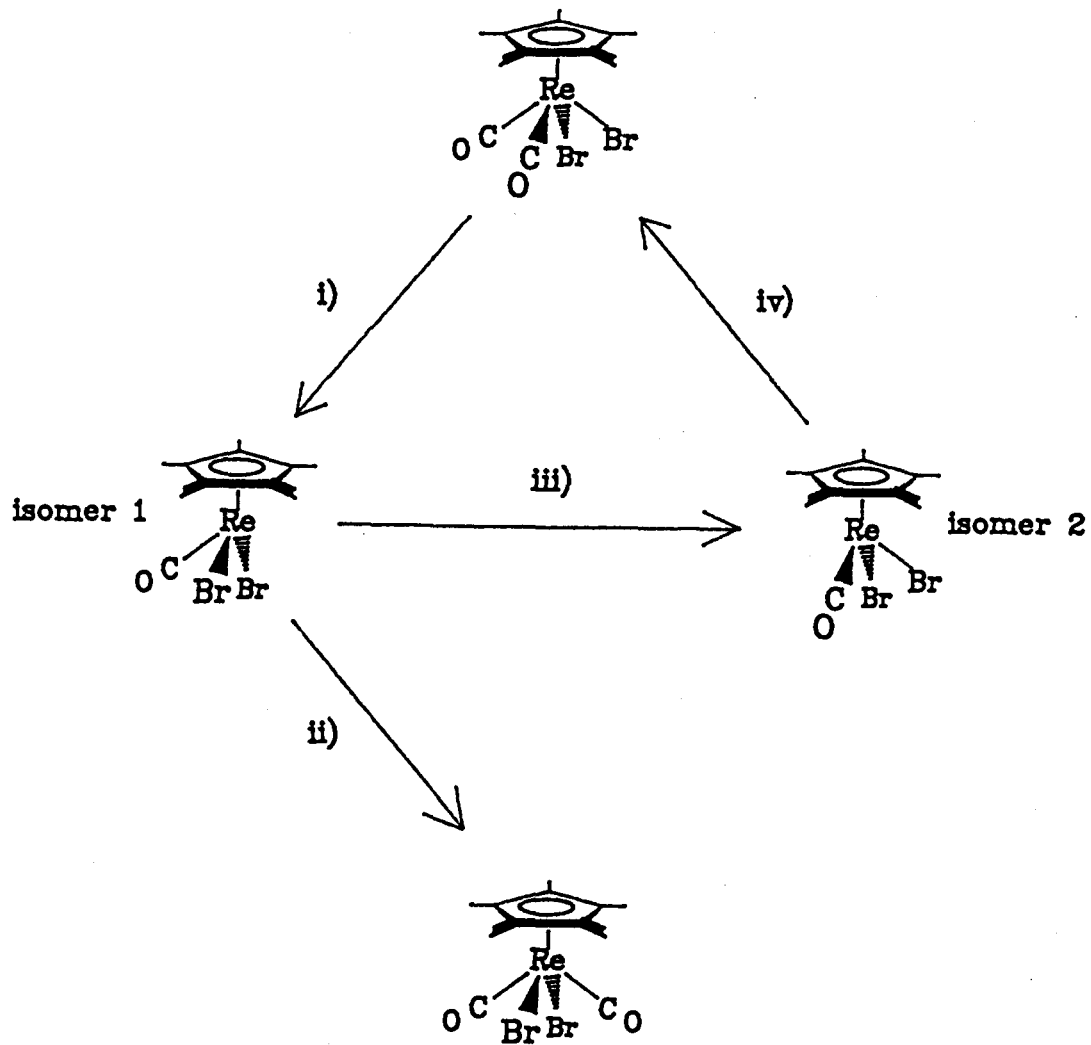


Figure 4-4.

(i) Photolysis in a glass at 77 K or 20 K, or photolysis in a film at 77 K. (ii) Warming either a surface film or glass. (iii) photolysis in a film at 77 K. (iv) warming of the photogenerated intermediate in a surface film.

in the thermal back reaction with free CO. This result explained why the solution isomerization occurred in the *cis* to *trans* direction only.<sup>35</sup>

The result of photolysing a film of  $(\eta^5\text{-C}_5\text{Me}_5)\text{Re}(\text{CO})_2\text{Br}_2$  and a low temperature glass containing  $(\eta^5\text{-C}_5\text{Me}_5)\text{Re}(\text{CO})_2\text{Br}_2$  was different. In a film, the photoisomerization of  $(\eta^5\text{-C}_5\text{Me}_5)\text{Re}(\text{CO})_2\text{Br}_2$ , was observable. However, in the film an additional intermediate was characterized. This demonstrated that the photochemistry of *trans*- $(\eta^5\text{-C}_5\text{Me}_5)\text{Re}(\text{CO})_2\text{Br}_2$  was altered by the change of phase from a low temperature glass to a surface film.

#### 4.4 Experimental Section

The compounds used, *cis*- and *trans*- $(\eta^5\text{-C}_5\text{Me}_5)\text{Re}(\text{CO})_2\text{Br}_2$ , were obtained from Professor D. Sutton, Simon Fraser University. However, they may be prepared by literature methods.<sup>68</sup>

The Si(111) wafers were obtained from Pacific Microelectronics Center, Canada. The wafers were *p*-type silicon with tolerances and specifications according to SEMI Standard M1.1.STD.5. The 4" wafers were cut to the approximate dimensions of 1 cm x 1 cm for use as substrates.

The FTIR transmittance spectra were obtained using a BOMEM Michelson MB-120 FTIR spectrophotometer operating at  $4\text{ cm}^{-1}$  resolution. The samples were held in a high conductivity copper sample mount. The sample mount was held within a  $\text{CaF}_2$  faced vacuum Dewar. The light source was a 100 W high pressure mercury lamp in an Oriel housing equipped with quartz condenser lenses.



#### 4.4.1 Calibration of the absorption of $(\eta^5\text{-C}_5\text{Me}_5)\text{Re}(\text{CO})_2\text{Br}_2$ on Si(111)

A stock solution of *cis*- $(\eta^5\text{-C}_5\text{Me}_5)\text{Re}(\text{CO})_2\text{Br}_2$  was prepared in dichloromethane (1.4 mM). A drop of the stock solution ( $3.1 \times 10^{-3} \text{ cm}^3$ ) was deposited on the surface of a silicon wafer, the solvent was allowed to evaporate, and the FTIR spectrum obtained. The coverage of the drop was found to be  $0.5 \text{ cm}^2$ . The process was repeated several times producing the data shown in Figure 4-1.

An analogous experiment was conducted using the *trans* isomer yielding slopes of  $6.0 \times 10^{-3}$  and  $7.3 \times 10^{-3}$  absorbance  $\text{\AA}^2/\text{molecules}$  for the high and low energy bands, respectively.

#### 4.4.2 Photolysis of $(\eta^5\text{-C}_5\text{Me}_5)\text{Re}(\text{CO})_2\text{Br}_2$ on silicon surfaces

Five drops of a dichloromethane solution containing  $(\eta^5\text{-C}_5\text{Me}_5)\text{Re}(\text{CO})_2\text{Br}_2$  were deposited on a silicon wafer and the solvent was allowed to evaporate. The silicon wafer was then mounted in a high conductivity copper holder and placed in a vacuum Dewar. The sample was then cooled, to 77 K, with liquid nitrogen and photolyzed for 80 seconds. The spectral changes associated with the photolysis of a film of  $(\eta^5\text{-C}_5\text{Me}_5)\text{Re}(\text{CO})_2\text{Br}_2$ , on Si(111), are summarized in Figure 4-2.

In a subsequent experiment, a cut-off filter (band pass  $\lambda > 420 \text{ nm}$ ) and a water filter (10 cm path length) with pyrex optics was placed between the light source and the sample. Spectral changes are summarized in Figure 4-3.

## Chapter 5: Photochemical reactions of $[(\eta^5\text{-C}_5\text{R}_5)\text{Mn}(\text{CO})_2(\text{NO})]^+$ ( $\text{R}_5 = \text{H}_5, \text{H}_4\text{Me}, \text{Me}_5$ ) as films and in low temperature glasses.

### 5.1 Introduction

There is a considerable amount of interest concerning the photochemistry of organometallic complexes in the gas phase<sup>72</sup> and on surfaces<sup>73</sup> due to the possible applications in the semiconductor industry. The photochemical deposition of conducting tracks directly on semiconductor surfaces is a preferable alternative to the present photoresist technologies.<sup>74</sup> Currently, one of the most significant problems with the photochemical beam writing of circuit components is that, although the initial film decomposition is photochemical, the final conversion to the metal is the result of thermal heating of the surface.<sup>75, 76b)</sup> Since the heating of the surface results in surface damage and altered interfacial properties, it would be advantageous to develop exclusively photochemical decompositions. Unfortunately, there is not a great deal known about the photochemistry of organometallics on surfaces.

Therefore, we chose to expand our study of reactions on surfaces to try to understand the basic science behind solid-state photochemistry. The cationic complexes,  $[(\eta^5\text{-C}_5\text{R}_5)\text{Mn}(\text{CO})_2(\text{NO})]^+$  ( $\text{R}_5 = \text{H}_5, \text{H}_4\text{Me}, \text{Me}_5$ ), were chosen because of their involatility and ease of <sup>15</sup>N<sup>15</sup>O labelling. Similar to the  $(\eta^5\text{-C}_5\text{Me}_5)\text{Re}(\text{CO})_2\text{Br}_2$  study, the photochemistry of surface films of  $[(\eta^5\text{-C}_5\text{R}_5)\text{Mn}(\text{CO})_2(\text{NO})]^+$  ( $\text{R}_5 = \text{H}_5, \text{H}_4\text{Me}, \text{Me}_5$ ) differed both from their photochemistry in solution and in a low temperature glass.

## 5.2 Results and Discussion

### 5.2.1 Photochemistry of $[(\eta^5\text{-C}_5\text{H}_4\text{Me})\text{Mn}(\text{CO})_2(\text{NO})][\text{PF}_6]$ in a low temperature glass

In order to compare the photochemistry in a film with that in a glass, an initial study was done in a low temperature glass. The results in a glass will be discussed before the results in a film.

A solution of  $[(\eta^5\text{-C}_5\text{H}_4\text{Me})\text{Mn}(\text{CO})_2(\text{NO})][\text{PF}_6]$  in (1,2-epoxyethyl)benzene was cooled to 77 K, forming a glass, without precipitation of the salt. Photolysis resulted in the spectral changes shown in Figure 5-1(a). The loss of intensity of the FTIR absorptions at  $2110\text{ cm}^{-1}$  and  $2070\text{ cm}^{-1}$ , associated with the carbonyls, and at  $1842\text{ cm}^{-1}$ , associated with the terminal nitrosyl, indicated the loss of starting material. Concomitant appearance of three absorption bands was observed. The band at highest energy,  $2132\text{ cm}^{-1}$ , was typical of free CO in (1,2-epoxyethyl)benzene.<sup>36</sup> The free CO band is weak and is only visible in Figures 5-1b) and 5-1c). The other two bands, at  $2050\text{ cm}^{-1}$  and  $1798\text{ cm}^{-1}$ , were assigned as due to the CO loss fragment  $[(\eta^5\text{-C}_5\text{H}_4\text{Me})\text{Mn}(\text{CO})(\text{NO})][\text{PF}_6]$ . The CO and NO absorptions of  $[(\eta^5\text{-C}_5\text{H}_4\text{Me})\text{Mn}(\text{CO})(\text{NO})][\text{PF}_6]$ , which appeared at lower energy than the absorptions due to the starting material, were consistent with the loss of a CO ligand. Photoextrusion of CO typically results in a shift of  $\nu(\text{CO})$  to lower energy.<sup>7,13,36,77</sup> The term unsaturated, as used here, is not meant to exclude the possibility of weak solvent coordination.<sup>77</sup> The assignment of the band at  $2050\text{ cm}^{-1}$  as  $\nu(\text{CO})$  and the band at  $1798\text{ cm}^{-1}$  as  $\nu(\text{NO})$  was confirmed by  $^{15}\text{NO}$  labelling. The lower energy band, at  $1798\text{ cm}^{-1}$ , appeared at  $1761\text{ cm}^{-1}$  after  $^{15}\text{NO}$  substitution (see Fig.

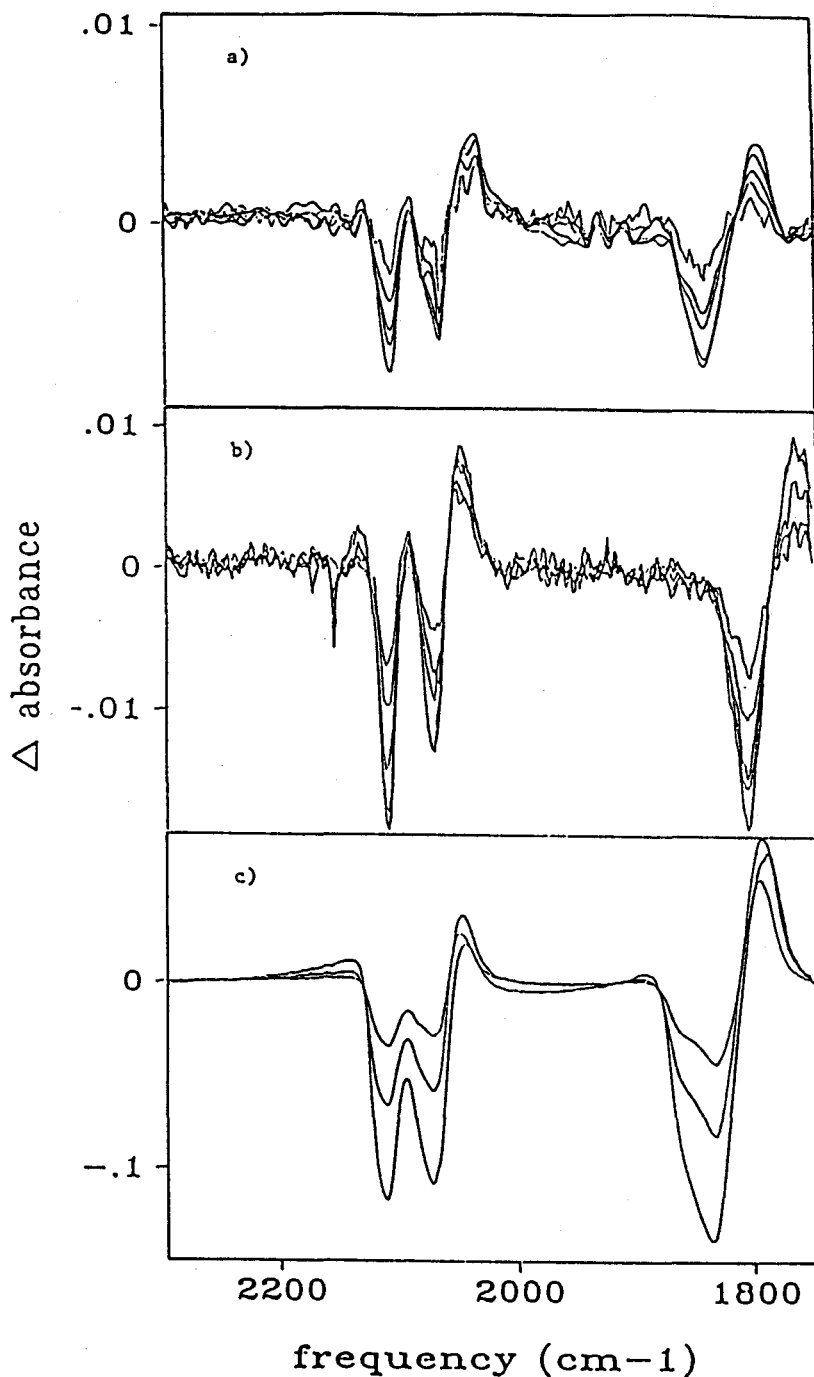
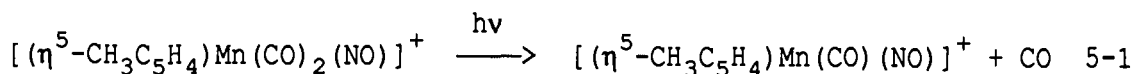


**Figure 5-1.** (a) FTIR difference spectra for the photolysis of  $[(\eta^5\text{-CH}_3\text{C}_5\text{H}_4)\text{Mn}(\text{CO})_2(\text{NO})][\text{PF}_6]$  for 15, 30, 45, 75 and 135 s at 77 K in a (1,2-epoxyethyl)-benzene glass. (b) FTIR difference spectra for the photolysis of  $[(\eta^5\text{-CH}_3\text{C}_5\text{H}_4)\text{Mn}(\text{CO})_2(^{15}\text{NO})][\text{PF}_6]$  for 15, 30, 45, 75 and 135 s at 77 K in a (1,2-epoxyethyl)-benzene glass. (c) FTIR difference spectra for the photolysis of  $[(\eta^5\text{-CH}_3\text{C}_5\text{H}_4)\text{Mn}(\text{CO})_2(\text{NO})][\text{PF}_6]$  for 15, 30 and 90 s, at 298 K in a film deposited on a Si(111) surface.

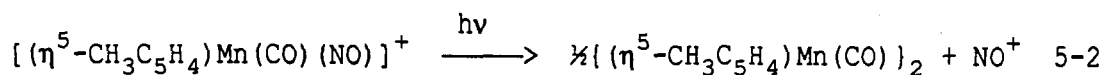
5-1(b)) whereas the 2050  $\text{cm}^{-1}$  band did not shift. The primary photoreaction in a (1,2-epoxyethyl)benzene glass at 77 K is summarized in equation 5-1. In a low temperature glass or matrix, the photochemical loss of a single CO ligand, forming an unsaturated species, is commonly observed.<sup>78</sup> However, the study on



$[(\eta^5\text{-C}_5\text{H}_4\text{Me})\text{Mn}(\text{CO})_2(\text{NO})]^+$  was a rare example of the photolysis of an ionic organometallic complex in a low temperature glass. The study of  $[(\eta^5\text{-C}_5\text{H}_4\text{Me})\text{Mn}(\text{CO})_2(\text{NO})]^+$  in a glass was possible as a result of the choice of solvent. (1,2-epoxyethyl)benzene is an excellent solvent for dissolving a variety of neutral and ionic complexes and forms a transparent glass at temperatures as low as 8 K.

The extended photolysis of a glass containing  $[(\eta^5\text{-C}_5\text{H}_4\text{Me})\text{Mn}(\text{CO})(\text{NO})][\text{PF}_6]$  resulted in further changes in the FTIR spectra. The secondary reaction was evidenced by the loss in intensity of the absorptions due to  $[(\eta^5\text{-C}_5\text{H}_4\text{Me})\text{Mn}(\text{CO})(\text{NO})][\text{PF}_6]$  and the appearance of a new band at 1728  $\text{cm}^{-1}$ . Upon  $^{15}\text{NO}$  substitution, the band at 1728  $\text{cm}^{-1}$  was unshifted. The insensitivity of the 1728  $\text{cm}^{-1}$  absorption to  $^{15}\text{NO}$  labelling indicated that it was not an NO absorption and, hence, was a CO absorption. The low energy of the CO band is indicative of a bridging mode of coordination. Therefore, the reaction was formulated as  $\text{NO}^+$  loss (see discussion in section 5.2.3) to generate a species of formula  $\{(\eta^5\text{-C}_5\text{H}_4\text{Me})\text{Mn}(\text{CO})\}_2$ . The reaction is summarized in equation 5-2. However, it should be noted that based on the IR spectral data the

formation of a trigonal planar ( $D_{3h}$ )  $[(\eta^5\text{-C}_5\text{H}_4\text{Me})\text{Mn}(\text{CO})]_3$  species can not be ruled out. In a glass,  $\{(\eta^5\text{-C}_5\text{H}_4\text{Me})\text{Mn}(\text{CO})\}_2$  was the final



observable photoproduct. Continued photolysis produced no spectral changes as monitored by FTIR spectroscopy.

### 5.2.2 Photochemistry of $[(\eta^5\text{-C}_5\text{H}_4\text{Me})\text{Mn}(\text{CO})_2(\text{NO})][\text{PF}_6]$ in a film at room temperature

The two complimentary substrates chosen for the surface studies were  $\text{CaF}_2$  and silicon. Calcium fluoride was chosen because it should have an oxide free, highly polar, surface. The silicon surface is covered by an oxide layer, the surface of which is believed to terminate with hydroxyl groups. No difference was observed in the chemistry when the films were deposited on the silicon or  $\text{CaF}_2$  surface. The studies of films deposited on silicon were done on either an untreated silicon surface or an etched surface. In industry, silicon wafers are commonly etched in a 10% hydrofluoric acid bath for 20 minutes to remove any surface oxide layer. Some of the wafers were treated with these standard cleaning procedures.<sup>79</sup> However, there was no detectable difference found between the behaviour of the untreated and the etched silicon surface. The silicon wafers were not sputtered, under high vacuum, to yield a pure silicon surface.

The substrate was unimportant as a result of the film thickness used which varied from 50 - 500 molecules/Å<sup>2</sup>. The photochemistry that occurred was in the bulk of the film and not at the film-substrate interface.

It should be pointed out that the photodecomposition of an organometallic film that is 50 - 500 molecules/Å<sup>2</sup> thick would result in a technically useful thickness of metal.<sup>80</sup> For example, the loss of all ligands in a film of 50 molecules/Å<sup>2</sup> would leave a metal surface 600 Å thick.

The initial photochemistry of  $[(\eta^5\text{-C}_5\text{H}_4\text{Me})\text{Mn}(\text{CO})_2(\text{NO})]^+$  was the same in a low temperature glass as in a film deposited on a surface. The initial result of the photolysis of a film of  $[(\eta^5\text{-CH}_3\text{C}_5\text{H}_4)\text{Mn}(\text{CO})_2(\text{NO})]^+$  was CO loss. The spectral changes associated with the photolysis of  $[(\eta^5\text{-C}_5\text{H}_4\text{Me})\text{Mn}(\text{CO})_2(\text{NO})]^+$ , deposited as a film on silicon, are illustrated in Figure 5-1(c). The photosensitivity of  $[(\eta^5\text{-C}_5\text{H}_4\text{Me})\text{Mn}(\text{CO})_2(\text{NO})]^+$  at 77 K in a glass and at ambient temperature in a film appeared to be comparable as evidenced by the spectral changes in Figure 5-1. The new bands, associated with the unsaturated species,  $[(\eta^5\text{-C}_5\text{H}_4\text{Me})\text{Mn}(\text{CO})(\text{NO})]^+$ , were only slightly shifted relative to the frequencies observed for the same species in a low temperature glass. In a room temperature film the bands due to coordinated CO and NO appeared at 2058 cm<sup>-1</sup> and 1803 cm<sup>-1</sup>, respectively. Whereas, in a glass the coordinated CO and NO bands appeared at 2050 cm<sup>-1</sup> and 1798 cm<sup>-1</sup>, respectively. The band at 1803 cm<sup>-1</sup>, in a film, was confirmed as being due to coordinated NO by <sup>15</sup>N<sup>15</sup>O substitution which resulted in a 34 cm<sup>-1</sup> shift to lower energy. The shift observed in the glass, as a result of

$^{15}\text{NO}$  substitution was  $37\text{ cm}^{-1}$ . This indicates that in a glass only weak solvation may have occurred. The basic reaction, described above, was insensitive to the choice of counter-ion ( $[\text{PF}_6]^-$ ,  $[\text{BF}_4]^-$  or  $[\text{ClO}_4]^-$ ) or to a change in methylation at the cyclopentadienyl ring (Table 5-1). The spectral data for the intermediates formed from the various salts are summarized in Table 5-1.

Room temperature photolysis of the photogenerated  $[(\eta^5\text{-C}_5\text{H}_4\text{Me})\text{Mn}(\text{CO})(\text{NO})][\text{PF}_6]$  species resulted in the loss of absorption bands due to the coordinated CO and NO ligands at  $2058\text{ cm}^{-1}$  and  $1803\text{ cm}^{-1}$ . The concomitant production of a single absorption band at  $1628\text{ cm}^{-1}$  was observed. This photoproduct was shown to be a result of the photolysis of  $[(\eta^5\text{-C}_5\text{H}_4\text{Me})\text{Mn}(\text{CO})(\text{NO})][\text{PF}_6]$  rather than the precursor molecule,  $[(\eta^5\text{-C}_5\text{H}_4\text{Me})\text{Mn}(\text{CO})_2(\text{NO})][\text{PF}_6]$ , by careful analysis of the growth of the bands. After the initial formation of the monocarbonyl, the absorption at  $1628\text{ cm}^{-1}$  was detected. The intensity of the band at  $1628\text{ cm}^{-1}$  increased to a maximum, concurrent with the increase in intensity of the bands due to the monocarbonyl. As the absorptions due to the monocarbonyl decreased, the intensity of the  $1628\text{ cm}^{-1}$  band also decreased indicating that it was photosensitive as well. No effect on the position of the  $1628\text{ cm}^{-1}$  band was observed upon  $^{15}\text{NO}$  substitution. Hence, the broad band at  $1628\text{ cm}^{-1}$  was attributed to bridging CO groups as the film degraded. It is possible that if a pure material was recovered it would be polymeric  $\{(\eta^5\text{-C}_5\text{H}_4\text{Me})\text{Mn}(\text{CO})\}_n$ . The  $\{(\eta^5\text{-C}_5\text{H}_4\text{Me})\text{Mn}(\text{CO})\}_n$  intermediate was also observed for  $[(\eta^5\text{-C}_5\text{H}_5)\text{Mn}(\text{CO})(\text{NO})][\text{PF}_6]$ , but it was not for  $[(\eta^5\text{-C}_5\text{Me}_5)\text{Mn}(\text{CO})(\text{NO})][\text{PF}_6]$ .



Table 5-1

## FTIR Spectral Data

Complex	Medium	$\nu(\text{CO})$ ( $\text{cm}^{-1}$ )	$\nu(\text{NO})$ ( $\text{cm}^{-1}$ )	Temp (K)
$[(\eta^5\text{-CH}_3\text{C}_5\text{H}_4)\text{Mn}(\text{CO})_2(\text{NO})][\text{PF}_6]$	Film	2114, 2074	1844	298
$[(\eta^5\text{-CH}_3\text{C}_5\text{H}_4)\text{Mn}(\text{CO})_2(\text{NO})][\text{PF}_6]$	Film	2108, 2067	1838	77
	Glass <sup>a</sup>	2110, 2070	1842	
$[(\eta^5\text{-CH}_3\text{C}_5\text{H}_4)\text{Mn}(\text{CO})_2(\text{NO})][\text{BF}_4]$	Film	2112, 2071	1840	298
$[(\eta^5\text{-CH}_3\text{C}_5\text{H}_4)\text{Mn}(\text{CO})_2(\text{NO})][\text{ClO}_4]$	Film	2110, 2068	1844	298
$[(\eta^5\text{-CH}_3\text{C}_5\text{H}_4)\text{Mn}(\text{CO})_2(^{15}\text{NO})][\text{PF}_6]$	Film	2114, 2076	1813	298
$[(\eta^5\text{-CH}_3\text{C}_5\text{H}_4)\text{Mn}(\text{CO})_2(^{15}\text{NO})][\text{PF}_6]$	Film	2106, 2064	1809	77
	Glass	2110, 2076	1805	298
$[(\eta^5\text{-C}_5\text{H}_5)\text{Mn}(\text{CO})_2(^{15}\text{NO})][\text{PF}_6]$	Film	2116, 2075	1846	298
$[(\eta^5\text{-C}_5\text{Me}_5)\text{Mn}(\text{CO})_2(^{15}\text{NO})][\text{PF}_6]$	Film	2089, 2042	1815	298
$[(\eta^5\text{-CH}_3\text{C}_5\text{H}_4)\text{Mn}(\text{CO})(\text{NO})][\text{PF}_6]$	Film	2058	1803	298
	Glass	2050	1798	
$[(\eta^5\text{-CH}_3\text{C}_5\text{H}_4)\text{Mn}(\text{CO})(\text{NO})][\text{BF}_4]$	Film	2048	1794	298
$[(\eta^5\text{-CH}_3\text{C}_5\text{H}_4)\text{Mn}(\text{CO})(\text{NO})][\text{ClO}_4]$	Film	2048	1794	298
$[(\eta^5\text{-CH}_3\text{C}_5\text{H}_4)\text{Mn}(\text{CO})(^{15}\text{NO})][\text{PF}_6]$	Film	2056	1769	298
	Glass	2048	1761	
$[(\eta^5\text{-C}_5\text{H}_5)\text{Mn}(\text{CO})(\text{NO})][\text{PF}_6]$	Film	2058	1803	298
$[(\eta^5\text{-C}_5\text{Me}_5)\text{Mn}(\text{CO})(\text{NO})][\text{PF}_6]$	Film	2023	1770	298
$[(\eta^5\text{-CH}_3\text{C}_5\text{H}_4)\text{Mn}(\text{CO})][\text{PF}_6]$	Film	2019		77
$[(\eta^5\text{-CH}_3\text{C}_5\text{H}_4)\text{Mn}(\text{CO})]$	Film	1929		77
$\{(\eta^5\text{-CH}_3\text{C}_5\text{H}_4)\text{Mn}(\mu\text{-CO})\}_2$	Film	1695		77
	Glass	1727		

Table 5-1 (Continued)

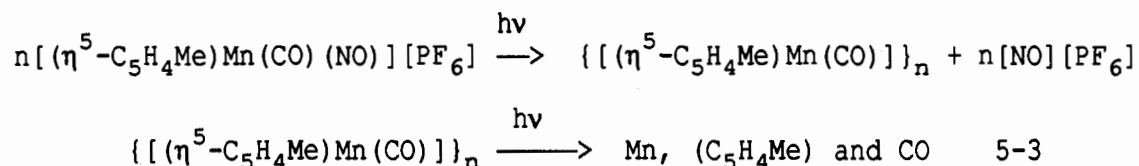
Complex <sup>a</sup>	Medium	ν (CH) (cm <sup>-1</sup> )
[(η <sup>5</sup> -CH <sub>3</sub> C <sub>5</sub> H <sub>4</sub> )Mn(CO) <sub>2</sub> ( <sup>14</sup> NO)][PF <sub>6</sub> ]	Film	3123
[(η <sup>5</sup> -CH <sub>3</sub> C <sub>5</sub> H <sub>4</sub> )Mn(CO) <sub>2</sub> ( <sup>14</sup> NO)][BF <sub>4</sub> ]	Film	3113
[(η <sup>5</sup> -CH <sub>3</sub> C <sub>5</sub> H <sub>4</sub> )Mn(CO) <sub>2</sub> (NO)][ClO <sub>4</sub> ]	Film	3106
[(η <sup>5</sup> -CH <sub>3</sub> C <sub>5</sub> H <sub>4</sub> )Mn(CO) <sub>2</sub> ( <sup>15</sup> NO)][PF <sub>6</sub> ]	Film	3125
[(η <sup>5</sup> -C <sub>5</sub> H <sub>5</sub> )Mn(CO) <sub>2</sub> ( <sup>15</sup> NO)][PF <sub>6</sub> ]	Film	3122

a) all glass measurements were conducted at 77 K

Upon subsequent photolysis, the band due to  $\{(\eta^5\text{-C}_5\text{H}_4\text{Me})\text{Mn}(\text{CO})\}_n$  no longer increased although other changes occurred. Prolonged photolysis led to the loss of bands due to both the coordinated ring system and the bridging CO's. The fact that the bridging carbonyls were lost was evidenced by a decrease in intensity of the absorption at  $1628\text{ cm}^{-1}$ . Loss of the methylcyclopentadienyl ligand was consistent with the loss of the sharp  $\nu(\text{CH})$  band at  $3123\text{ cm}^{-1}$  and the  $\nu(\text{CC})$  band at  $1429\text{ cm}^{-1}$ . The loss of the methylcyclopentadienyl absorptions was accompanied by the appearance of two broad  $\nu(\text{CH})$  bands at  $2918\text{ cm}^{-1}$  and  $2855\text{ cm}^{-1}$ . Analogously, when  $[(\eta^5\text{-C}_5\text{H}_5)\text{Mn}(\text{CO})(\text{NO})][\text{PF}_6]$  was photolyzed, the appearance of two broad  $\nu(\text{CH})$  bands at  $2937\text{ cm}^{-1}$  and  $2859\text{ cm}^{-1}$  was consistent with the loss of the coordinated cyclopentadienyl moiety. An analogous observation could not be made for the photolysis of  $[(\eta^5\text{-C}_5\text{Me}_5)\text{Mn}(\text{CO})(\text{NO})][\text{PF}_6]$  since there was no aromatic CH band. However, the appearance of two broad CH bands at  $2924\text{ cm}^{-1}$  and  $2864\text{ cm}^{-1}$  was consistent with the loss of the  $\text{C}_5\text{Me}_5$  ligand. In each case, mentioned above, the two bands in the  $2800\text{ cm}^{-1} - 3000\text{ cm}^{-1}$  region was consistent with the loss of the aromaticity of the cyclopentadienyl ring and the formation of hydrocarbon products derived from the cyclopentadienyl ring.

Associated with this, the final observed photoreaction resulted in the appearance of two peaks at  $1260\text{ cm}^{-1}$  and  $1160\text{ cm}^{-1}$ . These bands were insensitive to the change of methylation at the cyclopentadienyl ring and to  $^{15}\text{NO}$  substitution. The low energy bands, at  $1260\text{ cm}^{-1}$  and  $1160\text{ cm}^{-1}$ , were of comparable intensity to  $\nu(\text{NO})$  for the highest attained concentrations of  $[(\eta^5\text{-C}_5\text{H}_4\text{Me})\text{Mn}(\text{CO})(\text{NO})][\text{PF}_6]$ . The assignment of the

two bands was not obvious; however, it was confirmed that they were associated with the decomposition of the  $[\text{PF}_6]^-$  ion. The separate deposition and decomposition of  $[\text{NO}][\text{PF}_6]$ , on a silicon surface, gave rise to two bands in the same positions. The bands at  $1260 \text{ cm}^{-1}$  and  $1160 \text{ cm}^{-1}$  were not observed when the analogous  $[\text{ClO}_4]^-$  or  $[\text{BF}_4]^-$  salts were photolyzed. However, the  $[\text{ClO}_4]^-$  and  $[\text{BF}_4]^-$  salts gave rise to other intense bands in the same region as the  $[\text{PF}_6]^-$  salt. When the  $[\text{BF}_4]^-$  salt was photolyzed a broad band was observed at  $1172 \text{ cm}^{-1}$  concurrent with the loss of the  $1062 \text{ cm}^{-1}$  band associated with the  $[\text{BF}_4]^-$  ion. Similarly, the photolysis of the  $[\text{ClO}_4]^-$  salt showed a loss of the high energy band at  $1099 \text{ cm}^{-1}$ , due to the  $[\text{ClO}_4]^-$  ion, and the appearance of a single band at  $1167 \text{ cm}^{-1}$ . The final photoreaction was proposed to occur as shown in equation 5-3.

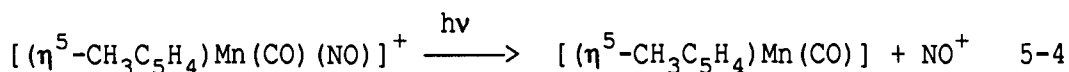


### 5.2.3 Photochemistry of $[(\eta^5\text{-C}_5\text{H}_4\text{Me})\text{Mn}(\text{CO})_2(\text{NO})][\text{PF}_6]$ in a film at low temperature

The result of the initial photolysis of a  $[(\eta^5\text{-C}_5\text{H}_4\text{Me})\text{Mn}(\text{CO})_2(\text{NO})]^+$  film, at 77 K, was the photoextrusion of a CO ligand. Although the photoextrusion of CO occurred at 77 K, the efficiency of the photoreaction was much lower than was observed for a room temperature film. The subsequent photochemistry of  $[(\eta^5\text{-C}_5\text{H}_4\text{Me})\text{Mn}(\text{CO})(\text{NO})]^+$  was temperature dependent.

Photolysis of the primary photoproduct,  $[(\eta^5\text{-C}_5\text{H}_4\text{Me})\text{Mn}(\text{CO})(\text{NO})]^+$ ,

at 77 K led to the loss of its absorption bands. Concomitant with the loss of the bands due to  $[(\eta^5\text{-C}_5\text{H}_4\text{Me})\text{Mn}(\text{CO})(\text{NO})]^+$  was the growth of three new bands at  $2232\text{ cm}^{-1}$ ,  $1929\text{ cm}^{-1}$  and  $1695\text{ cm}^{-1}$ . The band at  $2232\text{ cm}^{-1}$  shifts to  $2158\text{ cm}^{-1}$  as a result of  $^{15}\text{NO}$  labelling. The high energy band, at  $2232\text{ cm}^{-1}$ , was associated with the formation of  $\text{NO}^+$  in the film.<sup>81</sup> The band at  $1929\text{ cm}^{-1}$  was consistent with the formation of a new metal carbonyl species,  $[(\eta^5\text{-C}_5\text{H}_4\text{Me})\text{Mn}(\text{CO})]$ . The production of a neutral metal carbonyl fragment and free  $\text{NO}^+$  is summarized in equation



5-4. The remaining band, at  $1695\text{ cm}^{-1}$ , was not associated with the  $[(\eta^5\text{-C}_5\text{H}_4\text{Me})\text{Mn}(\text{CO})]$  complex as prolonged photolysis led to a continued increase in the intensity of the band at  $1929\text{ cm}^{-1}$ , whereas  $[(\eta^5\text{-C}_5\text{H}_4\text{Me})\text{Mn}(\text{CO})]$  reached a steady state concentration. Therefore, the low energy band at  $1695\text{ cm}^{-1}$  which was consistent with the formation of a bridging carbonyl was assigned to the formation of  $\{(\eta^5\text{-C}_5\text{H}_4\text{Me})\text{Mn}(\text{CO})\}_2$ . The complex,  $\{(\eta^5\text{-C}_5\text{H}_4\text{Me})\text{Mn}(\text{CO})\}_2$ , had an absorption band at  $1728\text{ cm}^{-1}$  in a low temperature glass. The  $33\text{ cm}^{-1}$  difference, between the absorption energy in the film and the glass, may have been the result of increased aggregation in the film. Alternatively, the  $33\text{ cm}^{-1}$  difference may be the result of solvation in the glass. The assignment of the low energy band as being due to a bridging carbonyl was supported by  $^{15}\text{NO}$  labelling which had no effect on the position of the band. The formation of the dimer complex is given in equation 5-2 and was competitive with the  $\text{NO}^+$  loss reaction summarized in equation 5-4. The supposition that the above result arose

from the photochemistry of the initial CO loss product was confirmed by the photolysis of  $[(\eta^5\text{-C}_5\text{H}_4\text{Me})\text{Mn}(\text{CO})(\text{NO})]^+$ , at 77 K, after its initial formation by room temperature photolysis.

Further photolysis of the film at 77 K resulted in the production of a sharp absorption band at  $2019\text{ cm}^{-1}$ . The absorption energy was insensitive to  $^{15}\text{NO}$  substitution. We were unable to determine what complex gave rise to the  $2019\text{ cm}^{-1}$  absorption, however, the band is consistent with coordinated CO. The complex was tentatively assigned as  $[(\eta^5\text{-C}_5\text{H}_4\text{Me})\text{Mn}(\text{CO})][\text{PF}_6]$ . The by-product of the formation of  $[(\eta^5\text{-C}_5\text{H}_4\text{Me})\text{Mn}(\text{CO})][\text{PF}_6]$  should be NO. However, no free NO was detected which may have been a result of its loss to vacuum.

Warming the sample resulted in a loss of the  $2232\text{ cm}^{-1}$  absorption assigned to  $\text{NO}^+$ , a further increase of the absorptions due to  $[(\eta^5\text{-C}_5\text{H}_4\text{Me})\text{Mn}(\text{CO})]$  and  $[(\eta^5\text{-C}_5\text{H}_4\text{Me})\text{Mn}(\text{CO})][\text{PF}_6]$  at  $1929\text{ cm}^{-1}$  and  $2019\text{ cm}^{-1}$  respectively, and the appearance of a band at  $1674\text{ cm}^{-1}$ . The band at  $1674\text{ cm}^{-1}$ , which was unchanged after  $^{15}\text{NO}$  substitution, was attributed to bridging CO groups within the film. At 77 K, an analogous band was observed at  $1695\text{ cm}^{-1}$ . The lower energy of the  $1695\text{ cm}^{-1}$  band, as the sample was warmed, was attributed to increased aggregation with increasing temperature.

After photolysing a  $[(\eta^5\text{-C}_5\text{H}_4\text{Me})\text{Mn}(\text{CO})_2(\text{NO})][\text{PF}_6]$  film, at 77 K, for 72 hours the observed final products were  $[(\eta^5\text{-C}_5\text{H}_4\text{Me})\text{Mn}(\text{CO})]$ ,  $\{(\eta^5\text{-C}_5\text{H}_4\text{Me})\text{Mn}(\text{CO})\}_2$ , and  $[(\eta^5\text{-C}_5\text{H}_4\text{Me})\text{Mn}(\text{CO})]^+$ . However, this was probably the result of the reduced photosensitivity of the films at 77 K. The photoextrusion of all ligands from a film of  $[(\eta^5\text{-C}_5\text{H}_4\text{Me})\text{Mn}(\text{CO})_2(\text{NO})][\text{PF}_6]$ , at room temperature, was achieved in less

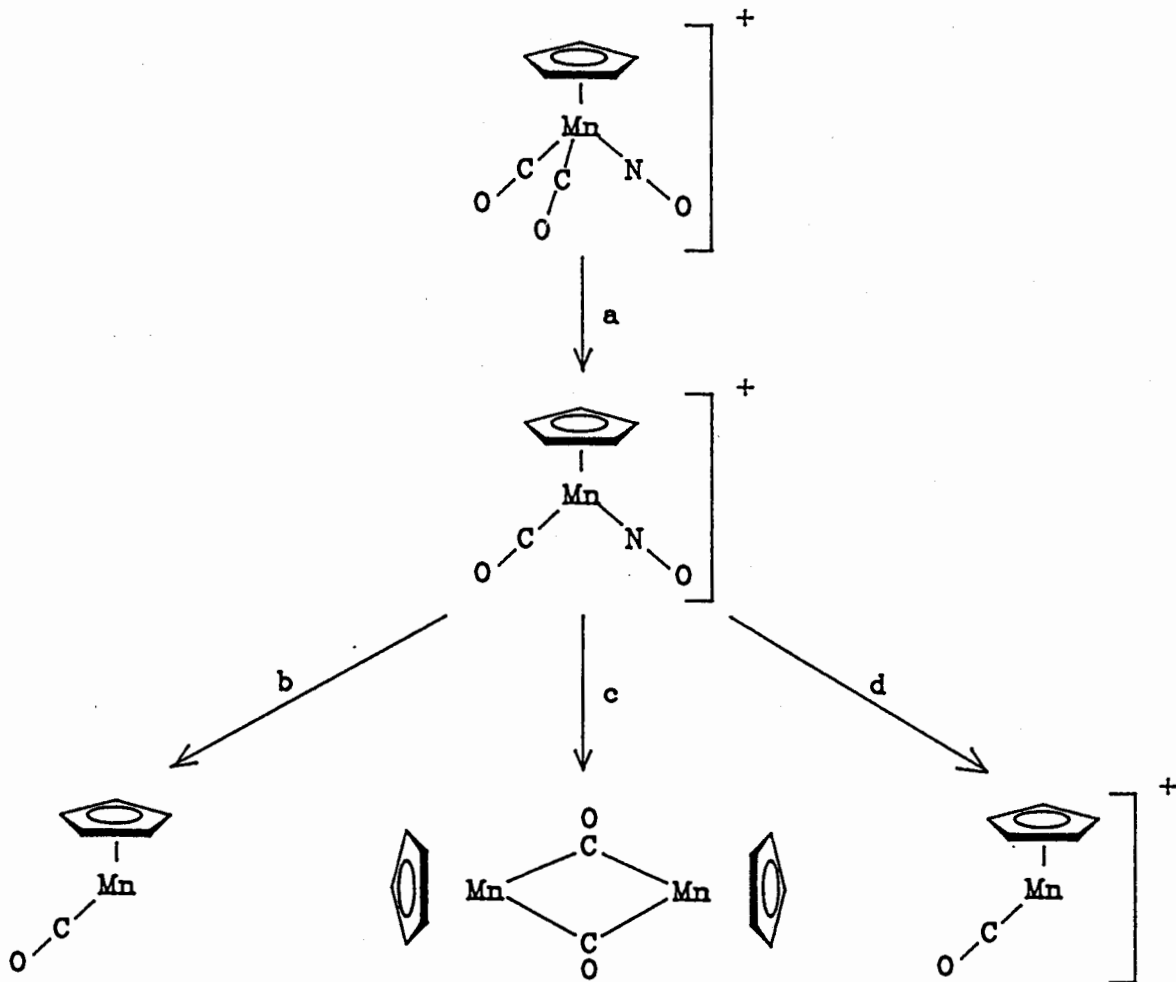


Figure 5-2.

Scheme of the photoreactions of  $(\eta^5\text{-C}_5\text{R}_5)\text{Mn}(\text{CO})_2(\text{NO})^+[\text{PF}_6]^-$  in a low temperature glass and in a film: (a) Photolysis in a glass or film at 77 K and in a film at 298 K; (b) Photolysis in a film at 77 K; (c) Photolysis in a glass at 77 K; (d) Photolysis in a film at 77 K.

than 24 hours. Presumably, if the films at 77 K were photolyzed for several days all ligands would have been lost as was the case for the room temperature films.

### 5.3 Conclusions

The photochemistry of  $[(\eta^5\text{-C}_5\text{H}_4\text{Me})\text{Mn}(\text{CO})_2(\text{NO})][\text{PF}_6]$  in different media is summarized in Figure 5-2. The loss of CO was the observed primary photoprocess for  $[(\eta^5\text{-C}_5\text{H}_4\text{Me})\text{Mn}(\text{CO})_2(\text{NO})][\text{PF}_6]$  whether in a low temperature glass or in a film. In a low temperature glass,  $\text{NO}^+$  loss followed CO loss. However, loss of both  $\text{NO}^+$  and NO was found to occur in a film. The observed products in a film were different from those found in a glass. In a film, aggregated and isolated  $(\eta^5\text{-C}_5\text{R}_5)\text{Mn}(\text{CO})$  fragments were produced, whereas only dimers were observed in a glass. Extended photolysis of a film, at room temperature, resulted in the loss of all ligands.

The study of  $[(\eta^5\text{-C}_5\text{R}_5)\text{Mn}(\text{CO})_2(\text{NO})]^+$  ( $\text{R}_5 = \text{H}_5, \text{H}_4\text{Me}, \text{Me}_5$ ) showed that a low energy photolytic process could result in the efficient reaction of organometallics in a film. However, the most important result of this study was that we were able to follow the photo-decomposition of organometallics that were deposited as surface films. It is apparent that photochemistry in the solid-state is rich and varied and deserves further study.

### 5.4 Experimental Section

The complexes  $[(\eta^5\text{-C}_5\text{H}_4\text{Me})\text{Mn}(\text{CO})_2(\text{NO})][\text{PF}_6]^{76a)}$  and  $[(\eta^5\text{-C}_5\text{H}_5)\text{Mn}(\text{CO})_2(\text{NO})][\text{PF}_6]^{82}$  were prepared by standard literature



methods.

The  $\text{CaF}_2$  crystals were purchased from Wilmad Glass Co. Inc.. The Si(111) wafers were obtained from Pacific Microelectronics Centre, Canada. The wafers were p-type with tolerances and specifications according to SEMI Standard M1.1.STD.5. The 4" wafers were cut to approximately 1cm x 1cm dimensions as required. The  $\text{Na}^{15}\text{NO}_2$  was purchased from MSD Isotopes and was 99 at.% enriched.

The Fourier transform infrared transmission spectra were collected using  $4\text{ cm}^{-1}$  resolution on a BOMEM Michelson M-120 FTIR spectrophotometer. The samples were held in a  $\text{CaF}_2$  faced cell for the glasses, or a high conductivity copper sample mount within a  $\text{CaF}_2$  faced vacuum Dewar (for the films).

The light source was a 100 W high pressure mercury lamp in an Oriel housing equipped with condenser lenses and filtered through a 10 cm water filter with pyrex optics (bandpass  $\lambda > 313\text{ nm}$ ).

#### 5.4.1 Preparation of $[(\eta^5\text{-C}_5\text{H}_4\text{Me})\text{Mn}(\text{CO})_2(\text{NO})][\text{X}]$ ( $\text{X} = [\text{BF}_4], [\text{ClO}_4]$ )

The salts  $[(\eta^5\text{-C}_5\text{H}_4\text{Me})\text{Mn}(\text{CO})_2(\text{NO})][\text{X}]$  ( $\text{X} = [\text{BF}_4], [\text{ClO}_4]$ ) may be prepared by the same procedure<sup>76a)</sup> as  $[(\eta^5\text{-C}_5\text{H}_4\text{Me})\text{Mn}(\text{CO})_2(\text{NO})][\text{PF}_6]$  using  $[\text{NH}_4][\text{BF}_4]$  and  $[\text{Na}][\text{ClO}_4]$  respectively, instead of  $[\text{NH}_4][\text{PF}_6]$ .

#### 5.4.2 Preparation of $[(\eta^5\text{-C}_5\text{H}_4\text{Me})\text{Mn}(\text{CO})_2(^{15}\text{NO})][\text{PF}_6]$

A solution of 0.320 g (1.47 mmol) of  $(\eta^5\text{-C}_5\text{H}_4\text{Me})\text{Mn}(\text{CO})_3$  in 5 ml of 95% EtOH and 0.9 ml of concentrated hydrochloric acid was heated to the boiling point and, at that temperature, a solution of 0.105 g (1.50 mmol) of  $\text{Na}^{15}\text{NO}_2$  in 0.25 ml of water was added. The reaction

mixture was allowed to boil for 5 min and then filtered, while hot, into a stirred solution of 0.3 g (1.8 mmol) of  $\text{NH}_4\text{PF}_6$  in 0.5 ml of water. After the mixture was allowed to cool to room temperature, the product was filtered, washed with  $\text{CH}_2\text{Cl}_2$  and dried under vacuum for 3 hours.

#### 5.4.3 Preparation of $[(\eta^5\text{-C}_5\text{Me}_5)\text{Mn}(\text{CO})_2(\text{NO})][\text{PF}_6]$

The complex  $[(\eta^5\text{-C}_5\text{Me}_5)\text{Mn}(\text{CO})_2(\text{NO})][\text{PF}_6]$ , prepared in our lab previously, may be prepared by the same method as  $[(\eta^5\text{-C}_5\text{H}_4\text{Me})\text{Mn}(\text{CO})_2(\text{NO})][\text{PF}_6]$ . However, the separation procedure was altered. The product, which was initially obtained from water-ethanol, was washed with hexane and then dissolved in dichloromethane. The product was recovered by precipitation using hexane.

#### 5.4.4 Photolysis of the compounds on a silicon surface

All of the experiments were conducted in an analogous manner. Therefore, a typical experiment will be described. A solution of  $[(\eta^5\text{-C}_5\text{H}_4\text{Me})\text{Mn}(\text{CO})_2(\text{NO})][\text{PF}_6]$  in methanol was prepared and 3-4 drops were placed on the Si(111) surface. After the solvent had evaporated, a film of  $[(\eta^5\text{-C}_5\text{H}_4\text{Me})\text{Mn}(\text{CO})_2(\text{NO})][\text{PF}_6]$  remained on the surface. The sample was transferred to a vacuum Dewar, evacuated, and cooled to 77 K. The Dewar was mounted on the optical bench of the FTIR spectrophotometer and the spectrum was obtained. Subsequently, the sample was photolyzed for 15, 30 and 90 s. A spectrum was collected after each photolysis. The spectral data and figures are given in Table 5-1 and Figure 5-1(c), respectively. The spectra obtained on a  $\text{CaF}_2$  surface were done in the

same manner.

The compounds,  $[\text{NO}][\text{PF}_6]$ ,  $[\text{NO}][\text{ClO}_4]$  and  $[\text{NO}][\text{BF}_4]$ , were independently deposited from a methanol solution on the silicon substrate. The resultant films were photodecomposed at both room temperature and 77 K utilizing the optical setup mentioned above.

Approximate surface coverages were determined in the following way. An aliquot (0.05 ml) taken from a stock solution of  $[(\eta^5\text{-C}_5\text{H}_4\text{Me})\text{Mn}(\text{CO})_2(\text{NO})][\text{PF}_6]$  (0.012 M) was deposited on the Si(111) surface in a dropwise fashion. The film area was  $0.785 \text{ cm}^2$  and the number of moles deposited was  $6 \times 10^{-7}$ . The final coverage was approximately  $5 \times 10^{17}$  molecules/ $\text{cm}^2$ . The results in Figure 5-1 represent the use of 10 drops. The results were independent of coverage in the range  $(5 - 50) \times 10^{17}$  molecules/ $\text{cm}^2$ .

## Chapter 6: The Photochemistry of $trans-(Et_3P)_2Ni(N_3)_2$ :

### Photodeposition of Nickel Films.

#### 6.1 Introduction

As mentioned previously, in Chapter 5, there is a limited amount of published information regarding the photochemistry of inorganic and organometallic species in the solid-state. The study of  $[(\eta^5-C_5R_5)Mn(CO)_2(NO)]^+$  showed that the photolysis of films of organometallic complexes containing CO ligands may result in the formation of dimers with bridging CO groups. The subsequent photolytic decomposition of these CO bridged dimer complexes could only be achieved, in a reasonable time-scale, in the case of a room temperature film. Also, the photoextrusion of the  $(\eta^5-C_5R_5)$  moiety resulted in hydrocarbon products being retained in the film.

In this study the azide ligand was chosen in order to circumvent the problems associated with the  $(\eta^5-C_5R_5)$  ligand. There is precedent in the literature that, in solution, the loss of  $N_2$  from a coordinated azide ligand and the loss of the azide ligand as a radical may be induced photochemically.<sup>83</sup> A recent study of the photochemistry of a related Ni(II) bis-azide complex  $(Ni(tet-a)(N_3)_2)$  was found to be consistent with both  $N_2$  loss and azide radical loss.<sup>84</sup> Hence, the azide ligand was an anionic ligand that could replace  $(\eta^5-C_5R_5)$  and was known to undergo photochemical decomposition. Since the azide ligand photodecomposes, the chance of dimer formation via a bridging azide should be remote. The  $^{15}N$  labelling of azide ligands is simple and may

yield additional information aiding in the characterization of intermediates. It is also important to point out that the azido group is an intense absorber in the IR which should allow the study of lower surface coverages than were possible in our previous studies.<sup>85,86</sup> The neutral ligand CO was not used in this study. The ligand  $\text{PEt}_3$ , which does not normally coordinate in a bridging manner was used. The high volatility of  $\text{PEt}_3$  also made it an ideal choice for this study since it was expected that the free  $\text{PEt}_3$  ligand would be lost from the surface. Therefore, the photochemical loss of all ligands from *trans*- $(\text{Et}_3\text{P})_2\text{Ni}(\text{N}_3)_2$  would leave metallic nickel which is used as part of a contact mixture for n-type ohmic contacts in GaAs devices.<sup>87</sup>

Also, in order that we could better interpret the photochemistry, the crystal structure of *trans*- $(\text{Et}_3\text{P})_2\text{Ni}(\text{N}_3)_2$  was determined by Professor Fred Einstein and Dr. Ray Batchelor (Simon Fraser University).<sup>88</sup> Discussed in this chapter is the photochemistry of *trans*- $(\text{Et}_3\text{P})_2\text{Ni}(\text{N}_3)_2$  films.

## 6.2 Results and Discussion

### 6.2.1 Spectroscopic data for the complexes.

The UV/Vis transitions of *trans*- $(\text{Et}_3\text{P})_2\text{Ni}(\text{N}_3)_2$  and related complexes<sup>89</sup> are summarized in Table 6-1. The lowest energy band was assigned to d-d transitions. Three transitions are expected in this region.<sup>90,91</sup> The lowest energy transition that was expected,  $d_z^2 \rightarrow d_{x^2-y^2}$ , was not resolved from the next highest energy transition,  $d_{xz,yz} \rightarrow d_{x^2-y^2}$ . The third d-d transition,  $d_{xy} \rightarrow d_{x^2-y^2}$ , was expected

Table 6-1

UV/Vis data for the relevant complexes<sup>a</sup>

Complex	LMCT	d-d ( $\epsilon$ )
	$\lambda$ (nm) $\epsilon$ ( $M^{-1} \text{ cm}^{-1}$ )	$\lambda$ (nm) $\epsilon$ ( $M^{-1} \text{ cm}^{-1}$ )
<i>trans</i> -(Et <sub>3</sub> P) <sub>2</sub> Ni(N <sub>3</sub> ) <sub>2</sub>	364 (10,000)	476 (230)
<i>trans</i> -(Et <sub>3</sub> P) <sub>2</sub> Ni(N <sub>3</sub> ) <sub>2</sub> <sup>b</sup>	360 (100) <sup>c</sup>	470 (2.5) <sup>c</sup>
<i>trans</i> -(Et <sub>3</sub> P) <sub>2</sub> Ni(Cl) <sub>2</sub> <sup>d</sup>	370 (14,200)	490 (450)
<i>trans</i> -(Et <sub>3</sub> P) <sub>2</sub> Ni(Br) <sub>2</sub> <sup>d</sup>	400 (6,200)	542 (350)
<i>trans</i> -(Et <sub>3</sub> P) <sub>2</sub> Ni(I) <sub>2</sub> <sup>d</sup>	373 (4,690) 459 (2,900)	610 (485)

- a) Spectra obtained in benzene unless otherwise stated.  
 b) Absorption spectra recorded on a film deposited on a quartz surface.  
 c) Intensity data is on an arbitrary scale and should be regarded with caution due to scattering.  
 d) Literature values from reference 89.

at slightly higher energy and resulted in a distinct asymmetry of the d-d absorption band. The next absorption band, which was resolved, was assigned to the  $N_3^-(\pi) \rightarrow d_{x^2-y^2}$  LMCT transition. The tentative assignments, stated above, were based on the assignments given for the halogen complexes,  $(Me_3P)_2Ni(X)_2$  ( $X = Cl, Br, I$ ).<sup>90</sup>

The first important feature in the data summarized in Table 6-1, is that the positions of the absorption maxima (LMCT and d-d) for the diazide complex changed only slightly upon changing from a non polar solvent (benzene) to a surface film (on quartz). The lack of a shift in the absorbance maxima of  $trans-(Et_3P)_2Ni(N_3)_2$  was consistent with the non coordinating nature of benzene and the absence of any significant interaction between molecules in the solid film. The variation of the UV/Vis absorption maxima of the dihalide nickel complexes was as expected. The high energy LMCT bands of the dihalogen complexes followed the trend expected from the optical electronegativities of Cl, Br, and I.<sup>91</sup> Analogously, the d-d transitions decrease in energy as a result of changing the halogens from Cl to Br to I as expected from the spectrochemical series.<sup>91</sup>

The FTIR spectra, in the region of azide antisymmetric stretches, of  $trans-(Et_3P)_2Ni(N_3)_2$  on a Si(111) surface is shown in Figure 6-1a). Since the plot of absorbance versus molecules per  $\text{\AA}^2$ , Fig. 6-1b), was linear over the concentration range studied it did not appear that any detectable thermal chemistry occurred upon film deposition. From the dimensions determined crystallographically the areal coverage of a molecule of  $trans-(Et_3P)_2Ni(N_3)_2$  was found to be  $64 \text{\AA}^2$ .<sup>88</sup> Assuming similar dimensions in the film, a total coverage of 1 molecule per  $\text{\AA}^2$

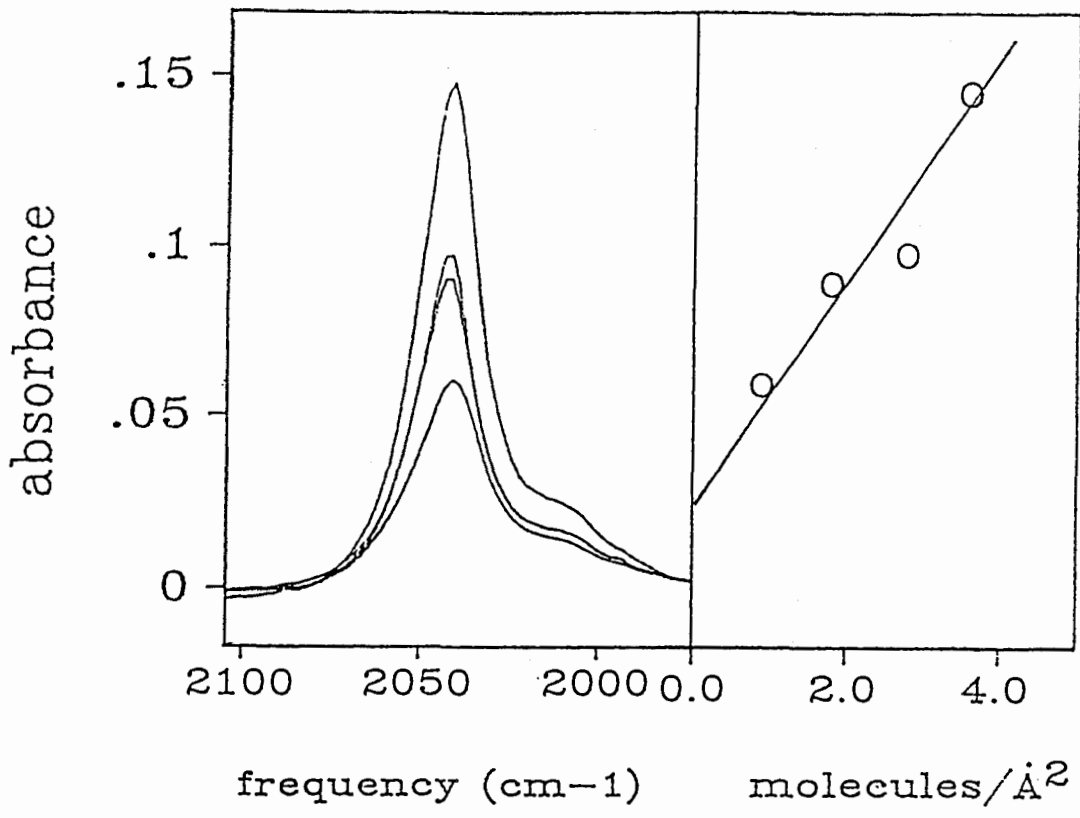


Figure 6-1

- a) A figure showing the antisymmetric azide stretch of  $\text{trans}-(\text{Et}_3\text{P})_2\text{Ni}(\text{N}_3)_2$  as a function of the amount deposited as a film.
- b) A plot of absorbance vs.  $\text{molecules}/\text{\AA}^2$  for the antisymmetric azide stretch of  $\text{trans}-(\text{Et}_3\text{P})_2\text{Ni}(\text{N}_3)_2$ .



corresponded to 64 monolayers. It is interesting to note that 64 monolayers is in the range required for technically useful films.<sup>80</sup> For each of the photochemical experiments discussed in this chapter the films studied were in excess of 60 monolayers. The interfacial layer, at either the vacuum or silicon interface, did not appear to be contributing significantly to the observed spectra.

The FTIR spectra of *trans*-(Et<sub>3</sub>P)<sub>2</sub>Ni(N<sub>3</sub>)<sub>2</sub> and its <sup>15</sup>N labelled derivatives are summarized in Table 6-2. The most intense band was associated with the antisymmetric azide stretch which appeared at 2041 cm<sup>-1</sup>. The 2041 cm<sup>-1</sup> band shifted to lower energy in the *trans*-(Et<sub>3</sub>P)<sub>2</sub>Ni(<sup>15</sup>NN<sub>2</sub>)<sub>2</sub> derivative. As a result of <sup>15</sup>NN<sub>2</sub><sup>-</sup> substitution, a mixture of isotopomers was possible. The mixture of isotopomers that could be formed are (Et<sub>3</sub>P)<sub>2</sub>Ni(<sup>15</sup>N<sup>14</sup>N<sub>2</sub>)<sub>2</sub>, (Et<sub>3</sub>P)<sub>2</sub>Ni(<sup>14</sup>N<sub>2</sub><sup>15</sup>N)<sub>2</sub> and (Et<sub>3</sub>P)<sub>2</sub>Ni(<sup>14</sup>N<sub>2</sub><sup>15</sup>N)(<sup>15</sup>N<sup>14</sup>N<sub>2</sub>) in a 1:1:2 ratio. As a result of the formation of the three different isotopomers the antisymmetric azide stretch was broadened by 25% and a superposition of the three spectra was observed. Previously, a mixture of isotopomers has been observed in the resonance Raman spectra of monoazido compounds.<sup>9</sup>

### 6.2.2 The photochemistry of *trans*-(Et<sub>3</sub>P)<sub>2</sub>Ni(N<sub>3</sub>)<sub>2</sub>.

The photolysis of *trans*-(Et<sub>3</sub>P)<sub>2</sub>Ni(N<sub>3</sub>)<sub>2</sub> in a (1,2-epoxyethyl)-benzene glass at 77 K, into either the charge transfer band or d-d transitions, had no effect on the complex as monitored by FTIR spectroscopy. The photolysis times were sufficiently long so that if the reaction in the glass had occurred with an efficiency comparable to the photoreaction

Table 6-2

FTIR spectral data for relevant complexes on Si(111)

Complex	$\nu_a$ ( $N_3$ ) cm <sup>-1</sup>
trans-(Et <sub>3</sub> P) <sub>2</sub> Ni(N <sub>3</sub> ) <sub>2</sub>	2041
<sup>15</sup> N) <sub>2</sub> -trans-(Et <sub>3</sub> P) <sub>2</sub> Ni(N <sub>3</sub> ) <sub>2</sub>	2029
[(Et <sub>3</sub> P) <sub>2</sub> Ni(N <sub>3</sub> )] <sup>+</sup>	2041
<sup>15</sup> N)-[(Et <sub>3</sub> P) <sub>2</sub> Ni(N <sub>3</sub> )] <sup>+</sup>	2029
N <sub>3</sub> <sup>-</sup>	2124
1- <sup>15</sup> N <sub>3</sub> <sup>-</sup>	2117
{(Et <sub>3</sub> P)Ni(N <sub>3</sub> ) <sub>2</sub> } <sub>2</sub>	2074, 2023
<sup>15</sup> N) <sub>4</sub> -{(Et <sub>3</sub> P)Ni(N <sub>3</sub> ) <sub>2</sub> } <sub>2</sub>	2060, 2015

in a surface film it would have been detected.

Prior to discussing the photochemistry of  $trans\text{-}(\text{Et}_3\text{P})_2\text{Ni}(\text{N}_3)_2$  as a film, it is necessary to mention the film thicknesses utilized. The thickness of the films discussed in this chapter may be approximated as 51 nm (calculation based on 64 monolayers). Since the film thickness was less than the wavelength of light used ( $350\text{ nm} < \lambda < 450\text{ nm}$ ) there was even irradiation throughout. Therefore, uneven irradiation which may cause preferential reaction at the film-vacuum interface is not expected. Experimentally, no indication of uneven irradiation was detected.

The photochemistry was conducted at room temperature, 77 K and 20 K. The only noticeable effect which the temperature variation had was to decrease the efficiency of the reaction at lower temperatures. Initially, photolysis of  $trans\text{-}(\text{Et}_3\text{P})_2\text{Ni}(\text{N}_3)_2$  on a silicon surface was carried out with visible light which resulted in d-d absorption. The FTIR spectral changes observed for the antisymmetric azide stretch are shown in Figure 6-2a). The loss of the antisymmetric stretch of the azide groups coincided with the growth of a new absorption at  $2124\text{ cm}^{-1}$ . The absorption at  $2124\text{ cm}^{-1}$  was clearly due to an azide species as confirmed by the  $^{15}\text{N}$  labelling of the precursor molecule. Upon  $^{15}\text{N}$  labelling the  $2124\text{ cm}^{-1}$  band had shifted to  $2117\text{ cm}^{-1}$ . The absorption was assigned as due to uncoordinated azide ion in the film. In order to confirm the assignment, a mixture of  $trans\text{-}(\text{Et}_3\text{P})_2\text{Ni}(\text{N}_3)_2$  and  $\text{NaN}_3$  were co-deposited from acetone. The azide ion showed a band at  $2124\text{ cm}^{-1}$  which was indistinguishable from the band formed after photolysing  $trans\text{-}(\text{Et}_3\text{P})_2\text{Ni}(\text{N}_3)_2$ . Labelled sodium azide,  $^{15}\text{NN}_2$ , co-deposited with

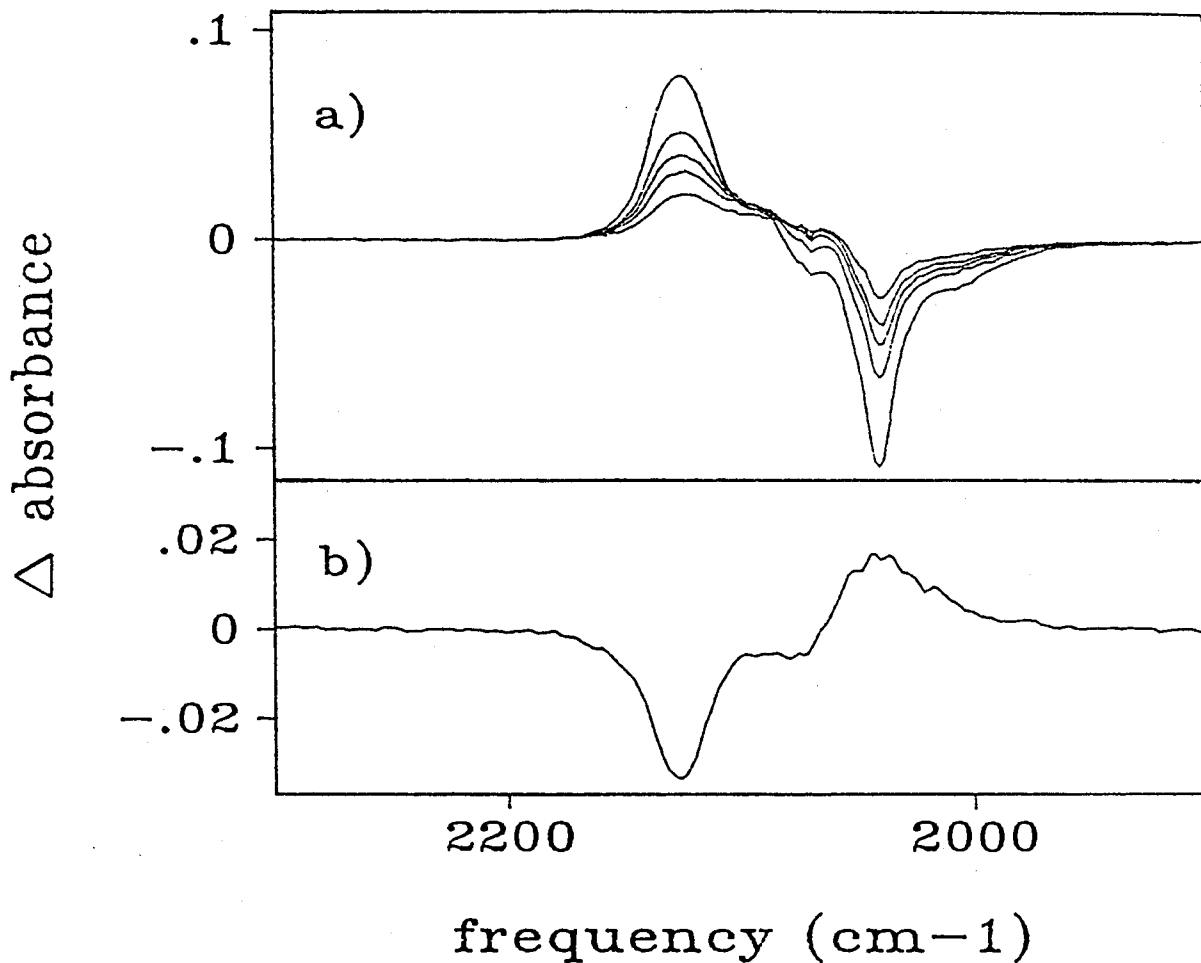


Figure 6-2

a) Spectral changes associated with the photolysis ( $\lambda > 420$  nm) of  $\text{trans}-(\text{Et}_3\text{P})_2\text{Ni}(\text{N}_3)_2$  on a silicon surface for 15, 35, 55, 90, and 240 min.

b) Spectral change associated with the subsequent photolysis (8 min.) of the sample shown in a) with  $\lambda > 313$  nm.

$trans-(Et_3P)_2Ni(N_3)_2$  gave rise to a band at  $2117\text{ cm}^{-1}$ . The assumption that the absorbance at  $2124\text{ cm}^{-1}$  was associated with the uncoordinated azide ion was supported by the band width. As mentioned earlier, a coordinated labelled azide would consist of isotopomers which would result in a broadened band. However, it was found that both  $N_3^-$  and  $^{15}NN_2^-$  had identical band widths consistent with a free ion.

In an effort to determine whether one or both azide ligands were photoextruded as a result of ligand field excitation a sample was irradiated exhaustively. The loss in intensity of the  $2041\text{ cm}^{-1}$  band, due to  $trans-(Et_3P)_2Ni(N_3)_2$ , never exceeded 50% of its original intensity. It should be noted that Figure 6-2 a) illustrates absorbance difference spectra and does not reflect the absolute loss in intensity. Several additional experiments were carried out, with extended photolysis, on films of varying initial thickness. In each instance, the band at  $2041\text{ cm}^{-1}$  decreased to approximately half its original value consistent with the experiments being independent of the coverages used. A plot of  $-\ln\{(A(t) - A(f))/(A(0) - A(f))\}$  vs. photolysis time was linear if a final absorbance of 0.53 times the initial absorbance was assumed. The plot is shown in Figure 6-3. Additionally, a plot of  $-\ln\{A(t)/A(0)\}$  vs. time was not linear (Fig. 6-3). The results plotted in Figure 6-3 are consistent with the antisymmetric azide absorption of the photoproduct occurring in the same region as the starting material's absorption (see section A-6 in the appendix for details). The azide loss product,  $(Et_3P)_2Ni(N_3)^+$ , has an absorbance that is nearly degenerate with the absorption of the starting complex,  $trans-(Et_3P)_2Ni(N_3)_2$ . The initial photoreaction is summarized in equation

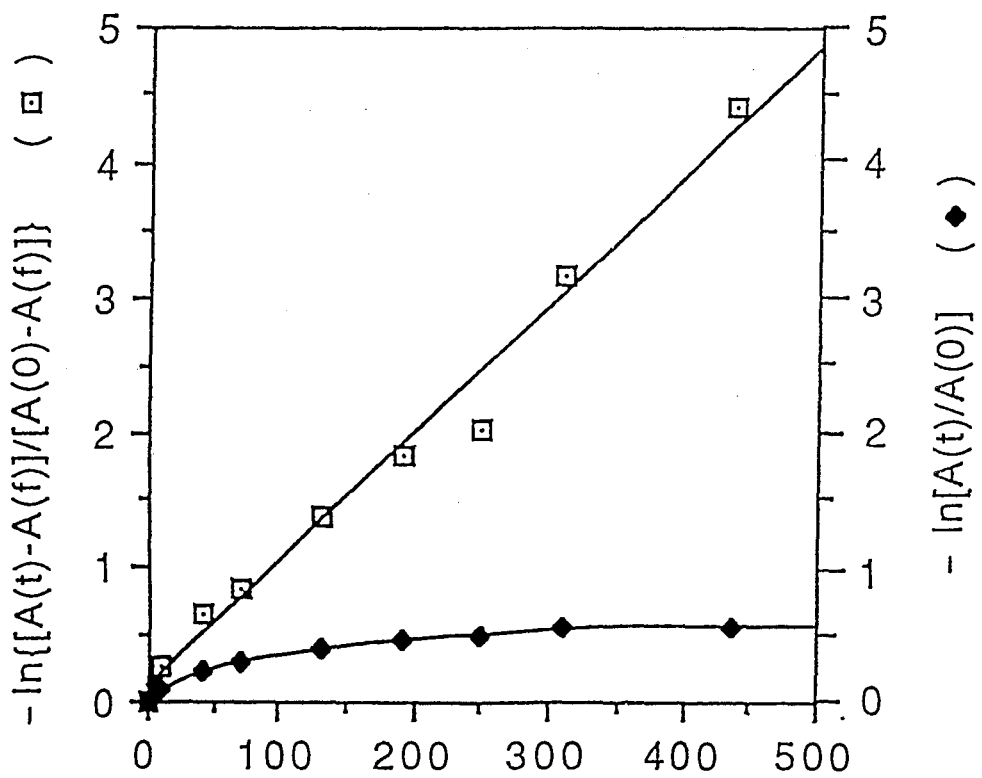
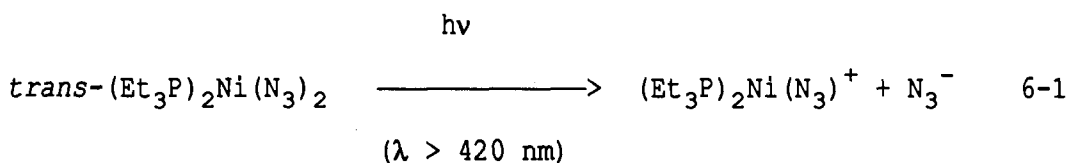


Figure 6-3

A plot of  $-\ln\left\{\frac{A(t)-A(f)}{A(0)-A(f)}\right\}$  and  $-\ln\left\{\frac{A(t)}{A(0)}\right\}$  vs. photolysis time

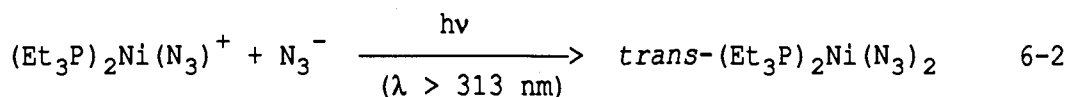
6-1.

The loss of a coordinated azide has been observed as a result of the d-d excitation of  $[\text{Co}(\text{CN})_5\text{N}_3]^-$ .<sup>92</sup> There does not appear to be any other example in the photochemistry of square planar  $d^8$  complexes where the loss of an azide ion, upon d-d excitation, has been shown. The loss of other anionic ligands is well established. Interestingly, the result of photolysis of  $\text{cis}-(\text{Ph}_3\text{P})_2\text{Pt}(\text{N}_3)_2$  was interpreted in terms of the



successive loss of  $\text{N}_3$  radicals to form  $\text{Pt}(\text{PPh}_3)_2$ .<sup>93</sup> We found no evidence for a similar process occurring as a result of d-d excitation of  $\text{trans}-(\text{Et}_3\text{P})_2\text{Ni}(\text{N}_3)_2$ . Recently, the photochemistry of  $(\text{Me}_3\text{P})_2\text{Ni}(\text{Cl})(\text{N}_3)$  has been studied in solution.<sup>94</sup> It was found that  $\text{N}_2$  was lost, after exposure to UV light, resulting in the eventual formation of clusters through the intermediacy of a nickel nitrido species.

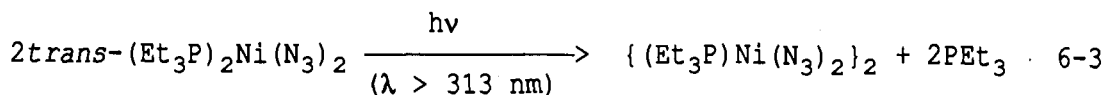
Photolysis of the primary photoproduct,  $(\text{Et}_3\text{P})_2\text{Ni}(\text{N}_3)^+$ , for less than ten minutes using Pyrex filtered light (bandpass greater than 313 nm) resulted in the loss of absorption due to free  $\text{N}_3^-$  and the growth of a band at  $2041 \text{ cm}^{-1}$  as shown in Figure 6-2b). This result was attributed to the regeneration of a coordinated terminal azide. The reaction is summarized in equation 6-2. The photogenerated species (Eq. 6-2) gave rise to a band that was degenerate with the starting material.



However, in some instances the band at  $2041 \text{ cm}^{-1}$  (as a result of UV photolysis) was broader than the absorption due to the starting complex when initially deposited. It is conceivable that the broadened absorption was the result of reorientation within the film. It should be emphasized that the photochemical re-coordination reaction did not occur thermally. In the dark, the FTIR spectra of films containing  $(\text{Et}_3\text{P})_2\text{Ni}(\text{N}_3)^+$  and  $\text{N}_3^-$  did not change over several hours.

The UV photolysis of either a newly deposited film of *trans*- $(\text{Et}_3\text{P})_2\text{Ni}(\text{N}_3)_2$  or a sample which had been through the above procedure resulted in the loss of intensity of the band at  $2042 \text{ cm}^{-1}$ . Associated with this was the appearance of two absorption bands at  $2074 \text{ cm}^{-1}$  and  $2023 \text{ cm}^{-1}$ . When an  $^{15}\text{N}$  labelled sample was subjected to the same procedure, two bands appeared at  $2060 \text{ cm}^{-1}$  and  $2015 \text{ cm}^{-1}$ . The two bands were assigned as due to the formation of a  $\{(\text{Et}_3\text{P})\text{Ni}(\text{N}_3)_2\}_2$  dimer.<sup>95</sup> The observation of two well separated bands in the spectra of azide complexes is commonly indicative of both terminal and bridging azides. The isoelectronic molecule,  $\{(\text{Ph}_3\text{P})\text{Pd}(\text{N}_3)_2\}_2$ , is known and showed azide stretches at  $2075 \text{ cm}^{-1}$  and  $2027 \text{ cm}^{-1}$ .<sup>96</sup> Interestingly, the monomeric palladium complex,  $(\text{Ph}_3\text{P})_2\text{Pd}(\text{N}_3)_2$ , has an antisymmetric azide stretch at  $2035 \text{ cm}^{-1}$  similar in energy to the antisymmetric azide stretch of *trans*- $(\text{Et}_3\text{P})_2\text{Ni}(\text{N}_3)_2$  at  $2041 \text{ cm}^{-1}$ . This suggests that the IR of analogous azide complexes of nickel and palladium are quite similar. The dimer formation reaction is summarized in equation 6-3.





The primary photoreaction is most likely the loss of a single  $\text{PEt}_3$  ligand and the formation of a three coordinate Ni(II) species,  $(\text{Et}_3\text{P})\text{Ni}(\text{N}_3)_2$ . Following the  $\text{PEt}_3$  ligand loss, an associative reaction to form the observed azide bridged dimer occurred. The proposed nickel dimer formation reaction is analogous to the thermal synthesis of  $\{(\text{Ph}_3\text{P})\text{Pd}(\text{N}_3)_2\}_2$  which occurred as a result of initial phosphine loss.<sup>96</sup> However, in solution, the palladium intermediate is probably solvated. The photoejection of  $\text{PPh}_3$  in a similar palladium complex,  $(\text{Ph}_3\text{P})_2\text{Pd}(\text{N}_3)_2$ , has been observed.<sup>97</sup>

Further photolysis of a film resulted in the gradual decrease in intensity of absorptions attributed to  $\{(\text{Et}_3\text{P})\text{Ni}(\text{N}_3)_2\}_2$ . However, the shape of the bands did not change to a great extent during the photolysis which may be consistent with the formation of a polymeric material. The prolonged photolysis most likely caused the formation of  $\text{N}_2$ , however, at no point was any species consistent with coordinated  $\text{N}_2$  detected by FTIR. Additionally, free  $\text{N}_2$  trapped within the film was not observed. Although,  $^{15}\text{N}^{14}\text{N}$  is expected to have a very low extinction coefficient.<sup>98</sup>

As a result of exhaustive photolysis, the absorption due to bridging azide decreased in intensity and a new band at  $1995 \text{ cm}^{-1}$  was detected. The  $1995 \text{ cm}^{-1}$  band reached a low steady state intensity and eventually was lost leaving no absorption in the azide region. The band was assigned to a new azide as confirmed by  $^{15}\text{N}$  labelling which gave

rise to a shift of  $9 \text{ cm}^{-1}$  to lower energy. This was an unusually low absorption energy for a metal azide. However, it is also possible in light of recent results<sup>99</sup> regarding free (ie., non ion-paired)  $\text{N}_3^-$  in a low temperature matrix that the  $1995 \text{ cm}^{-1}$  band is not associated with a coordinated azide. The reported antisymmetric azide frequency for  $\text{N}_3^-$  in an  $\text{N}_2$  matrix was  $2003.5 \text{ cm}^{-1}$  and shifted to lower energy by  $10.5 \text{ cm}^{-1}$  for  $^{14}\text{N}_2^{15}\text{N}^-$ . The formation of non ion-paired  $\text{N}_3^-$  ions, as the result of the continued photolysis of a  $(\text{Et}_3\text{P})_2\text{Ni}(\text{N}_3)_2$  film, would be expected as nickel metal was formed and the positive charge was no longer localized on a single metal. Exhaustive photolysis of the film at room temperature resulted in the disappearance of absorptions due to nitrogen containing ligands and the original phosphine (C-H) modes. The only absorptions that remained were due to uncoordinated  $\text{PEt}_3$ .

The final films, after exhaustive photolysis, were removed and transferred to an X-ray photoelectron spectrometer. The films were then analyzed by Auger and ESCA spectroscopies. The initial product on the surface was  $\text{NiO}$ , as evidenced by the nickel and oxygen peaks. The Auger spectrum gave rise to nickel signals at  $848 \text{ eV}$  ( $2p_{3/2}$ , LMM transition) and  $865 \text{ eV}$  ( $2p_{1/2}$ , LMM transition) and an oxygen signal at  $512 \text{ eV}$  (KLL transition). The relative amounts of nickel and oxygen were calculated using the formula given in equation 6-4. The elemental sensitivity factors for Auger transitions were obtained from a handbook of Auger spectroscopy.<sup>100</sup> The relative ratio of the Auger signals due to nickel and oxygen, for the unspattered sample, was 1:1. This is consistent with the formation of  $\text{NiO}$ . The surface layer was removed by sputtering with  $\text{Ar}^+$  ions. After 60 seconds of sputtering the relative

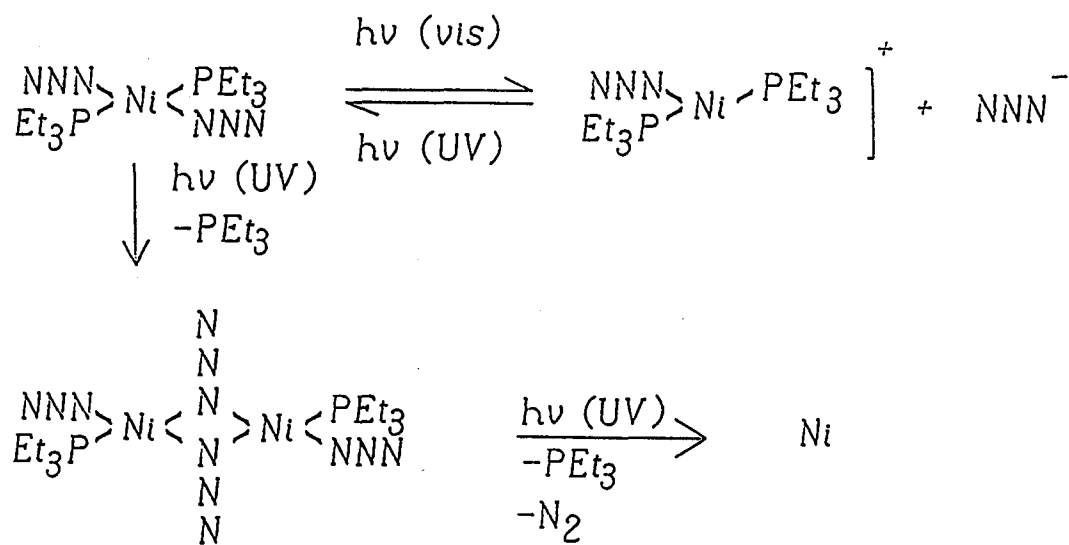


Figure 6-4

Summary of the photolysis of a  $\text{trans}-(\text{Et}_3\text{P})_2\text{Ni}(\text{N}_3)_2$  film

$$C_i = (I_i/S_i) / (\sum_i^n I_i/S_i)$$

6-4

where,  $C_i$  = concentration of species  $i$

$I_i$  = intensity of the Auger signal  
of species  $i$

$S_i$  = sensitivity factor of species  $i$

$n$  = number of species

ratio of the signals due to nickel and oxygen was approximately 6:1. Therefore, the composition beneath the surface of the film was consistent with the formation of elemental nickel. The nickel oxide layer was restricted to the surface of the film. No signal due to phosphorus was detected, consistent with all phosphorus containing species being lost from the surface. It is most likely that any phosphorus containing free ligand was lost to the vacuum in the Auger spectrometer. Trace amounts of nitrogen were detected and accounted for less than 2% of the original nitrogen content. The largest observed signal was due to carbon. Since the only carbon present in the molecule was associated with the  $\text{PEt}_3$  ligand, and no signal due to phosphorus was observed, this is most consistent with atmospheric contamination of the surface.

The surface analysis discussed above is consistent with the loss of all ligands from the coordination sphere of  $\text{trans}-(\text{Et}_3\text{P})_2\text{Ni}(\text{N}_3)_2$  resulting in the formation of elemental nickel. The  $\text{NiO}$  found on the surface of the film is consistent with oxygen adsorption after the sample was removed from the photolysis chamber.

The thickness of a surface film of nickel, produced by the

photolysis of a spin coated film of  $\text{trans}-(\text{Et}_3\text{P})_2\text{Ni}(\text{N}_3)_2$ , was measured by optical interferometry by comparison with a masked area of the substrate. The mask was removed, prior to the chip being photolyzed, resulting in a step in height between the nickel film and the silicon wafer. The step due to the nickel film was found to be 60 nm thick and showed no distinguishable variation in thickness near the step edge.

### 6.3 Conclusions

The results of photolysis under varying conditions are summarized in Figure 6-4. Most importantly, analogous to our previous work on surface films, the photochemistry in a low temperature glass, in this case not detectable, and in a film differed substantially. Also, the anionic ligand,  $\text{N}_3^-$ , was efficiently photodecomposed and its products lost to the vacuum. Finally, in this study on  $\text{trans}-(\text{Et}_3\text{P})_2\text{Ni}(\text{N}_3)_2$  films we were able to show that nickel films could be produced in a photochemical process at temperatures as low as 20 K.

### 6.4 Experimental Section

The  $\text{CaF}_2$  crystals were obtained from Wilmad Glass Co. Inc.. The Si(111) wafers were obtained from Pacific Microelectronics Center, Canada. The silicon substrates had the approximate dimensions of 1 cm x 1 cm. The  $^{15}\text{N}$  sodium azide was obtained from Cambridge Isotopes and was 99 atom percent  $^{15}\text{N}$  enriched in the one position.

The FTIR spectra were obtained with  $4\text{ cm}^{-1}$  resolution using a BOMEM Michelson 120 FTIR spectrophotometer. The samples were held in a  $\text{CaF}_2$  faced cell for glasses or in a high conductivity copper sample mount

within a  $\text{CaF}_2$  faced vacuum Dewar for films. Experiments at 20 K were conducted using a CTI Cryogenics Model 22 cryocooler and a 350R compressor system equipped with a Lake Shore Cryotronics DRC 80C temperature controller. The temperature was monitored with a Lake Shore Cryotronics silicon diode sensor (DTC500 DRC). The UV/VIS spectra were obtained with a Cary 17 spectrophotometer.

The photolysis source was a 100 W high pressure Hg lamp in an Oriel housing equipped with condenser lenses. For all of the experiments, the photolysis light was passed through a 10 cm. path length water filter equipped with pyrex optics. The combination of optics resulted, primarily, in LMCT excitation. In some experiments a band pass filter ( $\lambda > 420$  nm), interposed between the lamp and the sample, resulted in LF excitation.

X-ray photoelectron spectra were obtained using a PHI double pass CMA at 0.85 eV resolution at the Surface Physics Laboratory, Dept. of Physics, Simon Fraser University.

#### 6.4.1 Preparation of *trans*-( $\text{Et}_3\text{P}$ ) $_2\text{Ni}(\text{N}_3)_2$ .

The compounds discussed were prepared previously in our lab and the procedure used was a modification of that used by Bowman and Dori.<sup>101</sup> The subsequent details are for the  $^{15}\text{N}$  labelled derivative.

To a solution of *trans*-( $\text{Et}_3\text{P}$ ) $_2\text{Ni}(\text{Cl})_2$  (0.040 g) in acetone (20 ml) solid 1- $\text{Na}^{15}\text{NN}_2$  (0.026 g) was added. The mixture was allowed to stir for 24 hours, filtered, and the solvent was removed under reduced pressure. The solid was extracted with hexane which, once removed, yielded ( $^{15}\text{N}$ ) $_2$ -*trans*-( $\text{Et}_3\text{P}$ ) $_2\text{Ni}(\text{N}_3)_2$  (0.035 g, 85% yield).

#### 6.4.2 Photolysis of complexes in a (1,2-epoxyethyl)-benzene glass.

A sample of  $\text{trans}-(\text{Et}_3\text{P})_2\text{Ni}(\text{N}_3)_2$  was dissolved in (1,2-epoxyethyl)-benzene and loaded into a  $\text{CaF}_2$  faced cell. The sample was then cooled to 77 K whereupon the FTIR spectrum was obtained. Subsequently, the sample was photolyzed with broad band light for 20, 50, 87, 127 and 141 min. No change was detected in the FTIR spectra in the region of the antisymmetric azide stretch.

#### 6.4.3 Calibration of the absorption on a silicon surface.

A stock solution of  $\text{trans}-(\text{Et}_3\text{P})_2\text{Ni}(\text{N}_3)_2$  (0.0028 g) in  $\text{CH}_2\text{Cl}_2$  (3.0 ml) was prepared. A drop (0.0031 ml) of the stock solution was then deposited on the surface of a Si wafer and the solvent was allowed to evaporate. When the drop had dried, the FTIR spectrum was obtained. The area of the drop was determined to be  $0.5 \text{ cm}^2$ . The area of the drop and the absorption corresponded to a coverage of 0.9 molecules per  $\text{\AA}^2$ . The process was repeated several times.

#### 6.4.4 Spin coating of $\text{trans}-(\text{Et}_3\text{P})_2\text{Ni}(\text{N}_3)_2$ films.

A 1 cm. by 1 cm. silicon wafer was taped to a flat 1 inch disc which was subsequently attached to a small electrical motor. A solution of  $\text{trans}-(\text{Et}_3\text{P})_2\text{Ni}(\text{N}_3)_2$  in  $\text{CH}_2\text{Cl}_2$  was then prepared. As the wafer was spinning, a drop of the solution was allowed to fall onto the center of the wafer. The wafer was allowed to spin until the solvent had evaporated ( $\approx 1$  min.). The tape was then removed from the wafer leaving a 0.5 cm strip of the  $\text{trans}-(\text{Et}_3\text{P})_2\text{Ni}(\text{N}_3)_2$  film. After photolysing, interferometry was used to determine the film thickness.

The concentration of the solutions and the rate of rotation of the wafer were varied, from experiment to experiment, in order to achieve the most uniform film.

#### 6.4.5 Photolysis of the complexes on silicon surfaces.

Prior to photolysis a silicon surface was prepared with *trans*-(Et<sub>3</sub>P)<sub>2</sub>Ni(N<sub>3</sub>)<sub>2</sub>, as discussed above, and transferred to a vacuum Dewar. The sample was then photolyzed for 15, 35, 55, 90 and 240 min with a filter ( $\lambda > 420$  nm pass) positioned between the sample and the light source. Additional irradiation was conducted with only a water filter (10 cm path length with pyrex optics) for 8 min. The spectral changes are summarized in Figure 6-2 a) and 6-2 b), respectively. In some of the experiments the film was prepared by spin coating the *trans*-(Et<sub>3</sub>P)<sub>2</sub>Ni(N<sub>3</sub>)<sub>2</sub> complex from a CH<sub>2</sub>Cl<sub>2</sub> solution onto a silicon wafer. Spin coating produced a more uniform film but had absolutely no consequence on the observed photochemistry. Analogous experiments were conducted at 77 K and at 20 K.



**Chapter 7: The photochemistry of *fac*-Co(NH<sub>3</sub>)<sub>3</sub>(NO<sub>2</sub>)<sub>3</sub> and  
*mer*-Co(NH<sub>3</sub>)<sub>3</sub>(N<sub>3</sub>)<sub>3</sub> films.**

**7.1 Introduction**

The studies conducted on amorphous organometallic, and inorganic films have demonstrated that not only could these reactions be monitored but also that there was a wealth of chemistry occurring that was different than in other media. However, the photochemical decomposition of the organometallic compounds resulted in excessive hydrocarbon contamination of the resultant film. Additionally, when carbonyl containing organometallic compounds were photolyzed, inevitably, dimers with bridging carbonyl groups were formed which were difficult to photodecompose. Also, the choice of coordination compounds which had no carbon containing ligands seemed reasonable to demonstrate conclusively whether the carbon contamination of the resultant film occurred as a result of the precursor or from the atmosphere.

Discussed in this chapter is the photochemistry of *fac*-Co(NH<sub>3</sub>)<sub>3</sub>(NO<sub>2</sub>)<sub>3</sub> and *mer*-Co(NH<sub>3</sub>)<sub>3</sub>(N<sub>3</sub>)<sub>3</sub> films. The choice of these complexes seemed ideal for several reasons. The triazido and trinitro compounds were relatively easy to make and were air stable complexes. Also, the azide, ammine, and nitro groups are intense IR absorbers that can be easily monitored by infrared spectroscopy. But, most importantly, the photodecomposition of these complexes may result in the

formation of species that would be easily lost to the vacuum;  $\text{NH}_3$ ,  $\text{NO}_2$  and  $\text{N}_2$ . If the ligands were lost, photochemically, as gaseous molecules it would result in a relatively pure metal film.

## 7.2 Results and Discussion

### 7.2.1 Spectroscopic data for the complexes.

The UV/Vis spectra of the cobalt complexes in dimethyl sulfoxide were obtained. No other solvent was used since these compounds are insoluble in practically all other solvents. Both of the compounds, *fac*- $\text{Co}(\text{NH}_3)_3(\text{NO}_2)_3$  and *mer*- $\text{Co}(\text{NH}_3)_3(\text{N}_3)_3$ , have characteristic bands due to charge transfer and d-d transitions. The spectra for the cobalt complexes, in DMSO, are summarized in Table 7-1. The d-d transitions for each complex appeared as a single broad asymmetric band. The broad asymmetry of the band negated the assignment of individual transitions. The higher energy absorption bands are probably due to ligand to metal charge transfer (LMCT) transitions (as a result of  $\text{N}_3^-$  or  $\text{NO}_2^-$ ). No fine structure was observed for the charge transfer bands.

The proton NMR spectrum of the yellow complex,  $\text{Co}(\text{NH}_3)_3(\text{NO}_2)_3$ , consisted of a singlet at 3.34 ppm. A singlet in the N.M.R. spectrum is consistent with each  $\text{NH}_3$  group being *trans* to an  $\text{NO}_2$  group. The infrared and N.M.R. spectra of both the *fac*- and *mer*- isomers of  $\text{Co}(\text{NH}_3)_3(\text{NO}_2)_3$  have been recorded previously.<sup>102</sup> The N.M.R. spectrum, combined with the infrared data, confirmed the assignment of a *facial* geometry for  $\text{Co}(\text{NH}_3)_3(\text{NO}_2)_3$ .

The proton NMR spectrum of *mer*- $\text{Co}(\text{NH}_3)_3(\text{N}_3)_3$  had resonances at 3.33 ppm and 2.82 ppm which integrated in a 2:1 ratio. The position and

Table 7-1

UV/Vis data for the relevant complexes<sup>a</sup>

Complex	LMCT (nm)	d-d (nm)
	$\epsilon$ (M <sup>-1</sup> cm <sup>-1</sup> )	$\epsilon$ (M <sup>-1</sup> cm <sup>-1</sup> )
<i>mer</i> -Co(NH <sub>3</sub> ) <sub>3</sub> (N <sub>3</sub> ) <sub>3</sub>	336 (10,725)	586 (174)
<i>fac</i> -Co(NH <sub>3</sub> ) <sub>3</sub> (NO <sub>2</sub> ) <sub>3</sub>	344 (2,928)	425 (177)

a) Spectra recorded in dimethyl sulfoxide.

ratio of the two signals was consistent with a previous study.<sup>103</sup> The signal at 3.33 ppm, which integrated as two, was due to an ammine group *trans* to another ammine group. The peak which integrated as one, at 2.82 ppm, was assigned to an ammine group *trans* to an azide ligand.

The FTIR spectrum, of *mer*-Co(NH<sub>3</sub>)<sub>3</sub>(N<sub>3</sub>)<sub>3</sub>, contained two antisymmetric azide stretches at 2061(sh) cm<sup>-1</sup> and 2020 cm<sup>-1</sup>. The symmetric azide stretches appeared at 1311(sh) cm<sup>-1</sup> and 1287 cm<sup>-1</sup> (Table 7-2). As a result of the spectral data a meridional configuration was assigned to Co(NH<sub>3</sub>)<sub>3</sub>(N<sub>3</sub>)<sub>3</sub>, consistent with a previous study.<sup>102</sup> The FTIR data for all complexes is summarized in Table 7-2.

### 7.2.2 Photochemistry of *fac*-Co(NH<sub>3</sub>)<sub>3</sub>(NO<sub>2</sub>)<sub>3</sub> as a film.

The photolysis of *fac*-Co(NH<sub>3</sub>)<sub>3</sub>(NO<sub>2</sub>)<sub>3</sub>, as a film, was conducted at room temperature. Although the light source that was used radiates visible wavelengths it primarily emits in the UV region. The LMCT extinction coefficient (NO<sub>2</sub> → Co) was 2,928 M<sup>-1</sup> cm<sup>-1</sup> whereas the d → d extinction coefficient was 177 M<sup>-1</sup> cm<sup>-1</sup>. Therefore, although wavelengths greater than 313 nm were used for irradiation, LMCT absorbance probably led to the observed photochemistry.

The photolysis of a film of *fac*-Co(NH<sub>3</sub>)<sub>3</sub>(NO<sub>2</sub>)<sub>3</sub> for periods shorter than several hours resulted in very little spectral changes. The spectral changes associated with the photolysis of a *fac*-Co(NH<sub>3</sub>)<sub>3</sub>(NO<sub>2</sub>)<sub>3</sub> film for a total time of 70, 136.5, 191.5 and 359.5 hours are summarized in Figure 7-1. As can be seen in the Figure 7-1, the bands due to the NO<sub>2</sub> groups at 1427 cm<sup>-1</sup> (ν<sub>as</sub>(NO<sub>2</sub>)) and 1310 cm<sup>-1</sup> (ν<sub>s</sub>(NO<sub>2</sub>)) are decreasing in intensity. The bands due to the NH<sub>3</sub> ligands near 3250

Table 7-2

Summary of FTIR data<sup>a</sup>

	$\nu_{as}(N_3)$	$\nu_s(N_3)$	$\nu_{as}(\mu-N_3)$	$\nu_{as}(\mu-N_3)$
<i>mer</i> -Co(NH <sub>3</sub> ) <sub>3</sub> (N <sub>3</sub> ) <sub>3</sub>	2061 (sh), 2020	1311 (sh) 1287		
Co <sub>2</sub> ( $\mu$ -N <sub>3</sub> ) <sub>2</sub> (N <sub>3</sub> ) <sub>4</sub>	2060 2006	1206	2095	1283
{Co( $\mu$ -N <sub>3</sub> ) <sub>2</sub> } <sub>n</sub>			2058	1209

	$\nu_{as}(NO_2)$	$\nu_s(NO_2)$	$\nu_s(NO_2)$	$\delta(ONO)$
<i>fac</i> -Co(NH <sub>3</sub> ) <sub>3</sub> (NO <sub>2</sub> ) <sub>3</sub>	1427 (s)	1310 (sh)	1271 (w)	824

	$\nu_{as}(NO_2)$	$\nu_s(NO_2)$	$\rho_w(NO_2)$	$\nu(N=O)$	$\nu(NO_2)$	$\delta(ONO)$
Co(NH <sub>3</sub> ) <sub>3</sub> (NO <sub>2</sub> )(ONO) <sub>2</sub>	1422	1279	613	1464	1099	837

a: All band positions are for a film

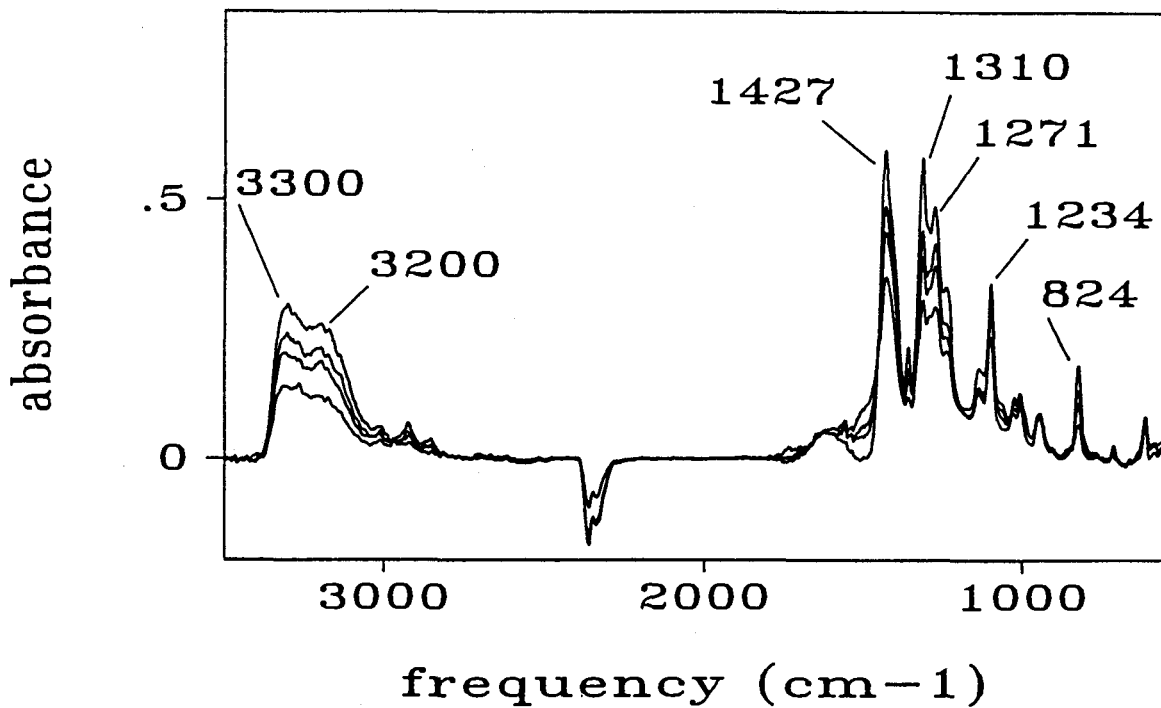


Figure 7-1

The absorbance difference spectra associated with the photolysis of a  $\text{fac-Co}(\text{NH}_3)_3(\text{NO}_2)_3$  film for a total time of 70, 136.5, 191.5 and 359.5 hours.

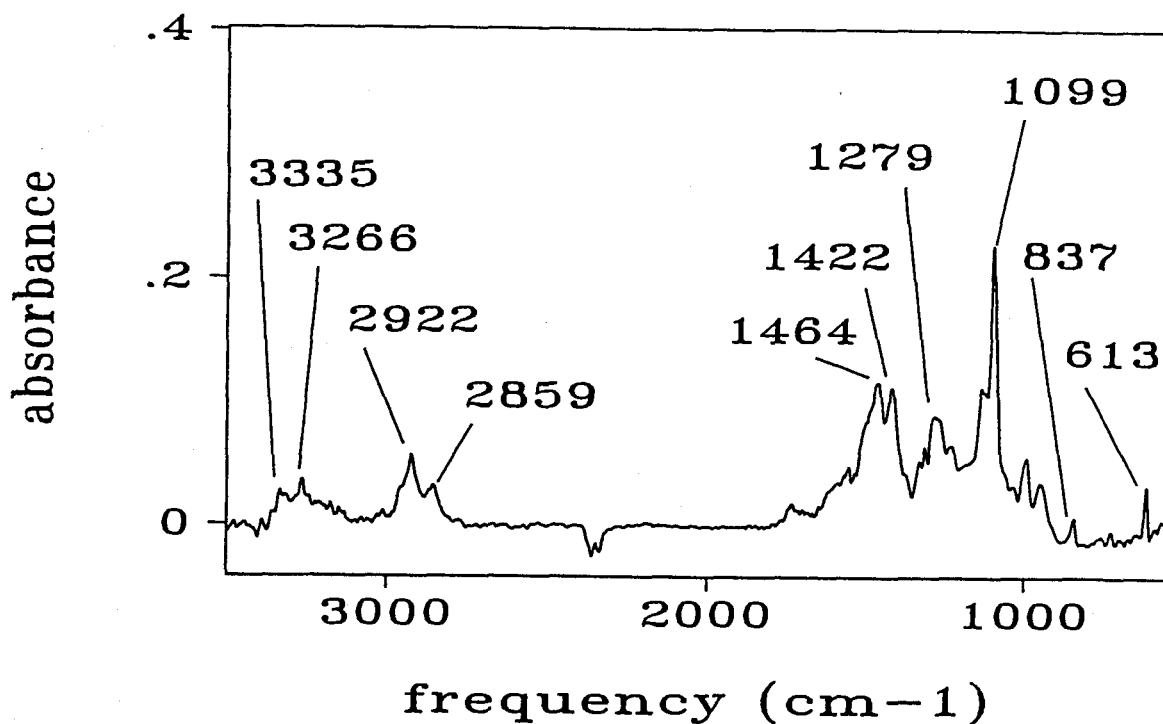


Figure 7-2

Spectrum of the intermediate,  $\text{Co}(\text{NH}_3)_3(\text{NO}_2)(\text{ONO})_2$ , obtained by subtraction of the spectrum of the starting complex from the final spectrum in Figure 7-1.

$\text{cm}^{-1}$  are also decreasing in intensity. In order to clearly identify the photoproduct, the spectrum of the starting material was subtracted from the final spectrum of the surface film following 359.5 hours of photolysis. The resultant spectrum is illustrated in Figure 7-2. Spectra with the same features could also be obtained by subtraction of the starting material spectrum from the spectra obtained at shorter photolysis times. The important observation in this spectrum is the bands at 1464 and 1099  $\text{cm}^{-1}$ . These bands are consistent with the formation of a nitrito ligand via a photochemical linkage isomerization. For the nitrito coordination, the symmetric and antisymmetric  $\nu(\text{NO}_2)$  modes are well separated,<sup>81</sup> in this case by 365  $\text{cm}^{-1}$ . This separation is typical of nitrito coordination. The presence of an absorption at 613  $\text{cm}^{-1}$  is indicative of the presence of remaining nitro ligation in the coordination sphere. The band at 613  $\text{cm}^{-1}$  is assigned as a wagging mode of the nitro ligand and is absent in nitrito complexes.<sup>81</sup> The presence of intense absorption bands at 1422 and 1279  $\text{cm}^{-1}$  is also consistent with this interpretation. The weak bands above 3000  $\text{cm}^{-1}$  are indicative of coordinated  $\text{NH}_3$ . The relative intensity of these bands to the bands associated with the  $\text{NO}_2^-$  ligands is slightly lower than in the starting material and may be indicative of the loss of some  $\text{NH}_3$  from the complex (see below). The photoproduct is tentatively assigned as containing  $\text{Co}(\text{NH}_3)_3(\text{NO}_2)(\text{ONO})_2$ .

The series of isomers,  $\text{Co}(\text{NH}_3)_3(\text{NO}_2)_n(\text{ONO})_{3-n}$  ( $n = 1-3$ ), have been prepared previously.<sup>104</sup> By comparison with the known spectra of these isomers the species present in the surface film is identified as being most consistent with  $\text{Co}(\text{NH}_3)_3(\text{NO}_2)(\text{ONO})_2$ . In spite of the agreement



with the reported spectra there is evidence that the complex is not a pure sample. The most important evidence for this statement arises from the intensity of the overtones associated with the  $\nu(\text{NO}_2)$  modes which appear at 2922 and 2859  $\text{cm}^{-1}$ . These absorptions are more intense than the absorption bands associated with the NH stretches at 3335 and 3266  $\text{cm}^{-1}$ . This is indicative of the loss of  $\text{NH}_3$  from the complex, however, the ratio of amines to nitro groups could not be confirmed with certainty.

The loss of  $\text{NH}_3$  would be expected to result in the formation of bridged  $\text{NO}_2$  ligands in the film. The spectra found do not allow us to exclude the possibility of some bridged  $\text{NO}_2$  within the film.

The major reaction, in any case, is linkage isomerization. Similar reactivity has been observed for related complexes in solution.<sup>2,105</sup> Presumably the net decomposition of the film is associated with some irreversible loss of the  $\text{NO}_2$  radical. When the  $\text{NO}_2$  radical reassociates with the complex it may do so by forming either linkage isomer. This is probably random as the nitro complex is the thermodynamically more stable isomer.<sup>104</sup>

After 359.5 hours of photolysis, the only FTIR spectral changes were the appearance of bands assigned to  $\text{Co}(\text{NH}_3)_3(\text{NO}_2)(\text{ONO})_2$ . Not only was the reaction of *fac*- $\text{Co}(\text{NH}_3)_3(\text{NO}_2)_3$  inefficient but no loss of the  $\text{Co}(\text{NH}_3)_3(\text{NO}_2)(\text{ONO})_2$  was observed. Since the starting material was not very photosensitive no further study of this complex was made.

### 7.2.3 Photochemistry of *mer*- $\text{Co}(\text{NH}_3)_3(\text{N}_3)_3$ as a film.

The photolysis of *mer*- $\text{Co}(\text{NH}_3)_3(\text{N}_3)_3$ , as a film, was conducted at

room temperature. The LMCT ( $N_3 \rightarrow Co$ ) extinction coefficient of  $mer-Co(NH_3)_3(N_3)_3$  was  $10,725 M^{-1} cm^{-1}$  whereas the  $d \rightarrow d$  extinction coefficient was  $586 M^{-1} cm^{-1}$ . Analogous to the trinitro complex, LMCT transitions probably dominated the observed photochemistry.

The spectral changes associated with photolysing a film of  $mer-Co(NH_3)_3(N_3)_3$  for a total time of 11, 21, 62, 122, 186, and 225 min are shown in Figure 7-3. As can be seen in Figure 7-3, bands due to the starting material are decreasing in intensity (negative bands), concomitant with the growth of bands due to the intermediate (positive bands). The bands due to the intermediate in the absorbance difference spectra appeared at  $2104 cm^{-1}$  and  $1204 cm^{-1}$ . To correct for the overlap of the bands due to the azide stretches of the intermediate and the starting material, the absorbances due to the starting material were added back in to the spectra. The computer addition of the starting material absorbances reveals the bands due solely to the intermediate and gives a more accurate measure of the peak positions. The spectra resulting from the computer addition of the starting material absorbances is given in Figure 7-4. The computer addition of the starting material absorbances showed that the intermediate possessed no absorptions consistent with coordinated ammine ligands. The antisymmetric azide stretches of the photo-generated intermediate appeared as two well separated bands at  $2095 cm^{-1}$  and  $2006 cm^{-1}$ . However, the band at  $2095 cm^{-1}$  was broad and asymmetric. By expanding the spectrum, in that region, it was clear that the  $2095 cm^{-1}$  band had a shoulder which appeared at  $2060 cm^{-1}$ .

The appearance of a higher energy band ( $2095 cm^{-1}$ ) and a lower

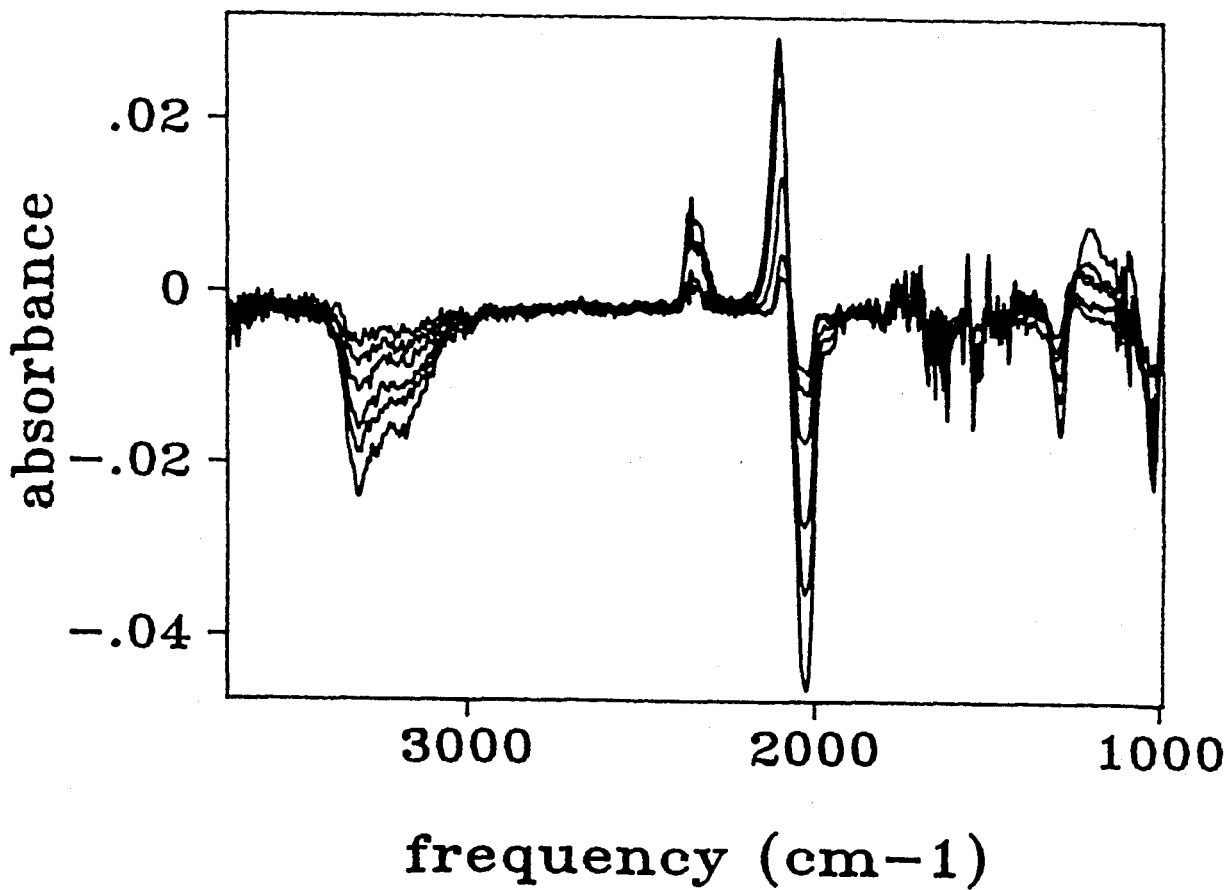


Figure 7-3

Absorbance difference spectra showing the growth of azide stretches, assigned to  $[\text{Co}_2(\text{N}_3)_6]$ , as a result of photolysing a film of *mer*- $\text{Co}(\text{NH}_3)_3(\text{N}_3)_3$  for a total time of 11, 21, 62, 122, 186, and 225 min.

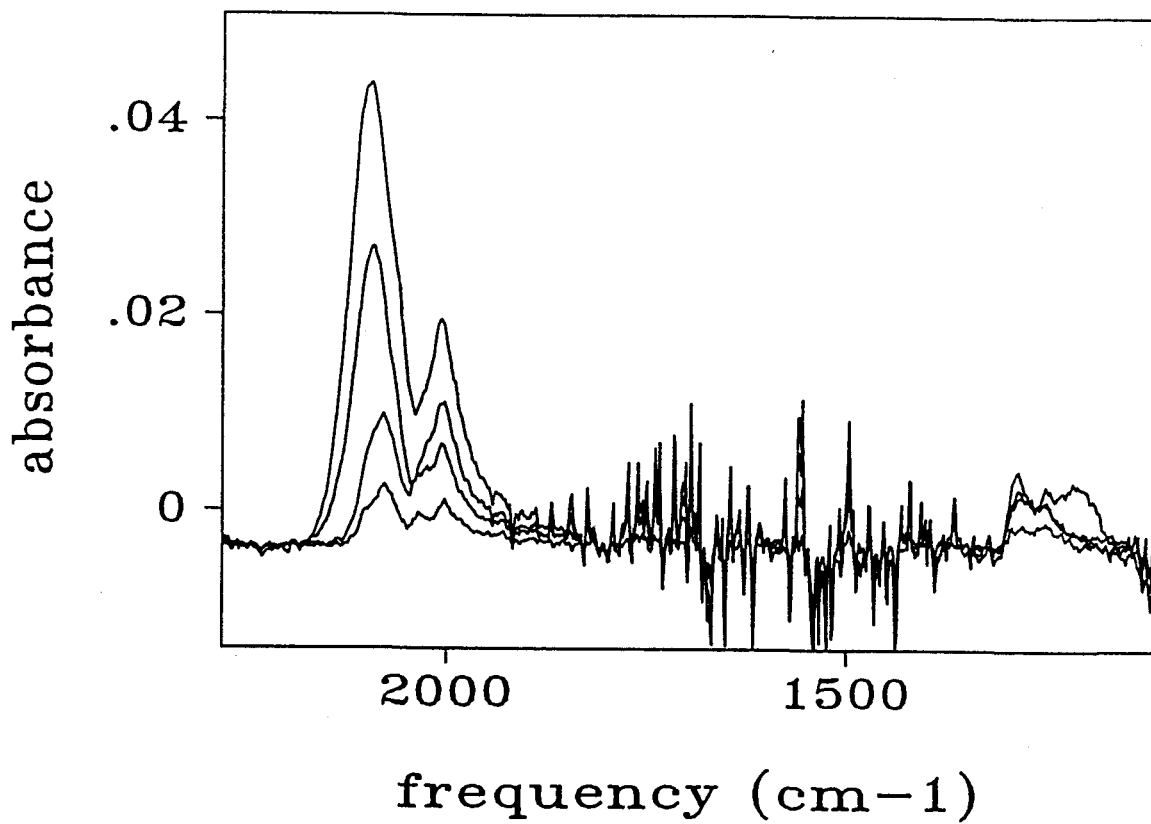


Figure 7-4

Absorbance spectra due to  $[\text{Co}_2(\text{N}_3)_6]$ , after starting material absorbances have been added in to Figure 7-3.

energy band ( $2006\text{ cm}^{-1}$ ), relative to the starting materials antisymmetric azide stretches, is indicative of the formation of a cobalt dimer containing bridging and terminal azido groups.<sup>106</sup> The band at  $2095\text{ cm}^{-1}$  was assigned as the antisymmetric stretch of a bridging azide ( $\nu_{as}(\mu\text{-N}_3)$ ). The bands at  $2060\text{ cm}^{-1}$  and  $2006\text{ cm}^{-1}$  are assigned as the antisymmetric stretches of terminal azide ligands.

The intermediate also had broad asymmetric azide stretches at  $1283\text{ cm}^{-1}$  and  $1206\text{ cm}^{-1}$ . The  $1283\text{ cm}^{-1}$  band is consistent with the symmetric stretch of a bridging azide ( $\nu_s(\mu\text{-N}_3)$ ). Whereas the  $1206\text{ cm}^{-1}$  band is consistent with the symmetric stretch of a terminal azide ( $\nu_s(\text{N}_3)$ ). Hence, the intermediate resultant from the loss of all amines was formulated as  $[\text{Co}_2(\text{N}_3)_6]$ . The proposed structure of the intermediate is given in Figure 7-5. The spectra of  $[\text{Co}_2(\text{N}_3)_6]$  are consistent with the spectra of analogous complexes.

The IR of a cobalt dimer complex containing bridging azide groups (no terminal azides), di- $\mu$ -azidotetrakis(acetylacetonato)dnicobalt(III),

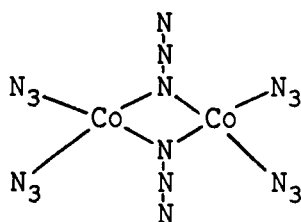


**Figure 7-5**

gave a sharp azide stretch ( $\nu_{as}(\mu\text{-N}_3)$ ) at  $2080\text{ cm}^{-1}$  and an absorption at  $1280\text{ cm}^{-1}$  ( $\nu_s(\mu\text{-N}_3)$ ).<sup>107</sup> The bridging azide stretch at  $2080\text{ cm}^{-1}$  appeared at a frequency  $50\text{ cm}^{-1}$  higher than the azide stretch of the monomeric species,  $[\text{Co}(\text{acac})_2(\text{N}_3)_2]^-$ .<sup>107</sup> There is precedent in the

literature showing that bridged azide complexes show a  $\nu_{as}(\mu-N_3)$  shift to higher frequency, relative to the monomeric species, of this magnitude.<sup>106</sup>

One of the antisymmetric azide stretches due to  $[Co_2(N_3)_6]$  ( $\nu_{as}(\mu-N_3)$ ), which appeared after photolysing *mer*- $Co(NH_3)_3(N_3)_3$  for 60 sec., was  $55\text{ cm}^{-1}$  to higher frequency of the starting materials azide stretches. The  $55\text{ cm}^{-1}$  shift is relative to the average band position of the antisymmetric azide stretches of the starting material.

The compound,  $[As(C_6H_5)_4]_2[Pd_2(N_3)_6]$ , is known and possesses both terminal and bridging azide groups. A single-crystal X-ray diffraction study revealed the structure to be that shown in Figure 7-6 ( $D_{2h}$ ).<sup>108</sup>

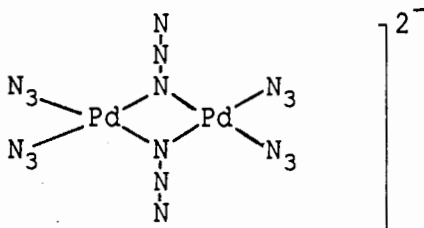


Figure 7-6

The palladium complex has an antisymmetric stretch at  $2060\text{ cm}^{-1}$  which was assigned as due to the bridging azides and two bands at  $2033\text{ cm}^{-1}$  and  $2000\text{ cm}^{-1}$  which were assigned to the antisymmetric stretches of the terminal azides.<sup>106,108</sup>

After photolysing a film of *mer*- $Co(NH_3)_3(N_3)_3$  for 225 min the bands due to  $[Co_2(N_3)_6]$  reached a maximum intensity. Subsequent photolysis resulted in the loss of the bands due to  $[Co_2(N_3)_6]$  at  $2095\text{ cm}^{-1}$ ,  $2060\text{ cm}^{-1}$ ,  $2006\text{ cm}^{-1}$ ,  $1283\text{ cm}^{-1}$ , and  $1206\text{ cm}^{-1}$  and the appearance of two new bands. The first was a broad asymmetric band centered at

2058  $\text{cm}^{-1}$ , the second band was also broad and asymmetric and centered at 1209  $\text{cm}^{-1}$  (Figure 7-7). The bands at 2058  $\text{cm}^{-1}$  and 1209  $\text{cm}^{-1}$  are likely due to the antisymmetric and symmetric stretches of a bridging azide, respectively. These bands were different, in position and appearance, from the bands due to both *mer*- $\text{Co}(\text{NH}_3)_3(\text{N}_3)_3$  and  $[\text{Co}_2(\text{N}_3)_6]$  (Fig 7-8). The bands at 2058  $\text{cm}^{-1}$  and 1209  $\text{cm}^{-1}$  were assigned to the formation of oligomers. The oligomers are formulated as repeating  $\{\text{Co}(\text{N}_3)_2\}_n$  units. No absorptions in the spectra of  $\{\text{Co}(\text{N}_3)_2\}_n$  could be assigned to terminal azide stretches, either antisymmetric or symmetric. Photolysis of  $\{\text{Co}(\text{N}_3)_2\}_n$  resulted in the decrease of absorptions due to  $\{\text{Co}(\text{N}_3)_2\}_n$ , however, no new bands were observed. Absorbance spectra showing the conversion of *mer*- $\text{Co}(\text{NH}_3)_3(\text{N}_3)_3$  to  $\{\text{Co}(\text{N}_3)_2\}_n$  through the intermediacy of  $[\text{Co}_2(\text{N}_3)_6]$  are summarized in Figure 7-8. After photolysing for 120 hrs., all bands due to azide ligands were lost.

The final film, resultant from exhaustive photolysis, was transferred to an X-ray photoelectron spectrometer and the Auger spectrum was obtained. The initial Auger spectrum of the sample showed that the film contained Co, O, and mostly carbon. The relative percentages of cobalt, oxygen and carbon were found to be 4%, 29%, and 66%, respectively. The high carbon and oxygen content, found on the surface of the film, were from atmospheric contamination of the film after the sample had been removed from the photolysis chamber. The surface layer of the film was removed by sputtering with 3 keV  $\text{Ar}^+$  ions. After two minutes of sputtering, the composition of the film had changed significantly. The relative percentages of cobalt, oxygen, and carbon were now 64%, 27%, and 9.5%, respectively. The shape and position of

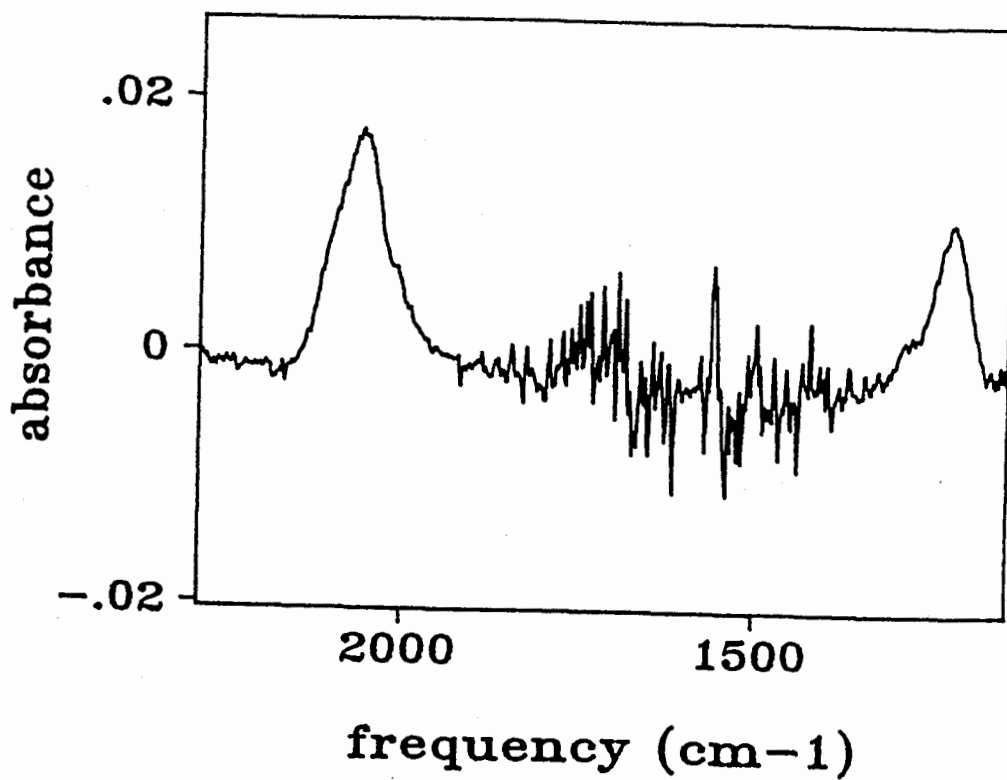


Figure 7-7

Absorbance spectrum due to  $\{\text{Co}(\text{N}_3)_2\}_n$



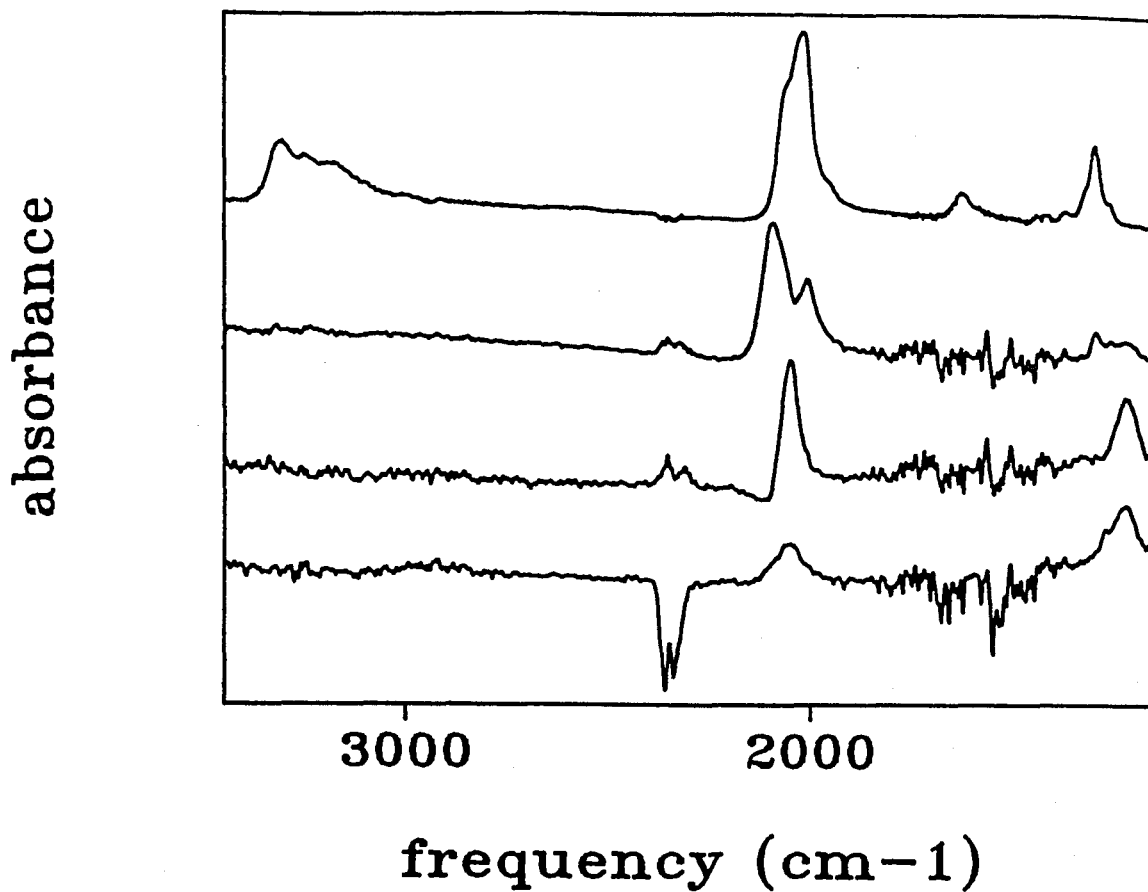


Figure 7-8

From top to bottom: Absorbance spectra showing the conversion of  $mer-Co(NH_3)_3(N_3)_3$  to  $\{Co(N_3)_2\}_n$  through the intermediacy of  $[Co_2(N_3)_6]$ .

the Co signals ( 2s at 652.8 eV, 2p<sub>1/2</sub> at 716.7 eV and 2p<sub>3/2</sub> at 772.2 eV) indicated the formation of elemental cobalt. The Auger spectra were consistent with the carbon and oxygen contamination being confined to the surface of the film. The relative composition of the bulk of the film was consistent with the formation of elemental cobalt.

### 7.3 Conclusions

The study of a *mer*-Co(NH<sub>3</sub>)<sub>3</sub>(N<sub>3</sub>)<sub>3</sub> film demonstrated that all ligands may be lost, photochemically, from coordination compounds. Also, the photodecomposition resulted in the production of a relatively pure cobalt metal film. The resultant film was shown to have very little contamination compared to the earlier studies on organometallic films. Also, we know that the carbon contamination did not come from the cobalt complexes being studied. Therefore, this particular study gives an indication of the amount of atmospheric contamination that occurs with our process. It is also important to point out that as a result of the limited solubility of *mer*-Co(NH<sub>3</sub>)<sub>3</sub>(N<sub>3</sub>)<sub>3</sub> and *fac*-Co(NH<sub>3</sub>)<sub>3</sub>(NO<sub>2</sub>)<sub>3</sub>, we were unable to spin-coat good quality films. From this study it was clear that some sort of organic ligand was essential for spin-coating uniform films from organic solvents.

### 7.4 Experimental Section

The experimental setup was identical to that discussed in Chapter 6. The UV/Vis spectra were obtained using a Cary 17 spectrophotometer. The photolysis source was also the same as that summarized in Chapter 6.

Auger spectra were obtained using a PHI double pass CMA at 0.85 eV resolution at the Surface Physics Laboratory, Dept. of Physics, Simon Fraser University.

#### 7.4.1 Preparation of *fac*-Co(NH<sub>3</sub>)<sub>3</sub>(NO<sub>2</sub>)<sub>3</sub>.

Trinitrotriammincobalt(III) was prepared using a standard literature method. The amount of reagents used, relative to the literature preparation, was scaled down.

Five grams of cobalt carbonate (0.042 mol) was dissolved in a hot mixture of 7.0 ml of glacial acetic acid and 20.0 ml of water. The above solution was then added to a cold mixture of 10.5 g (0.152 mol) of sodium nitrite, 50 ml aqueous ammonia, and 3.5 g of activated charcoal. The resulting solution was cooled in an ice bath while 30 ml of 3% hydrogen peroxide was slowly added to the stirred mixture. After the solution was in the ice bath for a further 20 minutes the liquid, contained in a 2-liter Erlenmeyer flask, was heated over a free flame in a fume hood for one hour (frequent swirling). Copious amounts of ammonia escaped during heating and the volume was kept constant by the addition of water. The hot solution was rapidly suction filtered to remove the charcoal, and the filtrate was cooled in an ice bath. The product that crystallized was filtered, washed with alcohol, ether and then allowed to air dry. The product may be purified by rapidly recrystallizing from thirty times its weight of boiling water that has been slightly acidified with acetic acid. The amount of product obtained was 2.6 g (yield, 25%).

#### 7.4.2 Preparation of $mer-Co(NH_3)_3(N_3)_3$ .

**WARNING:** The azido complexes of cobalt are detonators, especially sensitive at elevated temperatures! Discussed below is the preparation of  $mer-Co(NH_3)_3(N_3)_3$ .  $mer-Co(NH_3)_3(N_3)_3$  is explosive and extreme caution should be exercised when handling the compound.

The preparation procedure used was a modification of that used by Druding<sup>103</sup> et. al. However, in the interest of safety, the amount of reagents was reduced.

Cobalt(II) carbonate (reagent grade), 0.54g (0.0045 mol) and 0.50 g (0.0088 mol) of ammonium sulfate were dissolved in 20 ml water and 3 ml conc. sulphuric acid. After dissolution, 6 ml of 20% aqueous ammonia was slowly added, then 1.4 g (0.021 mol) sodium azide. Subsequently, air was bubbled through the solution for 2 hours. Afterwards, the solution was evaporated, to near dryness, on a steam bath. During evaporation a greenish-brown solid separated from the red solution.

**Warning:** Evaporation should be carried out behind a safety shield, since the hot residue is extremely shock sensitive. They should not be handled until they have cooled to room temperature. The greenish-brown residue was carefully transferred to a Buchner funnel. Solids that adhere to the beaker should not be scraped. The solid was washed with cold water until the filtrate was green, then washed with methanol and air-dried. The  $mer-Co(NH_3)_3(N_3)_3$  product was dark green in color.

#### 7.4.3 Deposition of $fac-Co(NH_3)_3(NO_2)_3$ and $mer-Co(NH_3)_3(N_3)_3$ as films.

$fac-Co(NH_3)_3(NO_2)_3$  and  $mer-Co(NH_3)_3(N_3)_3$  were dissolved in DMSO. However, spin coating the films was not possible, since DMSO is not

volatile enough. A drop of a DMSO solution containing either *fac*- $\text{Co}(\text{NH}_3)_3(\text{NO}_2)_3$  or *mer*- $\text{Co}(\text{NH}_3)_3(\text{N}_3)_3$  was deposited on a silicon chip. A film of the complex was formed by removing the solvent under reduced pressure.

## Chapter 8: The Photochemistry of $(\eta^5\text{-C}_5\text{H}_5)_2\text{Ti}(\text{N}_3)_2$ on Surfaces and in a Low Temperature Glass: Photodeposition of Titanium Dioxide Films

### 8.1 Introduction

As mentioned in the earlier chapters, metal films, metal oxides and metal nitrides are of paramount importance in the production of integrated circuits. In particular titanium dioxide has several practical applications in the semiconductor industry. The photodeposition of transition metals, specifically titanium, are of interest because of their applications as interconnects and in gate metallization in those situations where processing temperature is a critical factor. For example, a low process temperature is crucial in III-V device fabrication to avoid interfacial defects. The chemical vapour deposition of titanium dioxide<sup>110</sup> as well as the oxides of Ta<sup>111</sup>, Nb<sup>112</sup>, Hf<sup>37</sup>, and Zr<sup>37</sup> are being investigated since they are high-dielectric constant materials. The oxides of these metals may be suitable for applications such as storage capacitors in memory cells. One of the most useful applications of the photodeposition of a thin titanium metal film is on silicon wafers prior to the deposition of conducting aluminum tracks.<sup>37</sup> If a silicon wafer has an oxide coating prior to the deposition of aluminum tracks the adhesion of the aluminum is greatly diminished. However, a very thin film of titanium deposited first reacts with the oxide layer to form  $\text{TiO}_2$  leaving a silicon

surface. The scrubbing of the oxide layer by the titanium permits better adhesion of the aluminum tracks.<sup>37</sup>

As was discussed in the last chapter, the spin coating of good quality films of the inorganic cobalt complexes was complicated by their insolubility in most solvents. However the studies on the inorganic cobalt complexes demonstrated that the carbon contamination of the resultant film was primarily from the atmosphere. Therefore, the use of organic ligands probably does not account for a great deal of the hydrocarbon contamination of the photodecomposed film. Also, the presence of organic ligands in organometallic complexes greatly increase their solubility in organic solvents.

The choice of  $(\eta^5\text{-C}_5\text{H}_5)_2\text{Ti}(\text{N}_3)_2$  fulfilled several criteria. First, the  $(\eta^5\text{-C}_5\text{H}_5)$  moiety would allow the complex to be dissolved in organic solvents thereby permitting spin-coating of the films. Also, as demonstrated with the nickel and cobalt complexes, the azide ligands may be photoextruded. Similarly, the results of the study of  $(\eta^5\text{-C}_5\text{H}_5)_2\text{TiX}_2$  complexes in solution demonstrated that the cyclopentadienyl ligand may also be photoejected.<sup>113-115</sup> Precedent for photoextrusion of cyclopentadienyl from surface bound manganese complexes was discussed in Chapter 5. Photodecomposition of  $(\eta^5\text{-C}_5\text{H}_5)_2\text{Ti}(\text{N}_3)_2$  was expected to result in the formation of a titanium film.

In this chapter the photochemistry of  $(\eta^5\text{-C}_5\text{H}_5)_2\text{Ti}(\text{N}_3)_2$ , as a film and in glasses is discussed. The photolysis  $(\eta^5\text{-C}_5\text{H}_5)_2\text{Ti}(\text{N}_3)_2$ , as a film, led eventually to the production of a  $\text{TiO}_2$  film. High quality  $\text{TiO}_2$  films may be prepared by spray pyrolysis methods.<sup>116,117</sup>

Deposition of Ti films has also been achieved by laser assisted CVD.<sup>118,119</sup> However, the method described in this chapter to deposit TiO<sub>2</sub> films is the first example, as far as I am aware, of a single step process compatible with current mask photolithography methods.

## 8.2 Results and Discussion

### 8.2.1 Spectroscopic Data for the Complexes

The optical absorption spectra for  $(\eta^5\text{-C}_5\text{H}_5)_2\text{Ti}(\text{N}_3)_2$  consist of a number of bands, most of which are probably charge transfer in origin. The spectra for the Titanium complex, in different solvents, are summarized in Table 8-1. The transition near 400 nm and has an extinction coefficient in the range 2000-5000 M<sup>-1</sup>cm<sup>-1</sup>. This absorption is assigned as due to an azide to metal charge transfer transition. At higher energy a far more intense band was observed. The higher energy band had an extinction coefficient of approximately 20,000 M<sup>-1</sup> cm<sup>-1</sup>, and was assigned as due to a Cp to titanium charge transfer transition. The transition around 400 nm has been observed previously.<sup>89</sup>

A study of the photochemistry of analogous compounds,  $(\eta^5\text{-C}_5\text{H}_5)_2\text{TiX}_2$  (X = Cl, Br, I), has been done previously and their optical spectra have been discussed elsewhere.<sup>113-115</sup> Their spectra also consist of LMCT bands. The primary photochemistry discussed here is the result of photolysis into the low energy LMCT transition.

The FTIR spectrum in the region of the antisymmetric stretch ( $\nu_{\text{as}}(\text{N}_3)$ ) of  $(\eta^5\text{-C}_5\text{H}_5)_2\text{Ti}(\text{N}_3)_2$  on a Si(111) surface is given in Figure 8-1 a). It is interesting to note that there was a negligible deviation



Table 8-1

Optical data for  $(\eta^5\text{-C}_5\text{H}_5)_2\text{Ti}(\text{N}_3)_2$ 

Solvent	Wavelength (nm)	Extinction Coefficient $\ln(\text{M}^{-1}\text{cm}^{-1})^a$
Acetone	408	8.3
Toluene	412	8.5
	290	9.7
Ethanol <sup>b</sup>	404	7.7
	280	9.5
Ether	412	8.2
	288	9.4
$\text{CHCl}_3$	408	8.2
	284	9.9

- a) Due to the decomposition of the solutions, the extinction coefficients listed are approximate.
- b) For this solvent, the decomposition was so significant that the wavelengths and extinction coefficients should be considered very approximate.

from linearity (Fig 8-1 b)) when absorbance vs. coverage was plotted over a range of 0.9 - 4 molecules/Å<sup>2</sup>. The linear plot of Figure 8-1 b) is consistent with no detectable thermal chemistry occurring upon film deposition. The spectra of the complex on the surface did not change, in appearance, with increasing coverage. Based on the absorbance vs. coverage plot, the film thickness for each experiment was in excess of sixty monolayers. This coverage is in the region required for technically useful films.<sup>80</sup> The interfacial layer, at either the silicon or vacuum interface, did not make a detectable contribution to the observed spectra.

The FTIR spectra of  $(\eta^5\text{-C}_5\text{H}_5)_2\text{Ti}(\text{N}_3)_2$ , its <sup>15</sup>N labelled derivative and  $(\eta^5\text{-C}_5\text{H}_5)_2\text{TiCl}_2$  are summarized in Table 8-2. The most intense IR bands for  $(\eta^5\text{-C}_5\text{H}_5)_2\text{Ti}(\text{N}_3)_2$  are those due to the antisymmetric azide stretches at 2084 cm<sup>-1</sup> and 2051 cm<sup>-1</sup>. The symmetric azide stretch was found at 1348 cm<sup>-1</sup>. These assignments were consistent with the literature assignments of the solution IR.<sup>120</sup> The azide bands shifted to lower energy, as expected, for the <sup>15</sup>N labelled derivative. Analogous to the <sup>15</sup>N labelled *trans*-(Et<sub>3</sub>P)<sub>2</sub>Ni(N<sub>3</sub>)<sub>2</sub> complex discussed earlier, the <sup>15</sup>N labelled titanium complex consisted of a mixture of isotopomers;  $(\eta^5\text{-C}_5\text{H}_5)_2\text{Ti}({}^{15}\text{N}{}^{14}\text{N}_2)_2$ ,  $(\eta^5\text{-C}_5\text{H}_5)_2\text{Ti}({}^{14}\text{N}_2{}^{15}\text{N})_2$  and  $(\eta^5\text{-C}_5\text{H}_5)_2\text{Ti}({}^{15}\text{N}{}^{14}\text{N}_2)({}^{14}\text{N}_2{}^{15}\text{N})_2$  in a 1:1:2 ratio. The observed broad antisymmetric azide stretches were the result of the superposition of the stretches due to the three different isotopomers. The IR of the symmetric azide stretch showed a shift of 33 cm<sup>-1</sup> to lower energy, as a result of <sup>15</sup>N labelling but no fine structure was observed.

As well as the azide bands, both CH and CC absorptions due to the

Table 8-2

Table of FTIR spectral data for relevant complexes

Complex	Medium	$\nu_{as}(N_3)$ ( $\text{cm}^{-1}$ )	$\nu_s(N_3)$ ( $\text{cm}^{-1}$ )
$(\eta^5\text{-C}_5\text{H}_5)_2\text{Ti}(N_3)_2$	surface	2084,2051	1348
	glass	2077,2049	
$(^{15}\text{N})-(\eta^5\text{-C}_5\text{H}_5)_2\text{Ti}(N_3)_2$	surface	2063,2039	1315
	glass	2068,2036	
$(\eta^5\text{-C}_5\text{H}_5)_2\text{Ti}(N_3)$	surface	2077	1333
	glass	2069	
$(^{15}\text{N})-(\eta^5\text{-C}_5\text{H}_5)_2\text{Ti}(N_3)$	surface	2063	1311
	glass	2066	

Table 8-2 (cont.)

Complex	Medium	$\nu(\text{CH})$ ( $\text{cm}^{-1}$ )	$\nu(\text{CC})$ ( $\text{cm}^{-1}$ )
$(\eta^5\text{-C}_5\text{H}_5)_2\text{Ti}(\text{N}_3)_2$	surface	3106	1443
$(^{15}\text{N}) - (\eta^5\text{-C}_5\text{H}_5)_2\text{Ti}(\text{N}_3)_2$	surface	3106	1443
$(\eta^5\text{-C}_5\text{H}_5)_2\text{Ti}(\text{N}_3)$	surface	3107	1446
$(^{15}\text{N}) - (\eta^5\text{-C}_5\text{H}_5)_2\text{Ti}(\text{N}_3)$	surface	3107	1446
$(\eta^5\text{-C}_5\text{H}_5)_2\text{TiCl}_2$	surface	3105	1440

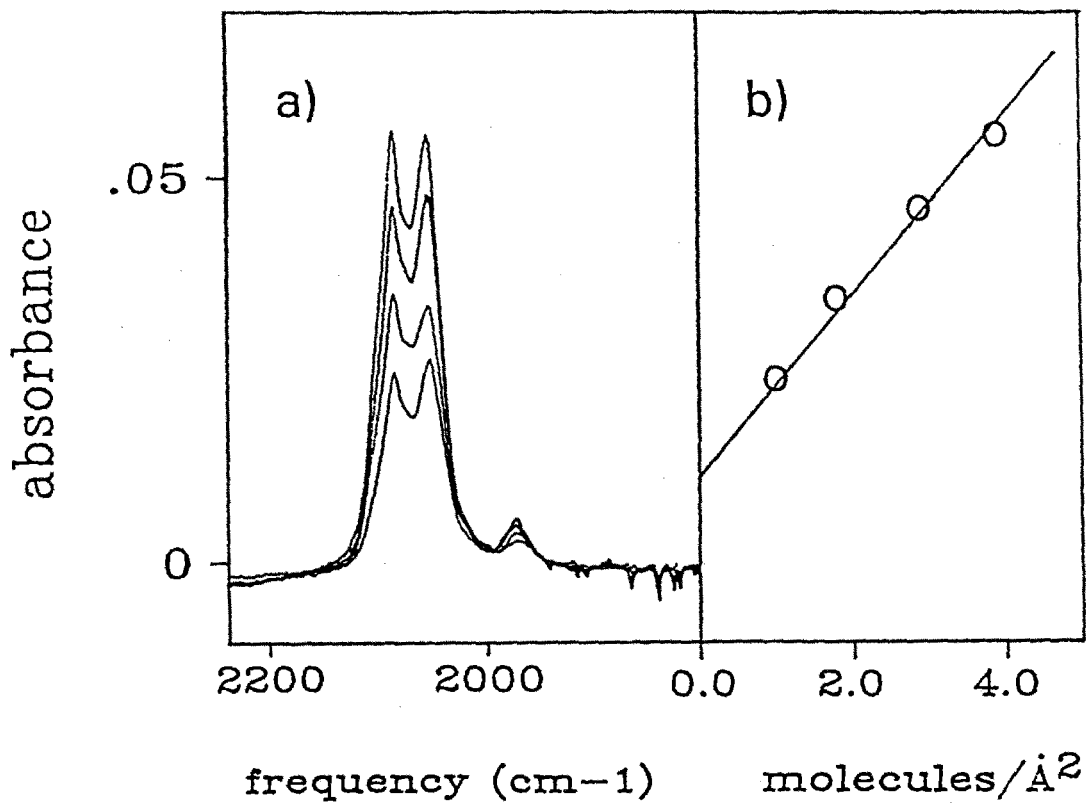


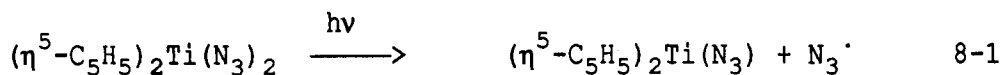
Figure 8-1

- a) FTIR spectra associated with 0.9, 1.8, 2.8, and 3.7 molecules of  $(\eta^5\text{-C}_5\text{H}_5)_2\text{Ti}(\text{N}_3)_2$  per  $\text{\AA}^2$  on a silicon surface.
- b) Plot of absorbance of the high energy component of the antisymmetric azide stretch of  $(\eta^5\text{-C}_5\text{H}_5)_2\text{Ti}(\text{N}_3)_2$  vs coverage, data from figure 8-1a).

cyclopentadienyl ligands were observed and are summarized in Table 8-2. The assignment of the CH and CC modes for  $(\eta^5\text{-C}_5\text{H}_5)_2\text{Ti}(\text{N}_3)_2$  were based on the published assignments for  $(\eta^5\text{-C}_5\text{H}_5)_2\text{TiCl}_2$ .<sup>121-123</sup> The spectral data for  $(\eta^5\text{-C}_5\text{H}_5)_2\text{TiCl}_2$  as a film on Si(111) are summarized in Table 8-2 and do not differ significantly from those in other media.

### 8.2.2 Photochemistry of $(\eta^5\text{-C}_5\text{H}_5)_2\text{Ti}(\text{N}_3)_2$ in a low temperature glass

Prior to discussion of the results obtained in a film, the results found in a (1,2-epoxyethyl)-benzene glass will be discussed. Photolysis was carried out at 77 K where (1,2-epoxyethyl)-benzene forms a transparent glass. The first photoreaction observed was the loss of intensity due to the azide antisymmetric stretches at  $2077\text{ cm}^{-1}$  and  $2049\text{ cm}^{-1}$ . Accompanying the loss in intensity due to the azide bands was the appearance of a new absorption at  $2069\text{ cm}^{-1}$ . Photolysis of the  $^{15}\text{N}$  labelled starting complex resulted in the appearance of this band at lower energy. This observation was consistent with the absorption being due to an azide. The spectral changes were indicative of the loss of a



single azide ligand and the formation of  $(\eta^5\text{-C}_5\text{H}_5)_2\text{TiN}_3$ . The reaction is summarized in equation 8-1.

The same overall result, summarized in equation 8-1, could be obtained at either 77 K or 20 K. The photoreaction could be initiated

with either the filtered (bandpass  $\lambda > 400$  nm or bandpass  $\lambda > 480$  nm) or unfiltered output of a high pressure Hg lamp. Presumably, the photoextruded azide radical thermally decomposed to yield  $N_2$ . No bands assignable to  $^{15}NN^{85}$  or  $N_3^{124}$  were detected in the FTIR spectra. However, that was not surprising, since  $^{15}N^{14}N$  is expected to have a very low extinction coefficient and is difficult to observe by IR spectroscopy.<sup>98</sup> Therefore, it was reasonable that the products derived from the thermal decomposition of the lost azide radical were not detected.

Extended photolysis resulted in no further photoreaction on a comparable time scale. One sample was photolyzed for more than six days at 20 K (three days with bandpass  $\lambda > 480$  nm and three days with a 10 cm path length quartz water filter equipped with pyrex optics) and no decomposition of the primary photoproduct,  $(\eta^5-C_5H_5)_2Ti(N_3)$ , was detected. As discussed below this photoproduct was far more sensitive in a film.

### 8.2.3 Photochemistry of $(\eta^5-C_5H_5)_2Ti(N_3)_2$ as a film

The room temperature photolysis of  $(\eta^5-C_5H_5)_2Ti(N_3)_2$  resulted in the initial loss of the antisymmetric stretches of the azides and the appearance of a new band. The spectral changes are summarized in Figure 8-2. The new band, which appeared between the antisymmetric azide stretches of the starting material, could be seen more clearly following the computer addition of the starting material absorptions. After computer addition of the starting material absorptions, the correct position of the new band was found to be  $2077\text{ cm}^{-1}$ . Repeating the

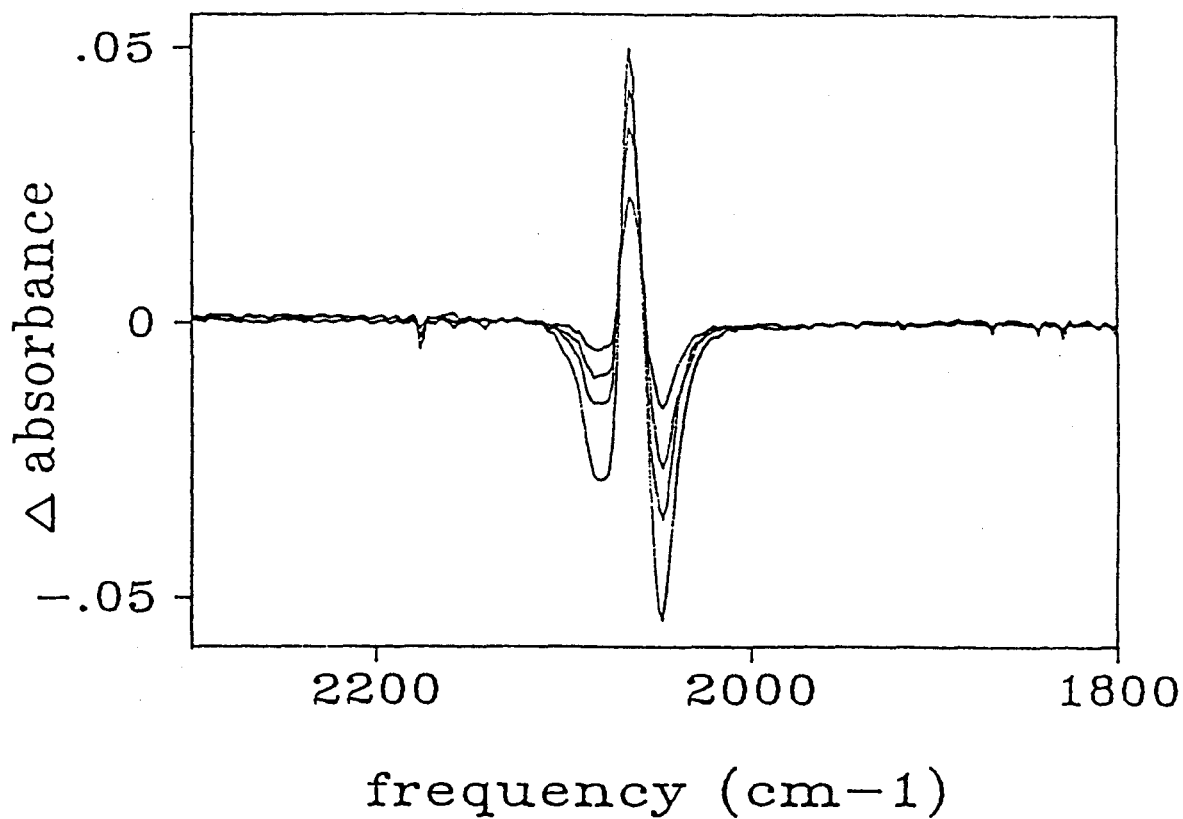


Figure 8-2

FTIR spectral changes associated with the photolysis of a film of  $(\eta^5\text{-C}_5\text{H}_5)_2\text{Ti}(\text{N}_3)_2$  on a silicon surface for 30, 60, 90, and 120 sec.



above procedure with  $^{15}\text{N}$  labelled starting material resulted in the appearance of the band due to the intermediate at  $2063\text{ cm}^{-1}$ . This band was substantially broadened (full width at half height of  $50\text{ cm}^{-1}$  compared to  $30\text{ cm}^{-1}$  for the unlabelled derivative). The photoreaction is summarized in equation 8-1. The width of the  $2063\text{ cm}^{-1}$  band of the  $^{15}\text{N}$  labelled complex was attributed to the formation of two isotopomers,  $(\eta^5\text{-C}_5\text{H}_5)_2\text{Ti}(^{15}\text{N}^{14}\text{N}_2)$  and  $(\eta^5\text{-C}_5\text{H}_5)_2\text{Ti}(^{14}\text{N}_2^{15}\text{N})$ . No other spectral changes were observed for this system in the initial stages of photolysis.

The initial reaction was assigned as being due to the loss of a single azide ligand. Photolysis of a film at either 77 K or 20 K showed an additional feature in the FTIR spectra. The antisymmetric azide stretch was split by a feature at slightly higher energy. The band, which appeared as a shoulder, shifted upon  $^{15}\text{N}$  labelling. A rotamer of the remaining azide may have been responsible for the shoulder since it is possible for the azide to coordinate in bent fashion.<sup>88</sup> It should be pointed out that when the film was photolyzed under an atmosphere of air no bands assignable to  $(\eta^5\text{-C}_5\text{H}_5)_2\text{Ti}(\text{N}_3)$  were observed.

Prolonged photolysis, *in vacuo*, of a film resulted in the spectral changes summarized in Figure 8-3. The disappearance of the  $(\eta^5\text{-C}_5\text{H}_5)_2\text{Ti}(\text{N}_3)$  complex, was evident from the decrease in the intensity of the absorptions due to the antisymmetric and symmetric stretches of the azide ligand, and the coordinated  $(\eta^5\text{-C}_5\text{H}_5)$  moiety. The only new absorptions observed were in the region of  $3000\text{ cm}^{-1}$  and  $1600\text{ cm}^{-1}$ . The bands remained unshifted upon  $^{15}\text{N}$  labelling and were therefore assigned as being due to the fragments derived from the uncoordinated  $(\text{C}_5\text{H}_5)$

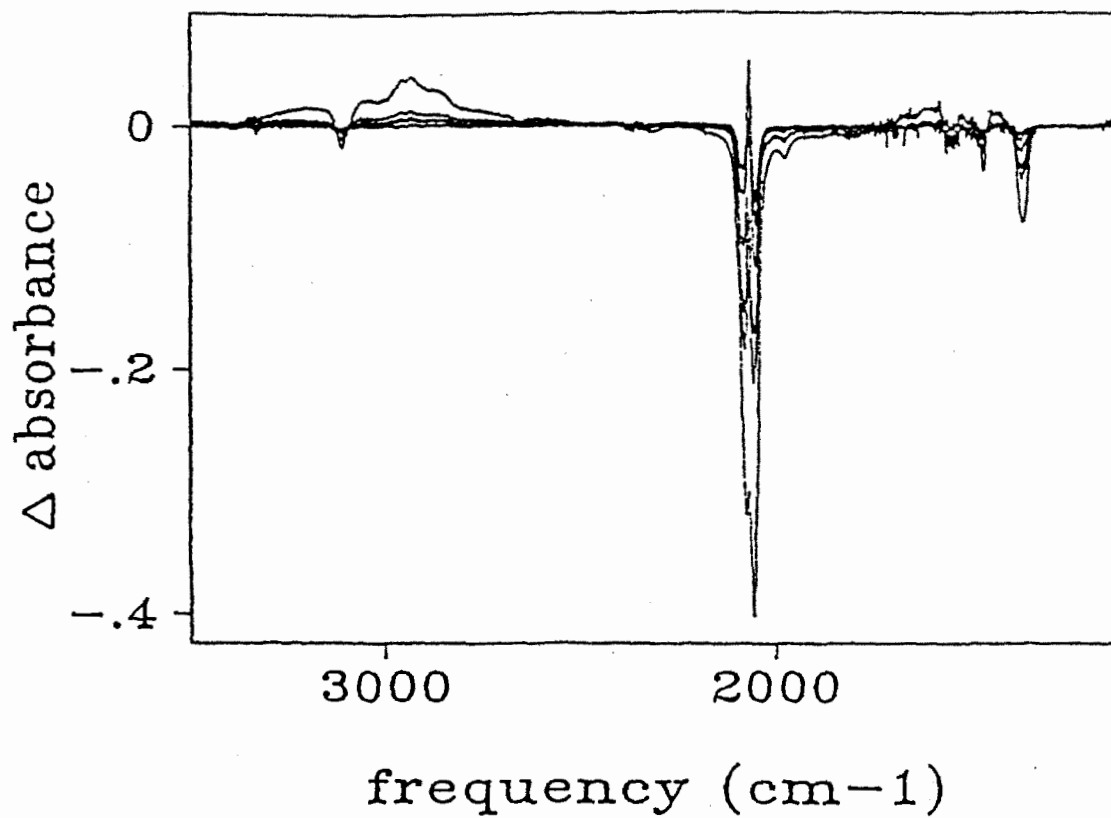
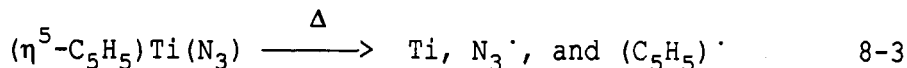
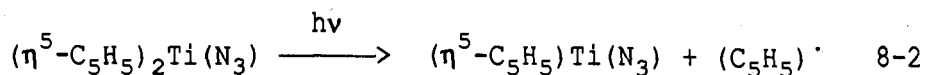


Figure 8-3

FTIR spectral changes associated with the photolysis of a  $(\eta^5\text{-C}_5\text{H}_5)_2\text{Ti}(\text{N}_3)_2$  film, on a silicon surface, for 3, 8, 35, 72, 102, and 1182 min.

ligand. The proposed reactions are summarized in equations 8-2 and 8-3.



It should be noted that the intermediate,  $(\eta^5\text{-C}_5\text{H}_5)\text{Ti}(\text{N}_3)$ , given in equation 8-2 was not observed. However, if the azide ligand was photoextruded from  $(\eta^5\text{-C}_5\text{H}_5)_2\text{Ti}(\text{N}_3)$ , rather than  $(\eta^5\text{-C}_5\text{H}_5)$ , the product would have been  $(\eta^5\text{-C}_5\text{H}_5)_2\text{Ti}$ . It has been shown that a form of  $(\eta^5\text{-C}_5\text{H}_5)_2\text{Ti}$  may be produced photochemically from  $(\eta^5\text{-C}_5\text{H}_5)_2\text{TiMe}_2$ .<sup>125</sup> The authors propose that the photochemically generated 'titanocene' is an oligomeric material made up of  $(\eta^5\text{-C}_5\text{H}_5)_2\text{Ti}$  and  $(\eta^1 : \eta^5\text{-C}_5\text{H}_4)\text{Ti}_2$  units. The oligomeric titanocene species is a photostable solid. The fact that we do not observe this product, or anything similar, indicated that an alternate photoprocess was occurring. Therefore, the second photoreaction was formulated as  $(\eta^5\text{-C}_5\text{H}_5)$  loss. Subsequently, the  $(\eta^5\text{-C}_5\text{H}_5)\text{Ti}(\text{N}_3)$  species thermally decomposed (eq. 8-3).

It is worth noting that the loss of  $(\eta^5\text{-C}_5\text{H}_5)$  has been postulated in the photochemistry of  $(\eta^5\text{-C}_5\text{H}_5)_2\text{TiCl}_2$ .<sup>125</sup> No spectral evidence consistent with the photoextrusion of a  $(\eta^5\text{-C}_5\text{H}_5)$  radical was observed as a result of photolysing  $(\eta^5\text{-C}_5\text{H}_5)_2\text{Ti}(\text{N}_3)_2$  in a glass or a film. However, the efficient recombination of  $(\eta^5\text{-C}_5\text{H}_5)$  and  $(\eta^5\text{-C}_5\text{H}_5)\text{Ti}(\text{N}_3)_2$  would be expected since diffusion of the photoproducts should be slow.

In some experiments, the films were produced by spin coating the complex onto the silicon wafer. The films produced in such a manner were thinner and more uniform. The spin coated films were typically on

the order of 120 nm thick. The results of the room temperature photolysis of spin coated films were consistent with the spectral changes discussed above, however, there was no evidence of hydrocarbon products in the IR spectra following prolonged photolysis. Presumably, the products derived from the thermal decomposition of uncoordinated  $(C_5H_5)$  were lost to the vacuum. The loss of the thermal decomposition products of  $(C_5H_5)$ , to the vacuum, is conceivable in the case of a thin film. Whereas in the thicker films the fragments are unlikely to diffuse out of the film.

Repetition of the above experiments, photolysing solely into the low energy transition, resulted in the same spectral changes as already discussed. The photosensitivity of a film of  $(\eta^5-C_5H_5)_2Ti(N_3)_2$  was markedly different from the complex in a glass. For example, a film held at 20 K, and photolyzed for 18 hours showed the loss of 75% of the  $(\eta^5-C_5H_5)_2Ti(N_3)$  intermediate.

The final films, after exhaustive photolysis, were removed and transferred to the X-ray photoelectron spectrometer. The resultant film contained Ti, O, C, and a small amount of N. The presence of  $TiO_2$  was confirmed by both the relative amounts of Ti and O and by the position of the Ti lines. The XPS lines due to Ti and  $TiO_2$  are well separated and easily distinguishable.<sup>126</sup> The  $2p_{3/2}$  and  $2p_{1/2}$  lines of Ti appear at 453.8 eV and 459.9 eV, respectively. Whereas the  $2p_{3/2}$  and  $2p_{1/2}$  lines of Ti in  $TiO_2$  appear at 458.8 eV and 464.2 eV, respectively. The titanium transitions in the XPS spectra of an exhaustively photolysed sample were found at 458.8 eV ( $2p_{3/2}$ ) and 464.5 eV ( $2p_{1/2}$ ). The Auger spectrum of the unspattered sample was used to calculate the

relative amounts of titanium and oxygen that were present (equation 6-4). The relative percentages of titanium and oxygen were found to be 23% and 39%, respectively. These relative amounts were consistent with the formation of  $TiO_2$ . In some experiments there was a slight asymmetry present in the Ti lines indicating the possible formation of TiN. Asymmetry also appeared in the N 1s line consistent with two peaks, one at 398.0 eV and one at 399.4 eV. This was indicative of the formation of nitrogen containing organic species or possibly TiN. The amount of carbon detected was dependent on the method of preparation of the initial film. If the initial film was prepared by the evaporation of a drop of a solution containing  $(\eta^5-C_5H_5)_2Ti(N_3)_2$ , then carbon was fifteen times more abundant than titanium. The films prepared by spin coating contained approximately three times the amount of carbon compared with the amount of titanium. The XPS results were in agreement with the observed infrared spectra.

The production of  $TiO_2$ , on the surface, was further confirmed by depth profile experiments. In the depth profile experiments, sputtering of the surface resulted in an initial decrease (i.e., sputtering for 6 minutes) of the oxygen to titanium ratio. Subsequent sputtering resulted in no further change in the ratio. The behaviour was consistent with the reduction of  $TiO_2$  upon sputtering. This effect has been reported previously.<sup>127</sup> The calculated ratio of titanium to oxygen, after 10 seconds of sputtering, was found to be approximately 1:1. The Auger studies indicated that the film was a homogeneous  $TiO_2$  layer rather than a mixture of oxides. Spin coated samples showed that the carbon signal decreased significantly after 15 seconds of sputtering.

At longer sputtering times a decreased rate of loss of the carbon signal was observed, however, the carbon signal did not decrease to baseline levels until silicon was the most intense spectral signal. At that point, the titanium signal was approximately half that of the silicon signal.

Surface Raman spectroscopy was done in the hope of identifying whether the  $\text{TiO}_2$  formed was anatase or rutile. However, the Raman spectra were complicated by the organic contaminants. The only observable signal was due to the intense fluorescent emission from the organic contamination. Repeated attempts to clean the surface, with various solvents, did not remove the contaminant.

The Ti, once formed, reacts with either the oxygen in the atmosphere or the oxide layer on the silicon substrate. The vacuum used in these experiments was on the order of  $10^{-3}$  torr. Therefore, there was a source of oxygen from the atmosphere with which the titanium could react to form  $\text{TiO}_2$ . Also, the oxide layer on the silicon was a source of oxygen for the formation of  $\text{TiO}_2$ .<sup>37</sup>

The approximate quantum yields for the decomposition of  $(\eta^5\text{-C}_5\text{H}_5)_2\text{Ti}(\text{N}_3)_2$ , under various atmospheres, were determined by photolysis with 366 nm light. The absorbance of the  $(\eta^5\text{-C}_5\text{H}_5)_2\text{Ti}(\text{N}_3)_2$  film was calculated from its solution extinction coefficient, at 366 nm. The quantum yield formula used is given in equation 8-4. The derivation of equation 8-4 is given in the appendix. Irradiation under a vacuum of about  $10^{-3}$  torr resulted in an approximate quantum yield, for the process, of 0.005. In air, where the  $(\eta^5\text{-C}_5\text{H}_5)_2\text{TiN}_3$  intermediate reacted thermally with oxygen, the decomposition quantum yield was

$$\Phi = [-\emptyset \times (\text{total number of moles}) / (I_0) (A(0))] \quad 8-4$$

where  $\Phi$  = quantum yield

$\emptyset$  = the slope of a plot of  $\ln(A(0)/A(t))$  vs. mJ of light, where,  $A(0)$  is the absorbance at time = 0 and  $A(t)$  is the absorbance at time = t

$I_0$  = Intensity of the incident light in mW

$A(0)$  = is the absorbance of the film at time = 0 based on the solution extinction coefficient at 366 nm

0.025. To support the idea that the differing quantum yields were the result of the oxygen content in the two atmospheres, a third quantum yield was determined in which the sample was under a nitrogen atmosphere (which contained a small amount of oxygen). The quantum yield under those conditions was found to be 0.010. The relevant quantities used in equation 8-2, for the three experimental conditions, are given in Table 8-3. The results were consistent with the varying stability of  $(\eta^5\text{-C}_5\text{H}_5)_2\text{TiN}_3$  under the differing conditions. In a vacuum  $(\eta^5\text{-C}_5\text{H}_5)_2\text{TiN}_3$  is more stable and required more light in order to affect its photochemical decomposition, resulting in a lower overall decomposition quantum yield. However, in air  $(\eta^5\text{-C}_5\text{H}_5)_2\text{TiN}_3$  was not stable and underwent thermal reactions with  $\text{O}_2$ . Therefore, since the  $\nu_{\text{as}}$  azide stretch of  $(\eta^5\text{-C}_5\text{H}_5)_2\text{TiN}_3$  overlaps with the absorbances due to the starting material, the apparent quantum yields were dependent on the lifetime of the  $(\eta^5\text{-C}_5\text{H}_5)_2\text{TiN}_3$  species.

The ability to produce thin films of  $\text{TiO}_2$  from smooth spin coated films of  $(\eta^5\text{-C}_5\text{H}_5)_2\text{Ti(N}_3)_2$  indicated that this system should be amenable

Table 8-3

Quantities used in the quantum yield calculations for  $(\eta^5\text{-C}_5\text{H}_5)_2\text{Ti}(\text{N}_3)_2$

Data for the low energy azide stretch

	Air	Nitrogen (with some O <sub>2</sub> )	Vacuum (10 <sup>-3</sup> torr)
$\phi$ (s <sup>-1</sup> )	1.80 x 10 <sup>-3</sup>	8.66 x 10 <sup>-4</sup>	3.27 x 10 <sup>-4</sup>
total # of moles	1.85 x 10 <sup>-8</sup>	2.07 x 10 <sup>-8</sup>	2.02 x 10 <sup>-8</sup>
I <sub>0</sub> (einstein/s)	2.29 x 10 <sup>-8</sup>	2.45 x 10 <sup>-8</sup>	2.29 x 10 <sup>-8</sup>
A(0) (cm <sup>2</sup> /mol) <sup>a</sup>	6.40 x 10 <sup>-2</sup>	7.10 x 10 <sup>-2</sup>	6.98 x 10 <sup>-2</sup>

Data for the high energy azide stretch

	Air	Nitrogen (with some O <sub>2</sub> )	Vacuum (10 <sup>-3</sup> torr)
$\phi$ (s <sup>-1</sup> )	2.14 x 10 <sup>-3</sup>	1.10 x 10 <sup>-3</sup>	4.24 x 10 <sup>-4</sup>
total # of moles	2.07 x 10 <sup>-8</sup>	2.45 x 10 <sup>-8</sup>	2.13 x 10 <sup>-8</sup>
I <sub>0</sub> (einstein/s)	2.29 x 10 <sup>-8</sup>	2.45 x 10 <sup>-8</sup>	2.29 x 10 <sup>-8</sup>
A(0) (cm <sup>2</sup> /mol) <sup>a</sup>	7.20 x 10 <sup>-2</sup>	8.50 x 10 <sup>-2</sup>	7.35 x 10 <sup>-2</sup>

a) Absorbance of a film calculated from the solution extinction coefficient determined at 366 nm ( $\epsilon = 1729 \text{ dm}^3/\text{mol cm}$ ).



01010 01010  
04-2 2010 19 202 323

to processing by standard lithographic techniques. In order to confirm this, a sample prepared by spin coating a Si wafer with  $(\eta^5\text{-C}_5\text{H}_5)_2\text{Ti}(\text{N}_3)_2$ , was photolyzed under a mask in contact with the wafer. The mask was obtained from IBM, and was a standard photomask. Once photolyzed, the sample was rinsed with  $\text{CH}_2\text{Cl}_2$  and imaged by a scanning electron microscope to yield the pattern shown in Figure 8-4. The pattern of five lines, of which the center line is twice as long as the remaining four, was clearly distinguishable. The lines were approximately 2 microns wide. This result demonstrated that the chemistry was compatible with current standard lithographic procedures.

### 8.3 Conclusions

The results of the photolysis, under the varying conditions, are summarized in Figure 8-5. In a film the loss of all ligands from  $(\eta^5\text{-C}_5\text{H}_5)_2\text{Ti}(\text{N}_3)_2$  was induced photochemically at temperatures as low as 20 K. The thermally produced nitrogen species, resultant from the photoextruded azide ligand, were lost to the vacuum. Conversely, the hydrocarbon species formed by the thermal decomposition of the photoextruded cyclopentadienyl moiety were not completely lost from the surface.

We have been able to show that  $\text{TiO}_2$ , which is a useful dielectric in VLSI devices,<sup>37</sup> could be produced photochemically at temperatures of 20 K. The deposition of dielectrics at such low temperatures would greatly reduce the chances of interdiffusion of species and surface defects. Clearly, the carbon contamination would present a significant barrier to using this process of depositing  $\text{TiO}_2$ . However, the process

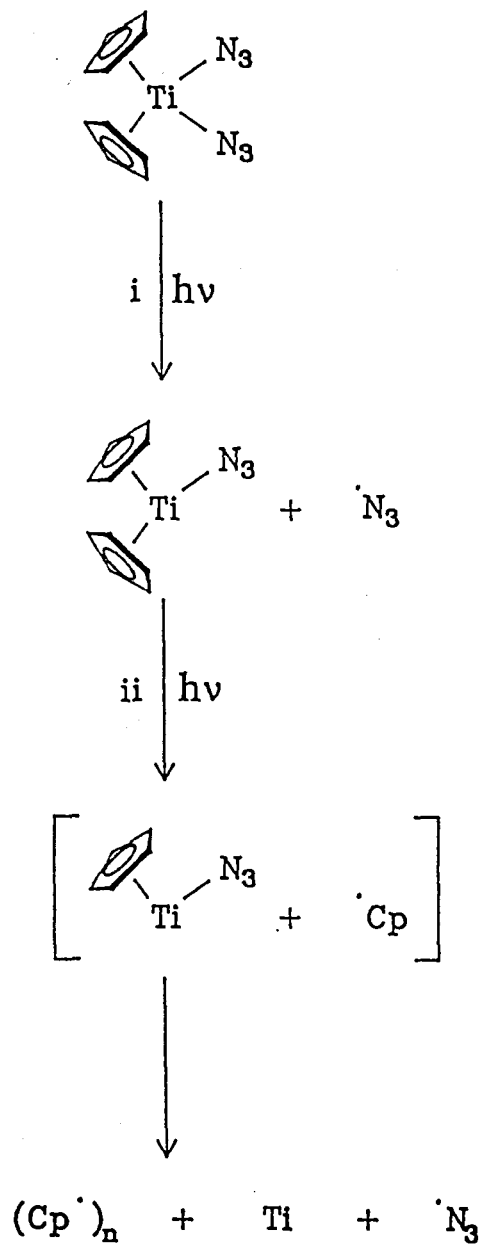


**Figure 8-5**

- i) Photolysis in a glass at either 77 or 20 K, or photolysis in a film at either 300, 77 or 20 K.
- ii) Photolysis in a film at 300, 77 or 20 K.

used here is unquestionably compatible with standard lithographic procedures.

#### 8.4 Experimental Section

The complex,  $(\eta^5\text{-C}_5\text{H}_5)_2\text{Ti}(\text{N}_3)_2$ , was prepared by literature methods.<sup>120, 128</sup> The  $\text{CaF}_2$  crystals were obtained from Wilmad Glass Co. Inc.. The Si(111) wafers were obtained from Pacific Microelectronics Center, Canada. The wafers were p-type silicon with tolerances and specifications as per SEMI Standard M1.1.STD.5. The 4" wafers were cut into pieces with the approximate dimensions of 1 cm x 1 cm. The  $^{15}\text{N}$  sodium azide was obtained from Cambridge Isotopes and was 99 atom percent  $^{15}\text{N}$  enriched in the 1 position.

The FTIR spectra were obtained using a BOMEM Michelson 120 FTIR spectrophotometer operating at  $4\text{ cm}^{-1}$  resolution. The samples were held in a  $\text{CaF}_2$  faced cell for glasses or in a high conductivity copper sample mount within a  $\text{CaF}_2$  faced vacuum Dewar for films. Experiments at 20 K were conducted using a CTI-Cryogenics Model 22 cryocooler and a 350R compressor system equipped with a Lake Shore Cryotronics DRC 80C temperature controller. The temperature was monitored with a Lake Shore Cryotronics silicon diode sensor (DTC500 DRC). The UV/VIS spectra were obtained with a Cary 17 spectrophotometer.

The photolysis source was a 100W high pressure Hg lamp in an Oriel housing equipped with condenser lenses and filtered through a 10 cm path length water filter equipped with pyrex optics.

X-ray photoelectron spectra were obtained using a PHI double pass CMA at 0.85 eV resolution at the Surface Physics Laboratory, Dept. of

Physics, Simon Fraser University. The depth profile was achieved by sputtering with 3 keV Ar<sup>+</sup> ions.

#### 8.4.1 Preparation of (<sup>15</sup>N) labelled ( $\eta^5$ -C<sub>5</sub>H<sub>5</sub>)<sub>2</sub>Ti(N<sub>3</sub>)<sub>2</sub>

To a solution containing ( $\eta^5$ -C<sub>5</sub>H<sub>5</sub>)<sub>2</sub>TiCl<sub>2</sub> (0.040 g) in acetone (20 ml) solid 1-Na<sup>15</sup>NN<sub>2</sub> (0.010 g) was added. The mixture was stirred for 24 hours. The solvent was then removed under reduced pressure and the solid was extracted with CH<sub>2</sub>Cl<sub>2</sub>. After the removal of the solvent the yield of (<sup>15</sup>N)-( $\eta^5$ -C<sub>5</sub>H<sub>5</sub>)<sub>2</sub>Ti(N<sub>3</sub>)<sub>2</sub> was 0.032 g (77%).

#### 8.4.2 Photolysis of complexes in a (1,2-epoxyethyl)-benzene glass.

A sample of ( $\eta^5$ -C<sub>5</sub>H<sub>5</sub>)<sub>2</sub>Ti(N<sub>3</sub>)<sub>2</sub> was dissolved in (1,2-epoxyethyl)-benzene and loaded into a CaF<sub>2</sub> faced cell. The sample was then cooled to 77 K and the FTIR spectrum obtained. Subsequently, the sample was photolyzed with UV light for 20, 30, 37, 60 and 120 min. Similar experiments were conducted at 20 K utilizing the cryocooler system.

#### 8.4.3 Calibration of the absorption on a silicon surface.

A stock solution of ( $\eta^5$ -C<sub>5</sub>H<sub>5</sub>)<sub>2</sub>Ti(N<sub>3</sub>)<sub>2</sub> (0.0060 g) in CH<sub>2</sub>Cl<sub>2</sub> (9.0 ml) was prepared. A drop (0.0031 ml) of this solution was then deposited on the surface of a Si wafer and the solvent was allowed to evaporate. Once the film had dried, the FTIR spectrum was obtained. The area of the drop was found to be 0.5 cm<sup>2</sup>. The area of the film and the absorption corresponded to a coverage of 0.94 molecules per Å<sup>2</sup>. The process was repeated several times. A calibration curve of absorbance vs. moles of ( $\eta^5$ -C<sub>5</sub>H<sub>5</sub>)<sub>2</sub>Ti(N<sub>3</sub>)<sub>2</sub> deposited is given in figure 8-1 b).

#### 8.4.4 The photolysis of complexes on silicon surfaces.

For photolysis, a Si surface was prepared with  $(\eta^5\text{-C}_5\text{H}_5)_2\text{Ti}(\text{N}_3)_2$ , as described above, and transferred to a vacuum Dewar. The sample was then photolyzed for 30, 60, 90, 120 sec. and 3, 8, 35, 72, 102 and 1182 min. The spectral changes are summarized in Figures 8-2 and 8-3. Analogous experiments were conducted at 77 K by cooling the vacuum Dewar with liquid  $\text{N}_2$ , and at 20 K using the cryocooler.

## Appendices

### A-2: Appendix for Chapter 2

Linert's equation and the definition of the terms (eq. 2-14 in Chapter 2) are restated here as equation A2-I. As stated in Chapter 2

$$k = A_0 s_N (h\omega x_{\text{bath}})^2 \exp[s_N(\omega/v - h\omega x_{\text{bath}})] \quad \text{A2-I}$$

- where;
- $A_0$  = constant
  - $s_N$  = is the number of reactant levels with energy lower than the reaction barrier
  - $h$  = Planck's constant
  - $\omega$  = is the vibrational frequency of the reaction site of the reactant
  - $x_{\text{bath}}$  = defined as  $1/kT$
  - $v$  = the active frequency of the heat-bath system in resonance with the reactant vibrations

there are two parameters characterizing the reactants;  $s_N$  and  $\omega$ .

Therefore, one form of Linert's equation is obtained by allowing  $s_N$  to vary and holding  $\omega$  constant.

The term  $x_{\text{bath}}$ , defined as  $1/kT$ , is substituted into equation A2-I yielding equation A2-II. Equation A2-II becomes equation A2-III if the squared term is expanded. If  $E_a$  is now set equal to  $N_A s_N h\omega$  and substituted into equation A2-III, equation A2-IV is obtained.

$$k = A_0 s_N (h\omega/kT)^2 \exp[s_N(\omega/v - h\omega/kT)] \quad \text{A2-II}$$

$$k = A_0 s_N (h\omega) (h\omega) / (kT)^2 \exp[s_N(\omega/v - h\omega/kT)] \quad \text{A2-III}$$

$$k = A_0 E h\omega / kRT^2 \exp[(E/N_A h\nu) - (E/RT)] \quad \text{A2-IV}$$

If A is now set equal to  $A_0 h\omega N_A$  and  $v$  is substituted for  $N_A h\nu$ , equation A2-IV becomes equation A2-V. Taking the natural logarithm of equation A2-V yields the final form of the equation (eq. A2-VI).

$$k = AE / (RT)^2 \exp[(E/v) - (E/RT)] \quad \text{A2-V}$$

$$\ln k = \ln(A \times E / (RT)^2) + (E/v) - (E/RT) \quad \text{A2-VI}$$

The other form of Linert's equation is obtained by substitution of  $h\omega$  by  $E_a / (s_N)$ ,  $N_A h\nu$  by  $v$  and  $A_0 / s_N$  by  $A$  in equation A2-IV. The result is shown as A2-VII. Taking the natural logarithm of equation A2-IX yields the final form of this equation (A2-VIII).

$$k = A \times (E/RT)^2 \exp[(E/v) - (E/RT)] \quad \text{A2-VII}$$

$$\ln k = \ln(A \times (E/RT)^2) + (E/v) - (E/RT) \quad \text{A2-VIII}$$



## A-6: Appendix for Chapter 6

The quantum yield for reaction,  $\Phi$ , is given in equation A6-I and was assumed to be a constant independent of the extent of reaction. For simplicity, the variables may be changed substituting the mole fraction,  $X$ , of  $trans-(Et_3P)_2Ni(N_3)_2$  which introduces a constant,  $c$ , into the equation (A6-II). Irradiation was conducted with a constant intensity light source. Therefore, the light absorbed by the starting material,  $d(h\nu)/dt$ , is given by equation A6-III where  $I$  is the intensity of the incident light and  $A'(0)$  and  $A'(f)$  are the initial and final absorbance of the film at the irradiation wavelength.

$$\Phi = -d(trans-(Et_3P)_2Ni(N_3)_2)/d(h\nu) \quad A6-I$$

$$c\Phi = -d(X)/d(h\nu) \quad A6-II$$

$$d(h\nu)/dt = I \left\{ \frac{(XA'(0))}{(XA'(0) + (1-X)A'(f))} \right\} \times (1 - \exp(-(XA'(0) + (1-X)A'(f)))) \quad A6-III$$

As a result of the film having a low overall coverage absorbance  $(1 - \exp(-(XA'(0) + (1-X)A'(f))))$  can be approximated by  $(XA'(0) + (1-X)A'(f))$ . Once the approximation is made, equation A6-III may be substituted into A6-II (through  $d(h\nu)$ ) leaving a differential equation in  $X$  and  $t$ , equation A6-IV. In equation A6-IV all of the constants have been combined into the quantum yield term to give a corrected constant,  $\emptyset$ .

$$dX/X = \emptyset dt \quad A6-IV$$

Integration of equation A6-IV, followed by converting the mole fraction into an absorbance at the monitored wavelength, gives rise to equation A6-V. In equation A6-V,  $A(t)$ ,  $A(0)$  and  $A(f)$  are the absorbance in the IR at the monitoring wavelength at time  $t$ , at time  $t=0$  and the final absorbance, respectively. Therefore, if the photoproduct does not absorb  $A(f)$  would be zero and a plot of  $-\ln\{A(0)/A(f)\}$  vs. time should be linear. If photoproduct absorption occurred, the more general form of the equation (A-V) would be needed to fit the data.

$$\ln\{(A(0) - A(f))/(A(t) - A(f))\} = \emptyset t \quad \text{A6-V}$$

### A-8: Appendix for Chapter 8

The quantum yield equation used in Chapter 8 is reproduced in equation A8-I. The general formula for the change in intensity of

$$\Phi = [-(\emptyset) \times (\text{total number of moles}) / (I_0) (A(0))] \quad \text{A8-I}$$

where  $\Phi$  = quantum yield

$\emptyset$  = the slope of a plot of  $\ln(A(0)/A(t))$  vs. mJ of light, where,  $A(0)$  is the absorbance at time = 0 and  $A(t)$  is the absorbance at time = t

$I_0$  = Intensity of the incident light in mW

$A(0)$  = is the absorbance of the film at time = 0 based on the solution extinction coefficient at 366 nm

a species is given in equation A8-II. Rearranging equation A8-II, and integrating yields equation A8-III. The general formula for quantum

$$dI = -\alpha[J]I dx \quad \text{A8-II}$$

where,  $dI$  = change in light intensity

$I$  = light intensity

$\alpha$  = proportionality constant

$[J]$  = concentration of absorbing species

$dx$  = sample thickness

$$I_f = I_0 e^{-\alpha[J]l} \quad \text{A8-III}$$

where,  $I_f$  = emergent light intensity

$I_0$  = incident light intensity

$l$  = path length

yield calculations is given in equation A8-IV. Substituting the mole fraction of starting material (X) for the number of moles, into equation A8-IV, introduces a constant and yields equation A8-V. Using equation

$$\phi = -d(\text{\#moles})/d(h\nu) \quad \text{A8-IV}$$

$$c\phi = -d(X)/d(h\nu) \quad \text{A8-V}$$

A8-III, the light absorbed by the starting material alone ( $I_a$ ) is given by equation A8-VI. Also, the absorbances may be defined in terms of

$$I_a = I_0[A(\text{s.m.})/A(\text{tot})](1 - e^{-A(\text{tot})}) \quad \text{A8-VI}$$

where,  $A(\text{s.m.})$  = absorbance due to the starting material alone

$A(\text{tot})$  = absorbance due to all species

the mole fraction. The absorbances, in terms of mole fractions are given in equations A8-VII and A8-VIII. The light absorbed by the starting material is also equal to the expression  $d(h\nu)/dt$ .

$$A(a) = XA(0) \quad \text{A8-VII}$$

$$A(\text{tot}) = XA(0) + (1-X)A(f) \quad \text{A8-VIII}$$

where,

$A(a)$  = absorbance of starting material

$A(f)$  = is the final absorbance

$X$  = mole fraction of starting material

Combining  $d(h\nu)/dt$  with equations A8-VI, A8-VII and A8-VIII yields the expression given in equation A8-IX. Because the quantum yields

$$d(h\nu)/dt = I_0 [XA(0)/(XA(0)+(1-X)A(f))] [1-e^{-(XA(0) + (1-X)A(f))}] \quad \text{A8-IX}$$

were done on thin films where the absorbance due to the starting material is much less than one, the following approximation was made;  $(XA(0)+(1-X)A(f)) \approx 1-e^{-(XA(0) + (1-X)A(f))}$ . Substituting the approximation into equation A8-IX yields equation A8-X. Now, combining equation A8-X and equation A8-V yields equation A8-XI. Integrating

$$d(h\nu)/dt = I_0 XA(0) \quad \text{A8-X}$$

$$-d(X)/X = \emptyset dt \quad \text{A8-XI}$$

where,  $\emptyset = c\Phi I_0 A(0)$

equation A8-XI and converting mol fraction, X, back into absorbance yields equation A8-XII. Taking the derivative of the relationship given in equation A8-XIII and rearranging gives the value of c in equation

$$\ln (A(0)/A(t)) = \emptyset t \quad \text{A8-XII}$$

$$(\# \text{ of moles Ti}) = X(\text{total } \# \text{ of moles})$$

A8-XIII

$$dX = d(\# \text{ of moles Ti})/(\text{total } \# \text{ of moles})$$

A8-XI. Therefore,  $c = 1/(\text{total } \# \text{ of moles})$ . Substituting the expression for  $c$  into equation A8-XI and rearranging yields the final form of the quantum yield expression (equation A8-XIV).

$$\Phi = [(\Phi) (\text{total } \# \text{ moles})]/[(I_0) (A_0)] \quad \text{A8-XIV}$$

## References

1. G.L. Geoffroy, M.S. Wrighton. *In Organometallic Photochemistry*. Academic Press, New York, NY. 1979.
2. P.C. Ford, R.E. Hintze, J.D. Peterson, *In Concepts of Inorganic Photochemistry*, Edited by A.W. Adamson, P.D. Fleischauer. Wiley, New York, NY. 1975. Chapter 5.
3. A.H. Jankowicz, R.G. Bergman. *J. Am. Chem. Soc.* **104**, 352 (1982).
4. a) J.K. Hoyano, W.A.G. Graham. *J. Am. Chem. Soc.* **104**, 3723 (1982).  
b) J.K. Hoyano, A.D. McMaster. W.A.G. Graham. *J. Am. Chem. Soc.* **105**, 7190 (1983).
5. M.L.H. Green, G. Giannotti. *J. Am. Chem. Soc. Chem. Commun.*, 1114 (1972).
6. M. Berry, N.J. Cooper, M.L.H. Green, S.J. Simpson. *J. Chem. Soc. Dalton Trans.*, 29 (1980).
7. J.G. Bentsen, M.S. Wrighton. *J. Am. Chem. Soc.* **109**, 4518 (1987).
8. J.P. Blaha, M.S. Wrighton. *J. Am. Chem. Soc.* **107**, 2694 (1985).
9. D.M. Kurtz Jr., D.F. Shriver, I.M. Klotz. *J. Am. Chem. Soc.* **98**, 5033 (1976).  
J.E. Pate, T.J. Thamann, E.I. Solomon. *Spectrochimica Acta.* **42A**, 313 (1986).
10. H.M. Manasevit. *Appl. Phys. Lett.* **12**, 156 (1968); *J. Crystal Growth.* **13/14**, 306 (1972); *J. Crystal Growth.* **22**, 125 (1974); *J. Crystal Growth.* **55**, 1 (1981).
11. W.E. Hoke, P.J. Lemomias, R. Korenstein. *J. Mat. Res.* **3**, 329 (1988).
12. *In Spectroscopy of Matrix Isolated Species*. Edited by R.J.H. Clark, R.E. Hester. John Wiley and Sons, New York, NY. 1989. pp. 6-12.
13. J.K. Burdett. *Coor. Chem. Rev.* **27**, 1 (1978).
14. L.R. Narasimhan, K.A. Littau, Dee William Pack, Y.S. Bai, A. Elschner, M.D. Fayer. *Chem. Rev.* **90**, 439 (1990).

15. J.D. Black, M.J. Boylan, P.S. Braterman, W.J. Wallace. *J. Organometal. Chem.* **63**, C21 (1973).
16. I.W. Stolz, G.R. Dobson, R.K. Sheline. *J. Am. Chem. Soc.* **84**, 3589 (1962).  
I.W. Stolz, G.R. Dobson, R.K. Sheline. *J. Am. Chem. Soc.* **85**, 1013 (1963).
17. J.D. Black, P.S. Braterman. *J. Organometal. Chem.* **63**, C19 (1973).
18. J.D. Black, P.S. Braterman. *J. Organometal. Chem.* **85**, C7 (1975).
19. J.K. Burdett, M.A. Graham, R.N. Perutz, M. Poliakoff, A.J. Rest, J.J. Turner, R.F. Turner. *J. Am. Chem. Soc.* **97**, 4805 (1975).
20. V.E. Bondybey, L.E. Brus. *J. Chem. Phys.* **64**, 3724 (1976).
21. *In Chemistry and Physics of Matrix-Isolated Species. Edited by L. Andrews, M. Moskovits. Elsevier Science Publishers, New York, NY. 1989. Chapter 9.*
22. W. Linert. *Chem. Phys.* **116**, 381 (1987).
23. J.U. Mondal, D.M. Blake. *Coord. Chem. Rev.* **47**, 205 (1982).  
G.W. Parshall. *Acc. Chem. Res.* **3**, 139 (1970).  
J. Halpern. *Acc. Chem. Res.* **3**, 386 (1970).  
J.P. Collman. *Acc. Chem. Res.* **1**, 136 (1968).  
J.P. Collman, W.R. Roper. *Adv. Organomet. Chem.* **7**, 53 (1968).
24. J.K. Stille, K.S.Y. Lau. *Acc. Chem. Res.* **10**, 343 (1978).
25. T.T. Tsou, J.K. Kochi. *J. Am. Chem. Soc.* **101**, 6319 (1979).
26. J.A. Labinger, J.A. Osborn. *Inorg. Chem.* **19**, 3230 (1980).
27. J.L. Speier. *Adv. Organomet. Chem.* **17**, 407 (1979) and references therein.
28. M. Hara, K. Ohno, J. Tsuji. *Chem. Comm.* 247 (1971).  
A.J. Archer, R.N. Haszeldine, R.U. Parish. *Chem Comm.* 524 (1971).
29. M. Kumada, K. Yamamoto, I. Ojima. *In Aspects of Homogeneous Catalysis. Edited by J.D. Morrison. Reidel: Dordrecht, 1977. Vol. 3. p. 186.*
30. W. Strohmeier. *Angew. Chem.* **76**, 873 (1964).



31. E. Koerner von Gustorf, F.-W. Grevels. *Fortschr. Chem. Forsch.* **13**, 366 (1969).
32. A.B.P. Lever. *In Inorganic Electronic Spectroscopy*. American Elsevier Publishing Company, New York, NY. 1968.
33. C.K. Jorgensen. *In Absorption Spectra and Chemical Bonding in Complexes*. Pergamon Press, New York, NY. 1962.
34. M. Wrighton. *Chem. Rev.* **74**, 401 (1974).
35. F.W.B. Einstein, A.H. Klahn-Oliva, D.Sutton, K.G. Tyers. *Organometallics*. **5**, 53 (1986).
36. R.H. Hill, B.J. Palmer. *Organometallics*. **8**, 1651 (1990).
37. S.P. Murarka, M.C. Peckerar. *In Electronic Materials Science and Technology*. Academic Press Inc., San Diego, CA. 1989.
38. J.J. Hood. *Phil. Mag.* **6**, 371 (1878).  
J.J. Hood. *Phil. Mag.* **20**, 323 (1885).
39. J.H. van't Hoff. *In Etudes de dynamique chimique*. F. Muller and Company, Amsterdam. 1884.
40. S. Arrhenius. *Z. Physik. Chem.* **4**, 226 (1889).
41. C. Masters. *In Homogeneous Transition Metal Catalysis*. Chapman Hall, London. 1981.
42. R.G. Bergman, P.F. Seidler, T.T. Wenzel. *J. Am. Chem. Soc.* **107**, 4358 (1985).
43. a) W. Jetz, W.A.G. Graham. *Inorg. Chem.* **10**, 4 (1971).  
b) J.K. Hoyano, W.A.G. Graham. *Organometallics*. **1**, 783 (1982).
44. W. Linert, A.B. Kurdjajtseu, R. Schmid. *Aust. J. Chem.* **36**, 1903 (1983).
45. W. Linert, A.B. Kurdjajtseu. *Aust. J. Chem.* **37**, 1139 (1984).
46. W. Linert, A.B. Kurdjajtseu, R. Schmid. *Aust. J. Chem.* **38**, 677 (1985).
47. W. Linert. *Aust. J. Chem.* **39**, 199 (1986).
48. W. Linert. *Chem. Phys.* **114**, 449 (1987).
49. W. Linert. *Chem. Phys.* **114**, 457 (1987).
50. W. Linert. *Inorganica. Chimica. Acta.* **141**, 233 (1988).

51. a) R.H. Hill, M.S. Wrighton. *Organometallics*. **6**, 632 (1987).  
b) R.H. Hill, M.S. Wrighton. *Organometallics*. **4**, 413 (1985).  
c) Kent M. Young, M.S. Wrighton. *Organometallics*. **8**, 1063 (1989).
52. Based on arguments similar to those in: F.A. Cotton, C.S. Kraihanzel. *J. Am. Chem. Soc.* **84**, 4432 (1962).
53. a) F. Carre, E. Colomer, F.J.B. Corriu, A. Vioux. *Organometallics*. **3**, 1272 (1984) and references cited therein.  
b) W.A.G. Graham. *J. Organomet. Chem.* **81**, 300 (1986).
54. U. Schubert, K. Ackermann, B.J. Wörle. *J. Am. Chem. Soc.* **104**, 7378 (1982).
55. U. Schubert, G. Scholz, J. Muller, K. Ackerman, B. Wörle, R.F.D. Stansfield. *J. Organomet. Chem.* **306**, 303 (1986).
56. 'SYSTAT', SYSTAT, Inc., version 5.1, 1990. Calculations were run on an I.B.M compatible personal computer equipped with a math co-processor.
57. R. Fletcher. *AERE R.*, 7125 (1972).
58. R. O'Neill. *Applied Statistics.*, 338 (1971).
59. P. Griffiths, I.D. Hill. *In Applied statistics algorithms*. Ellis Horwood Limited. Chichester. 1985.
60. L.L. Costarizo, S. Giuffrida, R. Romeo. *Inorg. Chim. Acta.* **38**, 31 (1980).
61. A.H. Janowicz, R.G. Bergman. *J. Am. Chem. Soc.* **105**, 3929 (1983). see note 28 for C-H bond formation evidence.
62. R.H. Hill, M.S. Wrighton. unpublished observations.
63. a) R.H. Hill, R.J. Puddephatt. *Organometallics*. **2**, 1472 (1983).  
b) A. Becalska, R.H. Hill. *J. Am. Chem. Soc.* **111**, 4346 (1989).
64. S. Fukuzimi, K. Ishikawa, T. Tanaka. *Organometallics*. **6**, 358 (1987).
65. This complex has been made on a synthetic scale: J.-M. Zhuang, D. Sutton. private communication.
66. T.L. Theodore, D.J. Darensbourg. *Inorg. Chem.* **6**, 971 (1967).
67. In our group, we have found that photolysis of a number of complexes in this solvent produce a simple CO loss product. In each of the cases no reaction of the epoxide ring was evident.

68. G. Diaz, A.H. Klahn-Oliva, C. Manzur. *Polyhedron*. **7**, 2743 (1988).
69. The complex, *cis*-( $\eta^5$ -C<sub>5</sub>Me<sub>5</sub>)Re(CO)<sub>2</sub>Me<sub>2</sub>, was prepared by the methylation of the dihalide: A.H. Klahn-Oliva, C. Manzur. manuscript in preparation.
70. J. Debad, R.H. Hill. *Can. J. Chem.* **68**, 2216 (1990).
71. W. Xia. *In The Study of Photochemical Intermediates of Selected Organometallic Compounds*. M.Sc. Thesis. Simon Fraser University. 1990.
72. M.J. Almond, D.A. Rice, C.A. Yates. *Chem. Br.* **24**, 1130 (1988).
73. K.A. Singmaster, F.A. Houle, R.J. Wilson. *Appl. Phys. Lett.* **53**, 1048 (1988).
74. H.H. Gilgen, T. Cacouris, P.S. Shaw, R.R. Krchnavek, R.M. Osgood. *Appl. Phys. B.* **42**, 55 (1987).
75. N.S. Gluck, Z. Ying, C.E. Bartosch, W. Ho. *J. Chem. Phys.* **86**, 4957 (1987).
76. a) T.A. James, J.A. McCleverty. *J. Chem. Soc. A.* 850 (1970).  
b) I.P. Herman. *Chem. Rev.* **89**, 1323 (1989).
77. R.N. Perutz, J.J. Turner. *J. Am. Chem. Soc.* **97**, 4791 (1975).
78. C.L. Randolph, M.S. Wrighton. *J. Am. Chem. Soc.* **108**, 3366 (1986).
79. V.A. Burrows, Y.J. Chabal, G.S. Higashi, K. Ragavachari, S.B. Christman. *Appl. Phys. Lett.* **53**, 998 (1988).
80. M.J. Rand. *J. Electrochem. Soc.* **120**, 686 (1973).
81. K. Nakamoto. *In Infrared and Raman Spectra of Inorganic and Coordination Compounds*. Third Edition. Johnson Wiley and Sons, New York, NY. 1963.
82. *In Organometallic Chemistry*. Vol. 1. Edited by J.J. Eisch, R.B. King. Academic Press, New York, NY. 1965. p. 163.
83. J.L. Reed, F. Wang, F. Basolo. *J. Am. Chem. Soc.* **94**, 7173 (1972).  
C. Bartocci, F. Scandola. *J. Chem. Soc. Chem. Commun.*, 531 (1970).  
J.F. Endicott, M.Z. Hoffman, L.S. Beres. *J. Phys. Chem.* **74**, 1021 (1970).
84. R. Ngai, Y-H. Wang, J.L. Reed. *Inorg. Chem.* **24**, 3802 (1985).

85. B.J. Palmer, A. Becalska, R.H. Hill. *J. Photochem. Photobiol. A: Chem.* **57**, 457 (1991).
86. B.J. Palmer, A. Becalska, R. Hader, R.H. Hill. *Polyhedron.* **8**, 877 (1991).
87. J.M. Woodall. *American Institute of Physics Conf. Proceed.* **138**, 223 (1986).
88. A. Becalska, R.J. Batchelor, F.W.B. Einstein, R.H. Hill, B.J. Palmer. *Inorg. Chem.*, in press.
89. C.R.C. Coussmaker, M.H. Hutchison, J.R. Mellor, L.E. Sutton, L.M. Venanzi. *J. Chem. Soc.*, 2705 (1961).
90. A. Merle, M. Dartiguenave, Y. Dartiguenave. *J. Mol. Struct.* **13**, 413 (1972).
91. G.J. Ferraudi. *In Elements of Inorganic Photochemistry*, Wiley, New York, NY. 1988.
92. G.J. Ferraudi, J.F. Endicott. *J. Chem. Soc. Chem. Commun.*, 674 (1973).  
P. Natarajan, A.W. Adamson. *J. Am. Chem. Soc.* **93**, 5599 (1971).
93. H. Knoll, R. Stich, H. Henning, D.J. Stufkens. *Inorg. Chimica. Acta.* **71**, 178 (1990) and references therein.
94. H-F. Klein, S. Haller, H. Konig, M. Dartiguenave, Y. Dartiguenave, M-J Menu. *J. Am. Chem. Soc.* **113**, 4673 (1991).
95. Attempts were made to form the dimer complex in solution by LMCT irradiation of an acetone solution of  $\text{trans}-(\text{Et}_3\text{P})_2\text{Ni}(\text{N}_3)_2$ . It was found that starting material was lost and no production of species containing coordinated azide was observed, as monitored by FTIR. Results analogous to those for the acetone solution were found in hexane.
96. W. Beck, W.P. Fehlhammer, P. Pollmann, R.S. Tobias. *Inorg. Chim. Acta.* **2**, 467 (1968).
97. H. Henning, R. Stich, H. Knoll, D. Rehorek. *Anorg. Allg. Chem.* **576**, 139 (1989).
98.  $^{15}\text{N}^{14}\text{N}$  is expected to have a very low extinction coefficient and is very difficult to observe in the IR; S. Pinchas, I. Laulight. *In Infrared Spectra of Labelled Compounds*. Academic Press, London. 1971.
99. R. Tian, J.C. Facelli, J. Michel. *J. Phys. Chem.* **92**, 4073 (1988).

100. *In Handbook of Auger Electron Spectroscopy*. Third Edition. Perkin-Elmer Corporation, Physical Electronics Industries Inc., Eden Prairie, Minnesota. 1978.
101. K. Bowman, Z. Dori. *Inorg. Chem.* **9**, 395 (1970).
102. L.F. Druding, H-C. Wang, R.E. Cohen, F.D. Sancilio. *J. Coord. Chem.* **3**, 105 (1973).
103. R.B. Hagel, L.F. Druding. *Inorg. Chem.* **6**, 1496 (1970).
104. V.H. Siebert. *Z. Anorg. Allg. Chem.* **441**, 47 (1978).
105. L. Costanzo, A. Giuffrida, G. Guglielmo, V. Ricevuto. *Inorg. Chim. Acta.* **33**, 29 (1973).
106. W. Beck, W.P. Fehlhammer, P. Pöllman, R.S. Tobias. *Inorg. Chim. Acta.* **2**, 467 (1968).
107. D.R. Herrington, L.J. Boucher. *Inorg. Nucl. Chem. Lett.* **7**, (1971).
108. W.P. Fehlhammer, L.F. Dahl. *J. Am. Chem. Soc.* **10**, 3377 (1972).
109. G.G. Schlessinger. *In Inorganic Laboratory Preparations*. Chemical Publishing Co. Inc., New York, N.Y. 1962. p. 262.
110. K.L. Sieferting, G.L. Griffin. *J. Electrochem. Soc.* **137**, 814 and 1206 (1990).
111. S. Zaima, T. Furata, Y. Yasuda. *J. Electrochem. Soc.* **137**, 1297 (1990).
112. C.C. Wang, K.H. Zaininger, M.T. Duffy, S. Patai. *J. Electrochem. Soc.* **126**, 1203 (1979).
113. R.W. Harrigan, G.S. Hammond, H.B. Gray. *J. Organometal. Chem.* **81**, 79 (1974).
114. Z-T. Tsai, C.H. Brubaker Jr.. *J. Organometal. Chem.* **166**, 199 (1979).
115. M.R.M. Bruce, A. Sclafani, D.R. Tyler. *Inorg. Chem.* **25**, 2546 (1986).
116. W.A. Badawy, E.A. El-Taher. *Thin Solid Films.* **158**, 277 (1988).  
W.A. Badawy, F. Decker, K. Doblhofer. *Solar Energy Materials.* **8**, 363 (1983).

117. W.W. Xu, R. Kershaw, K. Dwight, A. Wold. *Mat. Res. Bull.* **25**, 1385 (1990).
118. W.B. Chou, M.N. Azer, J.J. Mazumder. *J. Appl. Phys.* **66**, 191 (1989).
119. J.Y. Tsao, R.A. Becker, D.J. Ehrlich, F.J. Leonberger. *Appl. Phys. Lett.* **42**, 559 (1983).
120. R.S.P. Coutts, P.C. Wailes. *Aust. J. Chem.* **24**, 1075 (1971).  
J.E. Pate, T.J. Thamann, E.I. Solomon. *Spectrochimica Acta.* **42A** 2/3, 313 (1986).
121. P.M. Druce, B.M. Kingston, M.F. Lappert, T.R. Spalding, R.C. Srivastava. *J. Chem. Soc. (A)*, 2106 (1969).
122. E. Samuel, R. Ferner, M. Bigorgne. *Inorg. Chem.* **4**, 881 (1973).
123. G. Balducci, L. Bencivenni, B. De Rosa, R. Bibli, B. Martini, S.N. Cesaro. *J. Mol. Struct.* **64**, 164 (1980).
124. C.R. Brazier, P.F. Bernath, J.B. Burkholder, C.J. Howard. *J. Chem. Phys.* **89**, 1762 (1988).  
R. Tian, J.C. Facelli, J. Michl. *J. Phys. Chem.* **92**, 4073 (1988).  
J.I. Bryant. *Spectrochimica Acta.* **22**, 1475 (1966).
125. M.D. Rausch, W.H. Boon, H.G. Alt. *J. Organometal. Chem.* **141**, 299 (1977).
126. *In Handbook of X-Ray Photoelectron Spectroscopy. Second Edition.* Perkin-Elmer Corporation, Physical Electronics Industries Inc., Eden Prairie, Minnesota. 1977.
127. J. Gandon, J.C. Joud. *J. Less-Common Met.* **69**, 277 (1980).  
J.E. Bercaw, R.H. Marvich, L.G. Bell, H.H. Brintzinger. *J. Am. Chem. Soc.* **94**, 1219 (1972).
128. C.H. Langford, J.P. Aplington. *J. Organometal. Chem.* **4**, 271 (1965).